

INFORMATION TO USERS

This manuscript has been reproduced from the microfilm master. UMI films the text directly from the original or copy submitted. Thus, some thesis and dissertation copies are in typewriter face, while others may be from any type of computer printer.

The quality of this reproduction is dependent upon the quality of the copy submitted. Broken or indistinct print, colored or poor quality illustrations and photographs, print bleedthrough, substandard margins, and improper alignment can adversely affect reproduction.

In the unlikely event that the author did not send UMI a complete manuscript and there are missing pages, these will be noted. Also, if unauthorized copyright material had to be removed, a note will indicate the deletion.

Oversize materials (e.g., maps, drawings, charts) are reproduced by sectioning the original, beginning at the upper left-hand corner and continuing from left to right in equal sections with small overlaps.

ProQuest Information and Learning
300 North Zeeb Road, Ann Arbor, MI 48106-1346 USA
800-521-0600

UMI[®]

University of Alberta

Impact of anomalous surface forcing on the sub-polar North
Atlantic: Water mass formation and circulation

by

Duo Yang



A thesis submitted to the Faculty of Graduate Studies in partial fulfilment of the
requirements for the degree of Doctor of Philosophy

Department of Earth and Atmospheric Sciences

Edmonton, Alberta

Fall 2005



Library and
Archives Canada

Bibliothèque et
Archives Canada

0-494-08760-9

Published Heritage
Branch

Direction du
Patrimoine de l'édition

395 Wellington Street
Ottawa ON K1A 0N4
Canada

395, rue Wellington
Ottawa ON K1A 0N4
Canada

Your file *Votre référence*

ISBN:

Our file *Notre référence*

ISBN:

NOTICE:

The author has granted a non-exclusive license allowing Library and Archives Canada to reproduce, publish, archive, preserve, conserve, communicate to the public by telecommunication or on the Internet, loan, distribute and sell theses worldwide, for commercial or non-commercial purposes, in microform, paper, electronic and/or any other formats.

The author retains copyright ownership and moral rights in this thesis. Neither the thesis nor substantial extracts from it may be printed or otherwise reproduced without the author's permission.

AVIS:

L'auteur a accordé une licence non exclusive permettant à la Bibliothèque et Archives Canada de reproduire, publier, archiver, sauvegarder, conserver, transmettre au public par télécommunication ou par l'Internet, prêter, distribuer et vendre des thèses partout dans le monde, à des fins commerciales ou autres, sur support microforme, papier, électronique et/ou autres formats.

L'auteur conserve la propriété du droit d'auteur et des droits moraux qui protègent cette thèse. Ni la thèse ni des extraits substantiels de celle-ci ne doivent être imprimés ou autrement reproduits sans son autorisation.

In compliance with the Canadian Privacy Act some supporting forms may have been removed from this thesis.

Conformément à la loi canadienne sur la protection de la vie privée, quelques formulaires secondaires ont été enlevés de cette thèse.

While these forms may be included in the document page count, their removal does not represent any loss of content from the thesis.

Bien que ces formulaires aient inclus dans la pagination, il n'y aura aucun contenu manquant.


Canada

ABSTRACT

A regional eddy-permitting ocean model of the sub-polar North Atlantic under flux forcing, with a weak restoring term on salinity (to parameterize non-represented sea ice processes), has been developed based on a previous version using restoring boundary conditions. The flux forcing is based upon two different climatologies, from the Southampton Oceanography Center and the NCEP-NCAR reanalysis. With addition of a crude parameterization of the effect of high-frequency variability resulting from the passages of synoptic scale events on the heat flux over the convective region of the Labrador Sea during winter months, the model remains stable and all major features of the sub-polar gyre are represented, although temperature and salinity are still higher than observations, as seen in most high-resolution models of the sub-polar gyre, which appears to be dominated by internal advection processes rather than surface forcing.

The model is then utilized to examine the response of the sub-polar North Atlantic to distinct surface forcings corresponding to extreme North Atlantic Oscillation (NAO) phases and the Last Glacial Maximum (LGM). A potentially multi-decadal variability in Labrador Sea Water (LSW) formation and heat transport is observed in a high NAO experiment in contrast to a low NAO experiment. The results therefore suggest that LSW formation and heat transport processes are less stable under the high NAO phase and this feature appears to be brought about by internal oceanic processes, primarily attributable to changes in the strength and pathway of the North

Atlantic Current (NAC). During the LGM, the inclusion of sea ice effects in the atmospheric forcing shuts down Labrador Sea deep convection, as well as steers the NAC from its present northeastward path to a zonal path with an apparent southward shift. The meridional transport also reduces significantly. The results therefore emphasize the importance of the insulating effects of sea ice, in contrast to previous work. With such discrepant responses, this study stresses the importance of understanding how ocean circulation will evolve in some extreme circumstances, especially with the possibility for enhanced variability of the climate system under the high NAO phase which, as suggested by some model simulations, is more likely to occur in a warmer world.

ACKNOWLEDGEMENTS

I am very grateful to my supervisor, Dr. Paul Myers, who has been taking time and effort to make my transitions from atmospheric science to physical oceanography, as well as between different cultures, smoothly and successfully. Dr. Myers' stimulating suggestions and comments have greatly refined my original ideas in the course of my research and writing of this thesis. I feel honored to work and study with him. I believe that the experience I gain during this period will be of great benefit in my future career and my life.

I would like to express my gratitude to my committee members. Dr. Andrew Bush has given me constructive suggestions in my research, as well as looked closely of the thesis for English style and grammar. His assistance is as precious as that from a supervisor. Dr. Gerhard Reuter and Dr. Gordon Swaters have provided valuable advice polishing my thesis and their help during my study is as invaluable as those from friends. Dr. William Gough has offered motivated suggestions which helped improve the final version of my thesis.

Thanks to CFCAS and NSERC for providing funding (to Dr. Paul Myers) for my research.

I am deeply indebted to my husband, Shumin Wang, who has done everything he can to support me and take care of our family, and to my son, Chao Wang, for his understanding and help, as well as to my mother, sister and brother for their support and understanding throughout my study.

I am thankful to all my friends for their encouragement and advice, who have made my life during the study enjoyable.

Table of Contents

Abstract	ii
Acknowledgements	iv
List of Tables	viii
List of Figures	ix
1 Introduction	1
1.1 Significance of the subject	1
1.2 Methodology	11
1.3 Proposed research	16
References	20
2 A regional eddy-permitting ocean model of the sub-polar North Atlantic under flux forcing	30
2.1 Introduction	30
2.2 A brief description of the model	35
2.3 Surface boundary conditions and experiment design	36
2.3.1 Restoring control experiment	36
2.3.2 Forcing Data	36
2.3.3 Sub-polar North Atlantic SOC-NCEP flux comparison	38
2.3.4 Modifications	40
2.3.5 Experiment Design	43
2.4 Model results	44
2.4.1 Model stability	44
2.4.2 Experiment SOC1	45
2.4.3 Experiment NCEP1	49
2.4.4 A diagnosis of two modes of circulation in NCEP2	51
2.4.5 Adjusted SOC	55

2.5	Summary and discussion	58
References		60
3	Role of the high frequency portion of heat flux in Labrador Sea Water formation in an eddy-permitting ocean model	71
3.1	Introduction	71
3.2	Model description	73
3.3	Surface forcing algorithms	75
3.4	Model results	78
3.5	Summary and discussion	80
References		82
4	Response of the sub-polar North Atlantic to extreme NAO phase-related flux forcing in a regional eddy-permitting ocean model	87
4.1	Introduction	87
4.2	Model configuration and experiment design	89
4.3	Model response of the sub-polar North Atlantic	92
4.3.1	Less “stable” oceanic response in HNAO vs. LNAO	92
4.3.2	Anomalous NAC pathway	96
4.4	Discussion	98
4.5	Summary	99
References		101
5	Sensitivity of the sub-polar North Atlantic to LGM surface forcing and sea-ice distribution in an eddy-permitting regional ocean model	106
5.1	Introduction	106
5.2	A brief description of the model and experiment design	109
5.3	Model results	114
5.4	Discussion and Summary	118
References		119
6	Summary and Future Work	126
6.1	Summary and Conclusions	126
6.2	Future Work	129
References		130

List of Tables

2.1	Summary of experiments reported in this chapter	43
2.2	Properties of the LSW in March of 40th year (1: Averaged over years 37 ~ 40; 2: Clarke and Gascard (1983); Wallace and Lazier (1988); Lilly et al. (1999); <i>http : //www.mar.dfo-mpo.gc.ca/science/ocean/-woce/labsea/labsea_poster.html</i> ; 3: Levitus climatology)	49
3.1	Monthly heat flux means and maxima of instantaneous heat fluxes over the Labrador Sea convection region (55 ~ 59°N and 51 ~ 56°W) (unit: Wm^{-2})	77
5.1	Summary of experiments performed in this chapter	114
5.2	Maximum meridional stream function (Sv) for all experiments	115

List of Figures

1.1	Schematic diagram of surface and deep circulation in the subpolar North Atlantic (http://www.ifm.uni-kiel.de/allgemein/research/projects-sfb460/sfb460-e.htm)	4
1.2	Thickness (m) of the LSW layer from historical observations in the central Labrador Sea. The shaded is the NAO index (http://www.ifm.uni-kiel.de/allgemein/research/topics/fb1_select/fb1_s2.htm)	6
1.3	Major geographical and topographical features of the model domain. The legend for the numbered features is: 1)Flemish Cap; 2)Avalon Channel; 3)Mid-Atlantic Ridge; 4)Hudson Strait; 5)Denmark Strait; 6)Faeroe Island; 7)Cape Farewell; 8)Hamilton Bank; 9)Gulf of St. Lawrence. The contour interval is 1000 m, and the 500-m isobath is also indicated (Myers, 2002).	15
2.1	Heat fluxes averaged over Dec.-Feb. (unit: Wm^{-2}) for a) original SOC and b) NCEP; annual mean E minus P (unit: $cm yr^{-1}$) for c) original SOC and d) NCEP and the difference of NCEP minus original SOC for e) heat flux (unit: Wm^{-2}) and f) E minus P (unit: $cm yr^{-1}$). Some blank regions along Greenland and Labrador coasts indicate missing data in original SOC climatology due to sea ice.	39
2.2	Time series of a) temperature ($^{\circ}C$) and b) salinity (psu) for experiments SOC1, NCEP1 and RES, averaged over the entire model domain	45
2.3	Annual current fields (arrows) and EKE fields ($cm^2 s^{-2}$) (gray scale) at 52.5 m (3rd model level) averaged over years 37 ~ 40 for (a) SOC1; (b) RES; (c) NCEP1. Every second vector is plotted.	46
2.4	Annually-averaged PV over years 37 ~ 40 on $\sigma_0 = 27.6$ for a) SOC1 and b) NCEP1. Contour intervals are in $0.2 \times 10^{-10} m^{-1} s^{-1}$ but no value larger than $2.0 \times 10^{-10} m^{-1} s^{-1}$ is contoured. The small box indicates the central Labrador Sea region discussed in our analysis.	48
2.5	Time series of temperature ($^{\circ}C$) and salinity (psu) averaged over the entire model domain in NCEP2	52

2.6	Annually-averaged PV on $\sigma_0 = 27.6$ in NCEP2, a) for the 34th year and b) the 80th year. Contour intervals are in $0.2 \times 10^{-10} m^{-1} s^{-1}$ but no value larger than $2.0 \times 10^{-10} m^{-1} s^{-1}$ is contoured.	53
2.7	A time series of heat content over eastern basin convection region ($43 \sim 52^\circ N$, $12 \sim 24^\circ W$), from the surface to 915 m, and LSW volume ($\sigma_0 = 27.74 \sim 27.8$) over the central Labrador Sea region in NCEP2. .	54
2.8	Annual a) net heat influx b) net Ekman heat influx c) non-Ekman heat influx (a)-b) through four lateral faces of eastern region ($43 \sim 52^\circ N$, $12 \sim 24^\circ W$) for whole water column in NCEP1 and NCEP2 (units: <i>PW</i>).	56
2.9	Annually-averaged currents at a depth of 52.5 m for NCEP2 in a) the 35th year and b) the 80th year. Every second vector is plotted	57
3.1	Time series of wintertime heat fluxes at $57^\circ N$, $54^\circ W$ in the Labrador Sea	77
3.2	Time series of LSW volume on $\sigma_0 = 27.75 \sim 27.8$ over the central Labrador Sea Region	80
4.1	Heat flux anomalies averaged over Dec.-Feb. (NCEP-NCAR). HNAO anomalies are synthesized from three extreme high NAO years (1989, 1990 and 1995) and LNAO anomalies from three extreme low NAO years (1969, 1996 and 1963)	91
4.2	Time series of a) meridional stream function at $55^\circ N$; b) domain-averaged heat content; c) heat content in eastern basin ($43 \sim 52^\circ N$ $12 \sim 24^\circ W$) for HNAO (solid line) and LNAO (dashed line).	93
4.3	Snapshots of annual temperature anomalies in HNAO (with respect to annual temperature mean over the entire integration period - years $40 \sim 150$) averaged over the upper 658 m (model levels $1 \sim 14$) during a full oscillation (years $46 \sim 94$), plotted every six model years.	95
4.4	0 and -5 cm sea surface height contours for years 46 (dashed line), 76 (solid line) and 94 (dash-dot line) in HNAO and in year 80 (dotted line) in LNAO, output from our model.	97
5.1	Differences in a) winter (DJF) heat flux ($W m^{-2}$); b) annual E-P ($cm yr^{-1}$) between the LGM and present, based on CGCM output	111
5.2	LGM sea ice distributions. CGCM output in Feb. (maximum sea ice coverage) is indicated by the thick white line, north of which is covered by sea ice. Sea ice cover north of thick black line ($48^\circ N$) is based upon Crowley and North (1991). Shaded sea ice areas are consistent with de Vernal and Hillaire-Marcel (2000), with black color representing perennial sea ice, dark gray color winter (Dec.- May) sea ice cover, light gray color a shorter (Feb.- Apr.) sea ice season and the white area ice-free.	113

5.3	Annual temperature at 3rd model level (52 m) for a) SOCE b) LGME1	
	c) LGME2 d) LGME3	117

Chapter 1

Introduction

1.1 Significance of the subject

The earth receives more net radiation near the equator than near the poles. Instead of heating the tropics and cooling high latitudes all the time, this heat budget is balanced by poleward heat transport by the ocean and atmosphere. Although the relative importance of these two media in the transport is still a matter of debate (Trenberth and Caron, 2001), it has long been recognized that the transport and large heat capacity of the ocean have significant effect on the earth's climate. Oceanic heat transport is mainly carried out by the thermohaline circulation (THC), a complex global system of surface and subsurface ocean currents, described schematically by warm, salty surface waters transported poleward, replacing the equatorward flowing deep waters. Stability and variations in the THC have therefore attracted intensive attentions in term of its potential impact on the future stability of the climate system. An alternative term of the THC is the meridional overturning circulation (MOC) in

a sense that the flow is integrated zonally in the ocean (Wunsch, 2002), which implies a buoyancy flux for the major power source (Munk and Wunsch, 1998). Sometimes the MOC is even referred to as the THC owing to its dominance in the oceanic heat transport.

The sub-polar North Atlantic resides in the northern limit of the Atlantic Ocean, open to the south and mostly encompassed by land on its other sides but connecting to the Arctic through Baffin Bay, with the Labrador Sea situated in the westernmost portion of this region (Figure 1.1). The crucial role of this region in climate change and thus in socioeconomic implications is connected to its role in the MOC, and hence in poleward heat transport. This is linked to the North Atlantic Current, a branch of a large-scale cyclonic gyre prevailing in the upper layers of the ocean (from surface to 700 m or so), being further made a loop by other boundary currents along the shelves and over the shelf breaks, including the Irminger Current (IC), the East Greenland Current (EGC), the West Greenland Current (WGC) and the Labrador Current (LC) (Figure 1.1). The NAC, an extension of the Gulf Stream (a most swift and warm current) (Clarke et al., 1980), is unique in transporting warm waters to high latitudes (Rossby, 1996) as part of upper layer branch of the MOC. The NAC separates warm, saline waters of tropical-subtropical origin and the cold, relatively fresh waters from the Labrador Sea (Rossby, 1996). Its pathway is thus associated with the position of the Subarctic Front (SAF). In addition, the North Atlantic Deep Water (NADW - below 2000 m) - the major deep water component

of the MOC - passes through the Labrador Sea at the bottom, composed of the Island-Scotland Overflow Water (ISOW) and underlying Denmark Strait Overflow Water (DSOW) inflowing from the Nordic seas. Furthermore, at intermediate depths (500 ~ 2000 m), the intense air-sea exchange during winter leads to deep convection and the formation of the Labrador Sea Water (LSW), mostly offshore of the LC, around 56 ~ 58°N, 52 ~ 55°W (Clarke and Gascard, 1983; Wallace and Lazier, 1988; Lilly et al., 1999), under the preconditioning of local cyclonic oceanic circulation (uplifting the isopycnal surface) and weak stratification (Clarke and Gascard, 1983; Marshall and Schott, 1999). The LSW is a large volume of homogeneous water, characteristically cold (2.75 ~ 3.65 °C) and fresh (34.83 ~ 34.91 *psu*) (http://www.mar.dfo-mpo.gc.ca/science/ocean/woce/labsea/labsea_poster.html), with a weak vertical density gradient (Talley and McCartney, 1982). After its formation, the LSW spreads through the North Atlantic, northeastward to the Irminger Sea, eastward and southward. The southward-flowing portion of the LSW constitutes a component of the NADW, contributing to the MOC as part of the deep water flow (Figure 1.1). At intermediate layers also exist the sub-polar mode waters (SPMWs), which are large volumes of low stability water at a depth of a few hundred meters, formed locally by vertical mixing due to intensive wintertime cooling in the eastern sub-polar North Atlantic basin (Talley, 1999). These SPMWs circulate along the cyclonic gyre, eventually feeding the Labrador Sea through the IC where they help precondition the water column for LSW formation (Clarke, 1984; McCartney and Talley, 1982). Within the

Labrador Sea flows a counter-current (Lavender et al., 2000), extending through the whole water column, that is responsible for part of the LSW dispersal.

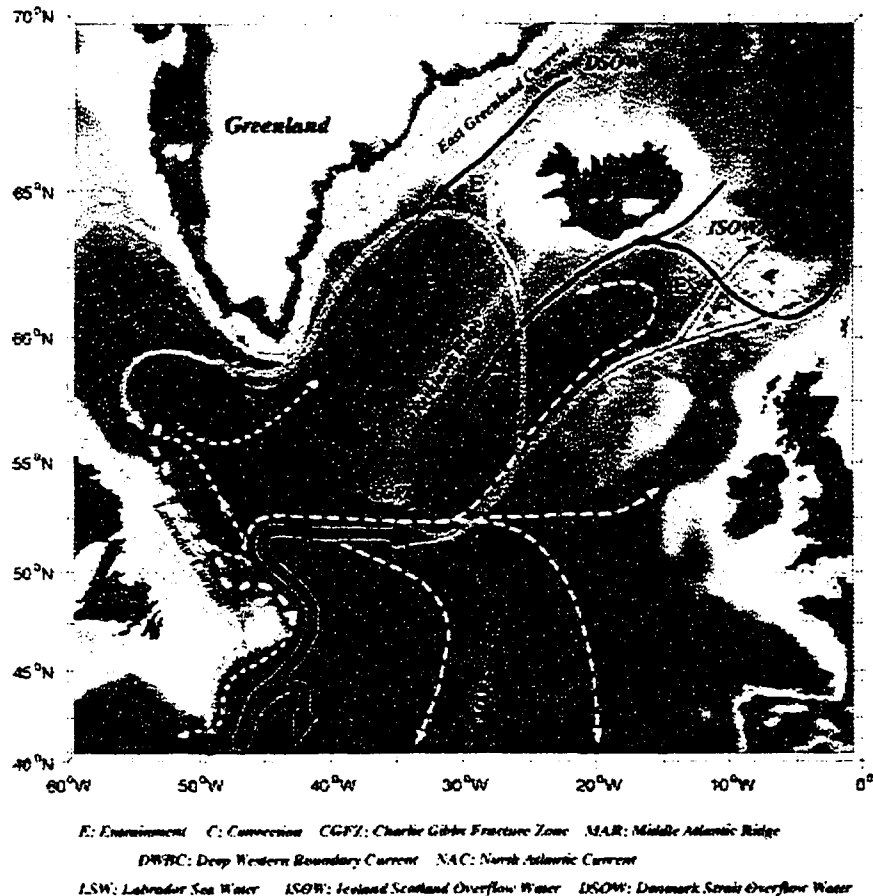


Figure 1.1: Schematic diagram of surface and deep circulation in the subpolar North Atlantic (<http://www.ifm.uni-kiel.de/allgemein/research/projects/sfb460/sfb460-e.htm>)

LSW formation and the NAC are the foci of this thesis. Observationally, they have displayed significant variability on interannual and interdecadal scales over the last five decades. Deep convection weakened and LSW layer thinned from the 1950s to 1970 with the convection effectively switched off in the late 1960s/early 1970s;

subsequent strengthening and thickening during 1971 ~ 76 was followed by thin conditions in the late 1970s/early 1980s; then deep convection resumed since 1984 with a record extreme strength and thick layer appeared in the 1990s (1990 ~ 1993), exceeding the normal 2000 m limit in depth (into the underlying ISOW layer); a drastic thinning ensued afterwards (since 1995) (Lazier, 1980; Talley and McCartney, 1982; Clarke and Gascard, 1983; Wallace and Lazier, 1988; Curry et al., 1998; Lazier, 1995; Lazier et al., 2002). These signals can be tracked to the subtropical large scale deep water with a lag of 6 yrs (Curry et al., 1998). The above variations are coincident to some extent with the variability in the North Atlantic Oscillation (NAO), a dominant mode of the atmospheric variability over the North Atlantic (Figure 1.2). The strong convection was accompanied by exceptionally cold and fresh LSW, and vice versa, thereby the variations of temperature and salinity of the LSW mutually compensated along the isopycnal (Dickson et al., 1996). This compensation was broken with a density increase due to extreme cooling and relative increase in salinity during 1990 ~ 1993 (that remained until 1995) (extreme high NAO phase) (Dickson et al., 1996; Lazier et al., 2002), indicating an invading of the LSW to the underlying cold but salty ISOW. The spreading of the LSW during the early 1990s showed surprisingly fast speeds: 6 months into the Irminger Sea (4.5 cm s^{-1}) although Pickart et al. (2003) suggested a possibility that the deep convection occurred within the Irminger Basin; 4 ~ 5.5 years to Rockall Trough (mean speed $1.5 \sim 2 \text{ cm s}^{-1}$) and 6 years into the subtropics (Sy et al., 1997; Curry et al., 1998). The speed from the

Labrador Sea to Rockall Trough is about three to four times faster than the previous estimate 0.47 cm s^{-1} , hence a circulation time of 18 ~ 19 years before 1991 (Read and Gould, 1992). All the evidence seems to indicate a far greater impact of the LSW during 1990s. Dickson et al. (1996) noticed that the variability of convection intensity in the Labrador Sea is roughly out of phase with those in the Greenland and Sargasso Seas. The link of these water mass properties to the NAO further suggests the non-local effect of the LSW. From this link, Dickson (1997) conjectured the connection between water mass formations and the sea surface temperature (SST) anomalies (e.g. Hansen and Bezdek, 1996), and hence a possible feedback of the ocean on the atmosphere that sets the NAO timescale.

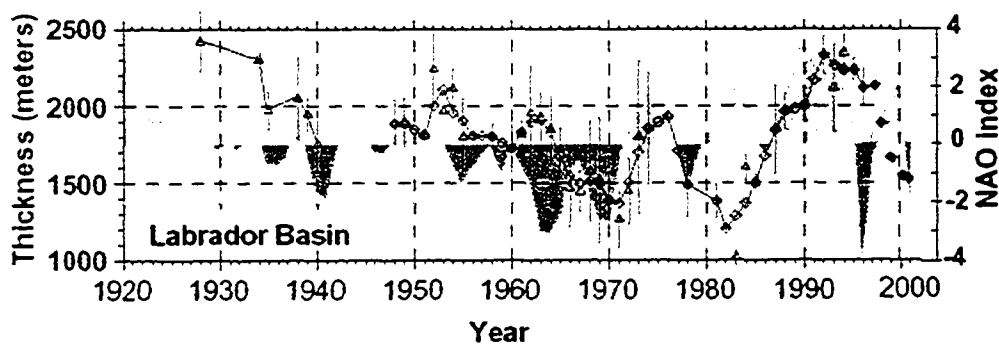


Figure 1.2: Thickness (m) of the LSW layer from historical observations in the central Labrador Sea. The shaded is the NAO index (http://www.ifm.uni-kiel.de/allgemein/research/topics/fb1_select/fb1_s2.htm)

There is also evidence that the NAC variability is linked to the NAO. Curry and McCartney (2001) suggest a gradual weakening of the Gulf Stream/NAC system during the low NAO interval and an intensification during persistently high NAO phase. Bersch (2002) proposes a subpolar gyre contraction with the SAF shifting

westward in the Iceland Basin and eastward in the Newfoundland when the NAO turned from high to low phase. Levitus (1989a,b) also found a redistribution of warm, saline subtropical waters and cold, fresh subarctic waters with the NAO.

The NAO index is defined as the surface pressure difference between the subpolar low (Stykkisholmur, Iceland) and the subtropical high (Lisbon, Portugal) and hence through geostrophy represents the strength of the westerly winds blowing over the North Atlantic Ocean between $40 \sim 60^{\circ}N$ (Hurrell, 1995). A high (low) or positive (negative) phase of the NAO indicates strengthening (weakening) of the meridional pressure gradient and thus westerly wind. The NAO's connection to the oceanic circulation is associated with its modulation to the surface fluxes (e.g. Cayan, 1992; Hurrell, 1996; Visbeck et al., 1998). For example, the Labrador Sea experiences considerably high heat loss during the high NAO phase, accompanied by enhanced westerly wind in the southern part of the basin (Pickart et al., 2002), and vice versa.

The impact of the NAO on the North Atlantic ocean dynamics has been investigated by a number of atmosphere-ocean coupled models. Delworth and Greatbatch (2000), using the Geophysical Fluid Dynamics Laboratory (GFDL) coupled model, reveal that the interdecadal variability in the intensity of the MOC can be viewed as an oceanic response to the NAO-related atmospheric forcing. Their further experiments with the oceanic component of the coupled model driven by surface fluxes suggests the dominant role of heat fluxes over the freshwater and momentum fluxes. Timmermann et al. (1998) however, employing ECHAM3/LSG coupled model of the Max Planck

Institute, emphasize the importance of evaporation and Ekman transport. Hakkinen (1999) analyzed a 43-year simulation of an ice-ocean (sigma-coordinate) coupled model forced by Comprehensive Ocean-Atmosphere Data Set (COADS) surface flux anomalies. Her results show the response of meridional heat transport (MHT) and the MOC to the NAO-related surface heat flux on interannual and decadal timescales. Eden and Willebrand (2001), using a North Atlantic ocean model driven by both NCEP-NCAR reanalysis anomalies for the years 1958 ~ 97 and idealized, stable forcing associated with the NAO, reveal that interannual oceanic variability is a fast barotropic response (involving a topographic Sverdrup balance) and a delayed (3 *yrs* and 6 ~ 8 *yrs*) baroclinic response to the NAO, stressing the importance of wind stress and heat flux. During a high NAO phase, the former forms a barotropic anti-cyclonic circulation anomaly near the sub-polar front with a diminished (enhanced) poleward heat transport in the sub-polar region (subtropics) due to changes in Ekman transport. The latter produces an increased sub-polar heat transport due to enhanced meridional overturning and a strengthening of the subpolar gyre. Using the same model, Eden and Jung (2001) found the lagged response of the North Atlantic circulation (Atlantic MOC - AMOC and the sub-polar gyre strength) to the NAO on the interdecadal timescale plays an important role in the development of interdecadal SST anomalies. Gulev et al. (2003), in a sigma-coordinate ocean model forced by NCEP-NCAR reanalysis anomalies for the years 1958 ~ 97 but with heat and freshwater fluxes being expressed as density flux linked to the NAO, identify

decadal-scale variability linked to the transformation of the LSW and sub-tropical Mode Waters (STMWs). A similar fast response as in Eden and Willebrand (2001) and delayed baroclinic response to the surface heat forcing are identified at time lags of 3 and 7 yrs. The authors stress the role of changes in stratification driven by formation processes of the LSW and the STMW in the 3 yr lag. While studies from Ocean General Circulation Models (OGCMs) have linked interannual or interdecadal variability in atmospheric forcing associated with the NAO to low-frequency variations in the horizontal and meridional circulations and heat transport, the internal oceanic fluctuations were revealed by a series of idealized models forced by idealized fluxes, independent of varying surface forcing (e.g. Weaver and Sarachik, 1991; Weaver et al., 1993; Greatbatch and Zhang, 1995; te Raa et al., 2004). Weaver and Sarachik (1991) revealed significant decadal oscillation in the THC with an alternation of deep water formation and collapse in a set of experiments using a coarse-resolution OGCM driven by steady forcing, with an advective mechanism involved. Weaver et al. (1993) observed a number of different states of the same model with respect to the relative importance of freshwater versus thermal fluxes, with self-sustained oscillations in the deep water formation rate existing in a case with sufficiently strong freshwater forcing case. Greatbatch and Zhang (1995), using a geostrophic ocean model with a box geometry of the North Atlantic driven by a constant, zonally uniform, surface heat forcing, show a fluctuation with a period of 50 years produced by the balance between the strength of the poleward heat transport and local heat storage. te Raa

et al. (2004) identified the internal interdecadal modes and the mechanism by using a hierarchy of increasingly complex model configurations. In light of the non-eddy-resolving feature of the above ocean models, it is of interest to examine the potential internal oceanic mode in a more realistic and high resolution regime.

The LSW formation and the NAC also experienced major fluctuations between the last glacial and the present interglacial. The Last Glacial Maximum (LGM - about 22 to 14 kyr BP) represents an extreme climate condition with large areas covered by great ice sheets and sea ice in the northern latitudes (Crowley and North, 1991). Paleo proxy data have provided us with some evidence that there was a weakening and shallowing of the NADW compared to today (e.g. Curry and Lohmann, 1983; Oppo and Fairbanks, 1987; Boyle and Keigwin, 1987) which was located in relatively southern latitudes (Alley and Clark, 1999) and was accompanied by a southward shifted and more zonally-orientated Gulf Stream/NAC system (Ruddiman and McIntyre, 1977, 1984; CLIMAP, 1981). Combined, these data suggest that the poleward ocean heat transport in the North Atlantic at the LGM was reduced (Miller and Russell, 1989), yet the mechanisms still need to be further clarified.

The goal of this study is therefore to inspect the sensitivity of water mass (the LSW) formation and circulation (the NAC) in the sub-polar North Atlantic to anomalous surface forcing (heat, freshwater and momentum fluxes and their sea ice modulation) and its mechanisms in a regional high resolution ocean model under flux forcing. These anomalies reflect the different phases of the NAO (both positive and negatives

phases), as well as potential changes associated with past climates (the LGM). The goal is to determine how possible future atmospheric states will affect the underlying ocean, and the potential of oceanic feedback upon the atmosphere as recent evidence suggests that the variability in SST plays an important role in setting the NAO's timescale (Kushnir and Held, 1996; Dickson, 1997; McCartney, 1997; Curry et al., 1998; Sutton and Allen, 1997).

1.2 Methodology

The model used in this study is the Sub-Polar Ocean Model (SPOM), a regional configuration of the Modular Ocean Model - Array (MOMA) (Myers, 2002). The original model formulation is based on a Bryan-Cox-Semtner type ocean general circulation model (Pacanowski et al., 1990) incorporating the inviscid version of the Killworth et al. (1991) free surface scheme. The governing equations are the primitive equations with incompressible, hydrostatic, Boussinesq and turbulent assumptions, listed below:

$$u_t + \vec{v} \cdot \nabla u + wu_z - fv = -\frac{1}{\rho_0} P_x + D^u + F^u \quad (1.1)$$

$$v_t + \vec{v} \cdot \nabla v + wv_z + fu = -\frac{1}{\rho_0} P_y + D^v + F^v \quad (1.2)$$

$$\theta_t + \vec{v} \cdot \nabla \theta + w\theta_z = D^\theta + F^\theta \quad (1.3)$$

$$S_t + \vec{v} \cdot \nabla S + wS_z = D^S + F^S \quad (1.4)$$

$$\nabla \cdot \vec{v} + w_z = 0 \quad (1.5)$$

$$P_z = -g\rho \quad (1.6)$$

$$\rho = \rho(\theta, S, P_0) \quad (1.7)$$

$$h_t^0 = (h^0 u^0)_x + (h^0 v^0)_y \quad (1.8)$$

The free surface equation (1.8) is closed by the following four equations:

$$u_t^0 = P_x^0 + f v^0 + T^u \quad (1.9)$$

$$v_t^0 = P_y^0 - f u^0 + T^v \quad (1.10)$$

$$P_x^0 = g h_x^0 \quad (1.11)$$

$$P_y^0 = g h_y^0 \quad (1.12)$$

where u , v , w , θ , S , ρ , P , h^0 , u^0 , v^0 and P^0 are three components of velocity, potential temperature, salinity, density, pressure, free surface height, two components of the barotropic velocity and the barotropic pressure, respectively. $D^{\vec{v}}$ and D^T (T denotes tracer) are diffusion terms. $F^{\vec{v}}$ and F^T are surface forcing terms resulted from wind stress and bouyancy fluxes respectively. T^u and T^v are the vertical-means of the baroclinic velocity tendencies (excluding the Coriolis term); $f = 2\Omega \sin\Theta$ is the

Coriolis parameter; ρ_0 the reference density of sea water (1 gcm^{-3}) and P_0 reference pressure field; g : gravitational acceleration.

$D^{\vec{v}}$ and D^T are expressed as

$$D^{\vec{v}} = -A_h \nabla^4 \vec{v} + A_v \vec{v}_{zz} \quad (1.13)$$

and

$$D^T = -K_h \nabla^4 T + K_v T_{zz} \quad (1.14)$$

The biharmonic horizontal viscosity coefficient $A_h = 7.5 \times 10^{18} \text{ cm}^4 \text{ s}^{-1}$ and the diffusion coefficient $K_h = 7.5 \times 10^{18} \text{ cm}^4 \text{ s}^{-1}$, the vertical diffusion is $K_v = 0.3 \text{ cm}^2 \text{ s}^{-1}$ and the momentum diffusion is $A_v = 1.5 \text{ cm}^2 \text{ s}^{-1}$. The constant viscosity and diffusion coefficients are not the best choice, but they represent an option of the model. Convective adjustment utilizes the complete convection scheme of Rahmstorf (1993). The model has a resolution of $1/3^\circ$, hence allowing eddies to be partially resolved. The Gent and McWilliams eddy parameterization is applied to deal with along-isopycnal mixing, with a constant of $2.0 \times 10^5 \text{ cm}^2 \text{ s}^{-1}$ used for the thickness diffusion parameter.

The model domain (Figure 1.3) covers the sub-polar North Atlantic ($68^\circ W \sim 0^\circ, 38 \sim 70^\circ N$). The southern boundary is open and connects to the rest of the North Atlantic. The baroclinic velocities along the boundary are calculated using the linear form of the equations (1.1) and (1.2) (Stevens, 1990). This choice keeps the velocities in agreement with the density field. The tracers are allowed to be advected or diffused out of the domain if the velocities (perpendicular to the boundary) at some level are

directed out of the domain and are restored smoothly to the Lozier et al. (1995) climatology (filled-in version of Grey and Haines (1999)) if the velocities are directed into the domain. The sea surface height is relaxed toward a diagnostic reference field (Myers, 2000). The open boundary condition produces a better representation of the inflowing Gulf Stream, outflowing NADW and the northward flowing Mediterranean Water. The northern boundary is closed and inlaid with restoring buffers in Hudson Strait, Baffin Bay and the region to the north of the Iceland. Myers (2005) has shown that increased freshwater export of the Canadian Arctic Archipelago through Davis Strait has negligible effect on freshwater content in both Labrador Sea interior and Labrador Sea. A partial cell finite-volume technique (Adcroft et al., 1997) is applied to better represent the topography. Restoring boundary conditions are used on the top surface layer, parameterizing as $F^T = \frac{1}{R}(T^S - T^{top})$, where T^S is monthly climatology, taken from NODC (1994), and T^{top} the model top layer tracer values. R is the relaxation timescale, a 2-hour given by Myers (2002) means the mixed layer properties are essentially fixed. Wind stress climatology (Trenberth et al., 1990) is substituted for $F^{\bar{v}}$ directly.

The model is solved using finite difference method. The horizontal grids are arranged as a staggered Arakawa B-grid (Arakawa and Lamb, 1977). This is a historical choice. Although it is widely believed that the B-grid gives better performance for course resolution (with respect to the Rossy deformation radius) (e.g. Mesinger and Arakawa, 1976), this fact holds only for inertia-gravity wave (Haidvogel and Beck-

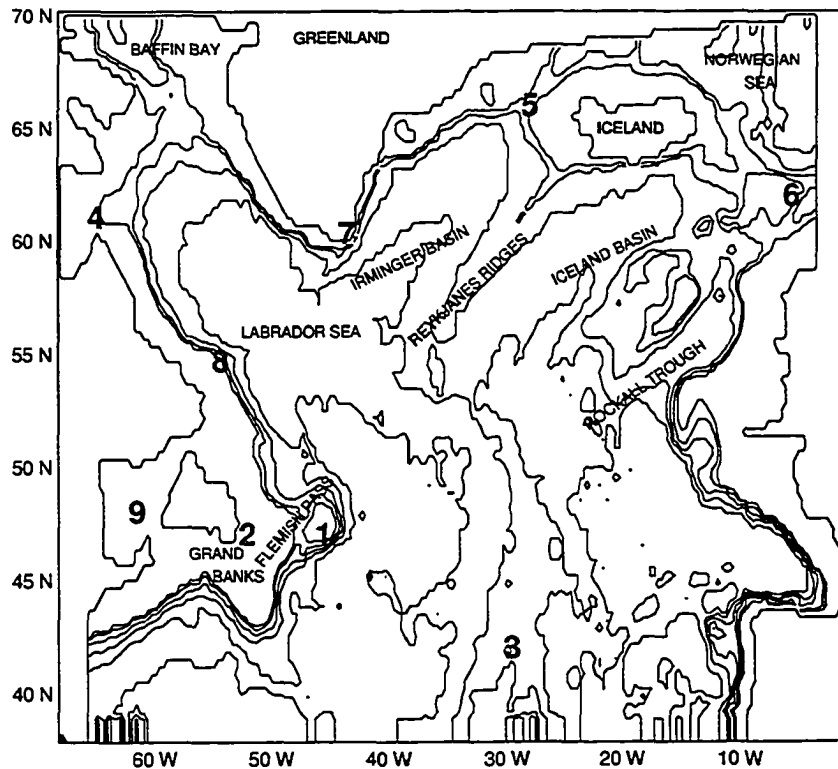


Figure 1.3: Major geographical and topographical features of the model domain. The legend for the numbered features is: 1)Flemish Cap; 2)Avalon Channel; 3)Mid-Atlantic Ridge; 4)Hudson Strait; 5)Denmark Strait; 6)Faeroe Island; 7)Cape Farewell; 8)Hamilton Bank; 9)Gulf of St. Lawrence. The contour interval is 1000 m, and the 500-m isobath is also indicated (Myers, 2002).

mann, 1999). The model has 36 z-levels, unevenly spaced, with finer resolution in the upper water column so as to better resolve the thermocline and mixed layer. The barotropic velocity fields and the free surface height are calculated using a small timestep (30 seconds) to resolve the fast external gravity waves whereas a larger timestep (1800 seconds) is used for the baroclinic velocity, as well as density and tracers, of the model.

The model reproduces the major features of the oceanic circulation and hydrography. The inclusion of the more realistic topography and sub-grid scale eddy parameterization improved large scale gyre structure (tighter and sharper), SPMW formation sites and LSW properties. However, limitations exist. For example, the relaxation of surface tracer values toward the prescribed climatology constrains the atmosphere-ocean exchange from freely penetrating the deep ocean. Like other high resolution models of this region, the LSW is still warmer and saltier in comparison with observations (see Chapter 2 for details).

1.3 Proposed research

This thesis is concerned with four themes, which converge to contribute to the above subject, including the establishment of a high resolution ocean model of the sub-polar North Atlantic, examination of the sensitivity of LSW formation to the high frequency fraction of atmospheric heat forcing, inspection of the effects of extreme high and low NAO phase - related surface forcing on the sub-polar North Atlantic and

investigation of the potential impact of atmospheric forcing and its sea ice modulation during the LGM.

Anomalous atmospheric signatures are delivered into the ocean through the ocean-atmosphere interface. This is implemented in ocean modelling by surface boundary conditions, which attempt to properly represent the ocean-atmosphere energy and mass exchanges. The parameterization of buoyancy fluxes is, however, a challenge owing to the inaccuracy of flux measurements over the ocean. This parameterization becomes particularly important when addressing the questions of climate variability and changes in the response of the subsurface oceanic circulation to anomalous atmospheric forcing. It is therefore a crucial process which needs to be represented in the model solution as accurately as possible. Basically, there are two types of boundary conditions in ocean modelling. Commonly used restoring boundary conditions restore the model tracer values towards climatology and hence keeps the model from drifting too far from the observations. However, these boundary conditions fix the surface conditions such that anomalous atmospheric forcing cannot be properly reflected in the model solution. Flux boundary conditions specify the fluxes either independent of (Rosati and Miyakoda, 1988) or with evolving temperature (Barnier et al., 1995) or salinity, and hence is more realistic and frees the surface conditions. However, some studies (e.g. Rosati and Miyakoda, 1988) show that they often lead to model instability or drifting problems. The first step of this study therefore aims at developing a flux-forced version of a regional eddy-permitting ocean model of the sub-polar North

Atlantic, based on its previous restoring version (Myers, 2002), while insuring model stability and minimizing the model drift.

Observations support the contention that convection in the Labrador Sea is forced by the high frequency portion of the heat flux, associated with synoptic events (e.g. Sathiyamoorthy and Moore, 2002). Yet, many oceans models are forced with monthly heat flux climatologies. This effect has therefore been crudely parameterized in the algorithm of surface forcing of the model mentioned above, where the monthly heat flux is simply multiplied by an ad hoc coefficient over a limited region within the Labrador Sea during the convective season (Nov.-Mar.). This parameterization improves significantly the properties of water mass formation and model hydrography and prevents the model tracer fields from drifting too far from the initial conditions (observations). However, are the model responses biased by increasing the heat fluxes over the entire winter instead of just during high frequency synoptic events? The second part of this thesis examines this issue with a series of experiments designed to represent different scenarios for synoptic events.

As discussed previously, the internal oceanic variability constitutes an important aspect of oceanic variation, in addition to external forcing. The third theme of this thesis therefore is to reexamine this issue in a more realistic (in terms of geometry, topography and NAO-related surface forcing) high resolution regional ocean model configuration. Eden and Willebrand (2001) also performed experiments with stable NAO-related surface forcing, which they called response to “idealized” forcing. Their

forcing is produced by the monthly regression patterns of the NCEP-NCAR fluxes to the NAO multiplied by three standard deviations of the NAO index for both high and low NAO phases. The differences of this study from theirs are that high resolution is used to better resolve eddy and frontal processes, there is a longer length of integration (allowing the development of a decadal internal mode), the sub-polar North Atlantic domain is chosen (consistent with the focus of this study), and hence different results are anticipated (they suggested a symmetric response of the model to the high and low NAO, i.e. same responses but with opposite sign).

There have been intensive efforts toward research about the discrepancy in the NADW (LSW) and its impact on the MOC and meridional heat transport at the LGM, with emphasis on the potential mechanism. The recent paleo reconstructions (de Vernal and Hillaire-Marcel, 2000, 2002) infer a low salinity surface layer and a strong stratification between the surface and the underlying waters attributable to the seasonal spreading of sea ice, implying a diminished LSW formation. Keffer et al. (1988) ascribe the southward migration in the Gulf/NAC system to the prevailing wind field modified by the great ice sheets (Manabe and Broccoli, 1985). This study instead inspects the impact of atmospheric forcing and its modulation of sea ice on LSW mass formation and circulation and hence emphasizes the significance of sea-ice insulation, which is difficult to clarify from paleo proxy data.

Following this Introduction, Chapter 2 describes the regional eddy-permitting ocean model of the sub-polar North Atlantic under flux forcing, which highlights re-

sults from three key experiments out of an extensive set of 34 experiments. Chapter 3 further explores sensitivity of water mass formation to different frequency and evolving patterns of synoptic events. Chapter 4 reexamines the issue of a low frequency internal oceanic mode by inspecting the effects of extreme NAO phase-related surface forcing in a more realistic and high-resolution regime. Chapter 5 examines the potential impact of atmospheric forcing and its sea ice modulation on LSW formation, the NAC pathway and hence poleward heat transport during the LGM. Finally, a summary and a discussion of future work are given in Chapter 6.

References

- Adcroft, A., C. Hill, and J. Marshall, 1997: Representation of topography by shaved cell in a height coordinate ocean model. *Mon. Weather Rev.*, **125**, 2293–2315.
- Alley, R. B. and P. U. Clark, 1999: The deglaciation of the Northern Hemisphere: A global perspective. *Annu. Rev. Earth Planet. Sci.*, **27**, 149–182.
- Arakawa, A. and V. R. Lamb, 1977: Computational design of the basic dynamical process of the UCLA general circulation model. *Methods in Computational Physics*, Academic Press, volume 17, 173–265.
- Barnier, B., L. Siefridt, and P. Marchesiello, 1995: Thermal forcing for a global ocean circulation model using a three-year climatology of ECMWF analyses. *J. Mar. Res.*, **6**, 363–380.

- Bersch, M., 2002: North Atlantic Oscillation-induced changes of the upper layer circulation in the North Atlantic Ocean. *J. Geophys. Res.*, **107**, 20-1-20-11.
- Boyle, E. A. and L. Keigwin, 1987: North Atlantic Thermohaline Circulation during the past 20,000 years linked to high-latitude surface temperature. *Nature*, **330**, 35-40.
- Cayan, D., 1992: Latent and sensible heat flux anomalies over the northern oceans: The connection to monthly atmospheric circulation. *J. Clim.*, **5**, 354-369.
- Clarke, R. A., 1984: Transport through the Cape Farewell-Flemish Cap section. *Rapp. P. -v. Reun. Cons. Int. Explor. Mer.*, **185**, 120-130.
- Clarke, R. A. and J.-C. Gascard, 1983: The formation of Labrador Sea Water. Part I: Large-scale processes. *J. Phys. Oceanogr.*, **13**, 1764-1778.
- Clarke, R. A., H. W. Hills, R. F. Reiniger, and B. A. Warren, 1980: Current system south and east of the Grand Banks of Newfoundland. *J. Phys. Oceanogr.*, **10**, 25-65.
- CLIMAP, 1981: Seasonal reconstruction of the earth's surface at the last glacial maximum. Geol. Soc. Am. Map Chart Ser. MC-36.
- Crowley, T. J. and G. R. North, eds., 1991: *Paleoclimatology*. New York: Oxford University Press; Oxford: Clarendon Press.
- Curry, R. G. and M. S. McCartney, 2001: Ocean gyre circulation changes associated with the North Atlantic Oscillation. *J. Phys. Oceanogr.*, **31**, 3374-3400.

- Curry, R. G., M. S. McCartney, and T. M. Joyce, 1998: Oceanic transport of subpolar climate signals to mid-depth subtropical waters. *Nature*, **391**, 575–577.
- Curry, W. B. and G. P. Lohmann, 1983: Reduced advection into Atlantic Ocean deep eastern basins during last glaciation maximum. *Nature*, **306**, 577–580.
- de Vernal, A. and C. Hillaire-Marcel, 2000: Sea-ice cover, sea-surface salinity and halo-/thermocline structure of the northwest North Atlantic: modern versus full glacial conditions. *Quaternary Sciences Reviews*, **19**, 65–85.
- 2002: Structure of the upper water column in the northwest North Atlantic: Modern versus Last Glacial Maximum conditions. *Paleoceanography*, **17**, 2–1–2–15.
- Delworth, T. L. and R. J. Greatbatch, 2000: Multidecadal Thermohaline Circulation variability driven by atmospheric surface flux forcing. *J. Clim.*, **13**, 1481–1495.
- Dickson, B., 1997: From the Labrador Sea to global change. *Nature*, **386**, 649–650.
- Dickson, R. R., J. R. N. Lazier, J. Meincke, P. Rhines, and J. Swift, 1996: Long-term coordinated changes in the convective activity of the North Atlantic. *Progress in Oceanogr.*, **38**, 241–295.
- Eden, C. and T. Jung, 2001: North Atlantic interdecadal variability: Oceanic response to the North Atlantic Oscillation (1865–1997). *J. Clim.*, **14**, 676–691.
- Eden, C. and J. Willebrand, 2001: Mechanism of interannual to decadal variability of the North Atlantic circulation. *J. Clim.*, **14**, 2266–2280.

- Greatbatch, R. J. and S. Zhang, 1995: An interdecadal oscillation in an idealized ocean basin forced by constant heat flux. *J. Clim.*, **8**, 82–91.
- Grey, S. M. and K. Haines, 1999: Climatological hydrography of the North Atlantic. *Int. WOCE Newsletter*, **36**, 23–25.
- Gulev, S. K., B. Barnier, H. Knochel, J. Molines, and M. Cottet, 2003: Water mass transformation in the North Atlantic and its impact on the meridional circulation: insights from an ocean model forced by NCEP-NCAR reanalysis surface fluxes. *J. Clim.*, **16**, 3085–3110.
- Haidvogel, D. B. and A. Beckmann, 1999: *Numerical Ocean Circulation Modeling*. Imperial College Press.
- Hakkinen, S., 1999: Variability of the simulated meridional heat transport in the North Atlantic for the period 1951–1993. *J. Geophys. Res.*, **104**, 10991–11007.
- Hansen, D. V. and H. F. Bezdek, 1996: On the nature of decadal anomalies in North Atlantic sea surface temperature. *J. Geophys. Res.*, **101**, 8749–8758.
- Hurrell, J. W., 1995: Decadal trends in the North Atlantic Oscillation: Regional temperatures and precipitation. *Science*, **269**, 676–679.
- 1996: Influence of variations in extratropical wintertime teleconnections on Northern Hemisphere temperature. *Geophys. Res. Lett.*, **23**, 665–668.

- Keffer, T., D. G. Martinson, and B. H. Corliss, 1988: The position of the Gulf Stream during quaternary glaciations. *Science*, **241**, 440–442.
- Killworth, P. D., D. Stainforth, D. J. Webb, and S. M. Peterson, 1991: The development of a free-surface Bryan-Cox-Semtner ocean model. *J. Phys. Oceanogr.*, **21**, 1333–1348.
- Kushnir, Y. and I. M. Held, 1996: Equilibrium atmospheric response to North Atlantic SST anomalies. *J. Clim.*, **9**, 1208–1220.
- Lavender, K. L., R. E. Davis, and W. B. Owens, 2000: Mid-depth recirculation observed in the interior Labrador and Irminger seas by direct velocity measurements. *Nature*, **407**, 66–68.
- Lazier, J., R. Hendry, A. Clarke, I. Yashayaev, and P. Rhines, 2002: Convection and restratification in the Labrador Sea, 1990–2000. *Deep-Sea Research*, **49**, 1819–1835.
- Lazier, J. R. N., 1980: Oceanographic conditions at O. W. S. Bravo 1964–1974. *Atmos. Ocean*, **18**, 227–238.
- 1995: The salinity decrease in the Labrador Sea over the past thirty years. *Natural Climate Variability on Decade-to-Century Time Scales*, National Academy Press, Washington DC, volume 40, 295–304.
- Levitus, S., 1989a: Interpentadal variability of salinity in the upper 150m of the North Atlantic Ocean, 1970–1974 versus 1955–1959. *J. Geophys. Res.*, **94**, 9679–9685.

- 1989b: Interpentadal variability of temperature and salinity at intermediate depths of the North Atlantic Ocean, 1970-1974 versus 1955-1959. *J. Geophys. Res.*, **94**, 6091-6131.
- Lilly, J. M., P. B. Rhines, M. Visbeck, R. Davis, J. R. N. Lazier, F. Schott, and D. Farmer, 1999: Observing deep convection in the Labrador Sea during winter 1994/95. *J. Phys. Oceanogr.*, **29**, 2065-2098.
- Lozier, M. S., W. B. Owens, and R. G. Curry, 1995: The climatology of the North Atlantic. *Prog. Oceanogr.*, **36**, 1-44.
- Manabe, S. and A. J. Broccoli, 1985: The influence of continental ice sheets on the climate of an ice-age. *J. Geophys. Res.*, **90**, 2167-2190.
- Marshall, J. and F. Schott, 1999: Open-ocean convection: observation, theory, and model. *Review of Geophysics*, **37**, 1-64.
- McCartney, M. S., 1997: Is the ocean at the helm? *Nature*, **388**, 521-522.
- McCartney, M. S. and L. D. Talley, 1982: The subpolar mode water of the North Atlantic Ocean. *J. Phys. Oceanogr.*, **12**, 1169-1188.
- Mesinger, F. and A. Arakawa, 1976: *Numerical methods used in atmospheric models. Vol. I.* GARP Publications Series. 17.
- Miller, J. R. and G. L. Russell, 1989: Ocean heat transport during the Last Glacial Maximum. *Paleoceanog.*, **4**, 141-155.

- Munk, W. and C. Wunsch, 1998: Abyssal recipes II: energetics of tidal and wind mixing. *Deep-Sea Research I*, **45**, 1977–2010.
- Myers, P. G., 2000: A time-dependent, non-linear finite element model of the barotropic vorticity equation. Physics and physical oceanography technical report 2000-4, Memorial University of Newfoundland. 21pp.
- 2002: SPOM: A regional model of the sub-polar North Atlantic. *Atmosphere-Ocean*, **40**, 445–463.
- 2005: Impact of freshwater from the Canadian Arctic Archipelago on Labrador Sea Water formation. *Geophys. Res. Lett.*, **32**, 1–4.
- NODC, 1994: World ocean atlas 1994 cd-rom data set documentation, tech. rep. noaa. US Department of Commerce.
- Oppo, D. W. and R. G. Fairbanks, 1987: Variability in the deep and intermediate water circulation of the Atlantic Ocean during the past 25,000 years: North Hemisphere modulation of the Southern Ocean. *Earth and Planetary Science Letters*, **86**, 1–15.
- Pacanowski, R. C., K. Dixon, and A. Rosati, 1990: *The GFDL Modular Ocean Model users guide, version 1.0 Tech. rep.2 GFDL*.
- Pickart, R. S., F. Straneo, and G. W. K. Moore, 2003: Is Labrador Sea Water formed in the Irminger Basin? *Deep-Sea Research I*, **50**, 23–52.

- Pickart, R. S., D. J. Torres, and R. A. Clarke, 2002: Hydrography of the Labrador Sea during active convection. *J. Phys. Oceanogr.*, **32**, 428–457.
- Rahmstorf, S., 1993: A fast and complete convection scheme for ocean models. *Ocean Modelling*, **101**, 9–11.
- Read, J. F. and W. J. Gould, 1992: Cooling and freshening of the subpolar North Atlantic Ocean since the 1960s. *Nature*, **360**, 55–57.
- Rosati, A. and K. Miyakoda, 1988: A general circulation model for upper ocean simulation. *J. Phys. Oceanogr.*, **18**, 1601–1626.
- Rossby, T., 1996: The North Atlantic Current and surrounding waters: at the crossroads. *Rev. Geophys.*, **34**, 463–481.
- Ruddiman, W. F. and A. McIntyre, 1977: Late quaternary surface ocean kinematics and climate change in the high-latitude North Atlantic. *J. Geophys. Res.*, **82**, 3877–3887.
- 1984: Ice-age thermal response and climatic role of the surface North Atlantic Ocean, 43°–63°. *Geological Society of America Bulletin*, **95**, 381–396.
- Sathiyamoorthy, S. and G. W. K. Moore, 2002: Buoyancy flux at ocean weather station Bravo. *J. Phys. Oceanogr.*, **26**, 458–474.
- Stevens, D. P., 1990: On open boundary conditions for three dimensional primitive equation ocean circulation model. *Geophys. Astrophys. Fluid Dynam.*, **51**, 103–133.

- Sutton, R. T. and M. R. Allen, 1997: Decadal predictability of North Atlantic sea surface temperature and climate. *Nature*, **388**, 563–567.
- Sy, A., M. Rhein, J. R. N. Lazier, K. P. Koltermann, J. Meinck, A. Putzka, and M. Bersch, 1997: Surprisingly rapid spreading of newly formed intermediate waters across the North Atlantic Ocean. *Nature*, **386**, 675–679.
- Talley, L. D., 1999: Mode waters in the subpolar North Atlantic in historical data and during the WOCE period. *Int. WOCE Newsletter*, **37**, 3–6.
- Talley, L. D. and M. S. McCartney, 1982: Distribution and circulation of Labrador Sea Water. *J. Phys. Oceanogr.*, **12**, 1189–1205.
- te Raa, L. A., J. Gerrits, and H. A. Dijkstra, 2004: Identification of the mechanism of interdecadal variability in the North Atlantic ocean. *J. Phys. Oceanogr.*, **34**, 2792–2807.
- Timmermann, A., M. Latif, R. Voss, and A. Groetzner, 1998: Northern Hemispheric interdecadal variability: A coupled air-sea mode. *J. Clim.*, **11**, 1906–1931.
- Trenberth, K. E. and J. M. Caron, 2001: Estimates of meridional atmosphere and ocean heat transports. *J. Clim.*, **15**, 3433–3443.
- Trenberth, K. E., W. G. Large, and J. G. Olson, 1990: The mean annual cycle in global ocean wind stress. *J. Phys. Oceanogr.*, **20**, 1742–1760.

- Visbeck, M., H. Cullen, G. Krahnmann, and N. Naik, 1998: An ocean model's response to North Atlantic Oscillation-like wind forcing. *Geophys. Res. Lett.*, **25**, 4521–4524.
- Wallace, D. W. R. and J. R. N. Lazier, 1988: Anthropogenic chlorofluoromethanes in newly formed Labrador Sea Water. *Nature*, **332**, 61–63.
- Weaver, A. J., J. Marotzke, P. F. Cummings, and E. S. Sarachik, 1993: Stability and variability of the thermohaline circulation. *J. Phys. Oceanogr.*, **23**, 39–60.
- Weaver, A. J. and E. S. Sarachik, 1991: Evidence for decadal variability in an ocean general circulation model: An advective mechanism. *Atmos.-Ocean*, **29**, 197–231.
- Wunsch, C., 2002: What is the Thermohaline Circulation? *Science*, **298**, 1179–1181.

Chapter 2

A regional eddy-permitting ocean model of the sub-polar North Atlantic under flux forcing

2.1 Introduction

The dependence of water mass formation and properties on atmospheric forcing requires accurate representation of surface flux fields in ocean modelling. Specified climatological wind stress is usually employed for momentum forcing (McWilliams, 1996), whereas proper parameterization of heat and freshwater fluxes remains a challenge for ocean modelling due to inaccuracy of flux measurements over the ocean. This deficiency becomes larger as questions of climate variability and change are to be considered, as the surface boundary conditions are the link to convey anomalous atmospheric signatures to the ocean.

⁰A version of this chapter has been submitted for publication. Duo Yang and Paul G. Myers 2005. *Journal of Geophysical Research*.

Restoring boundary conditions, an expression of heat and freshwater fluxes as terms proportional to the differences between model surface (or upper layer) and climatological tracer values, have commonly been utilized in oceanic simulations. This approach is simple to implement and keeps the model from drifting too far from the observations. However, it is the approach of the tracer values to the observations that fixes the surface conditions and constrains the model from addressing variability questions. Furthermore, the formulation of restoring boundary conditions implies false fluxes, i.e. non-zero fluxes are produced by incorrect model temperature or salinity fields (Weaver and Hughes, 1992; Killworth et al., 2000).

Restoring boundary conditions on temperature can be traced back to Haney's pioneering work (1971), where a model's temperature is relaxed toward an effective air temperature. Haney's work, as well as others since (e.g. Han, 1984; Large et al., 1997; Barnier et al., 1995), stresses the importance of the interactivity between ocean and atmosphere in understanding ocean physics and the resulting model stability. These authors therefore formulate flux-like thermal boundary conditions, which impel an ocean model toward an equilibrium state with a prescribed atmosphere. For example, Barnier et al. (1995) expressed the heat flux as a sum of an estimated climatological flux and a relaxation of the model surface temperature toward the climatological sea surface temperature (SST). This formulation has been recently applied in a number of ocean modelling efforts (e.g. Smith et al., 2000; Willebrand et al., 2001; Treguier et al., 2005).

The thermal boundary conditions mentioned above are plausible owing to the fact that long-wave radiation and turbulent fluxes strongly rely on the temperature. The lack of a direct feedback from surface salinity to the freshwater flux (evaporation minus precipitation) however means a restoring boundary condition on salinity is physically unjustified (e.g. Weaver and Sarachik, 1991; Huang, 1993; Tziperman et al., 1994). Mixed boundary conditions (restoring on temperature and a specified freshwater flux on salinity) avoid this (Bryan et al., 1986) and have been widely applied to force ocean models to examine the role of anomalous salt fluxes in the thermohaline circulation (e.g. Weaver and Sarachik, 1991; Tziperman et al., 1994). Greatbatch and Zhang (1995) suggest that the most robust results are obtained by using flux boundary conditions on both temperature and salinity, in comparison to restoring surface temperature and salinity, “mixed” or “reversed mixed” boundary conditions.

Flux boundary conditions specify heat and freshwater fluxes. Some studies show that these boundary conditions can often lead to significant drifts in temperature and salinity (e.g. Rosati and Miyakoda, 1988). Surface flux fields currently used by general circulation models are based on either observational derivations or output of reanalysis systems. In either case, the fields are based on climatological monthly averages, such that extreme cooling events associated with the passage of synoptic scale events are removed (Killworth, 1996). A comparison of the results under monthly mean versus 12-hourly averaged forcing highlights the role of high frequency

variability unrepresented in monthly means in producing more realistic mixing-layer structure (Rosati and Miyakoda, 1988). Philander and Seigel (1985) showed that parameterizing high-frequency wind fluctuations in monthly mean winds could avoid overly high surface temperatures (discussed by Rosati and Miyakoda, 1988).

The significance of the sub-polar North Atlantic in the global thermohaline circulation (THC) depends on the Labrador Sea, which provides a relay for deep water export from Nordic Seas to the rest of world oceans and a site for Labrador Sea Water (LSW) formation. Air-sea exchange thus plays a crucial role. The variability in water mass formation and circulation in this region, in response to anomalous atmospheric conditions, has been documented by a number of authors (e.g. Dickson et al., 1996; Curry et al., 1998; Eden and Willebrand, 2001; Eden and Jung, 2001; Bersch, 2002). LSW formation is triggered by intensive atmospheric forcing, combined with the local cyclonic circulation and weak stratification (Clarke and Gascard, 1983). This strong atmospheric forcing is most likely related to its high frequency component (Moore et al., 1996; Rasmussen et al., 1996; Sathiyamoorthy and Moore, 2002). An inclusion of the effect of high frequency variability in the monthly flux forcing fields may be favorable to the representation of major properties for the large-scale sub-polar circulation.

A growing number of modeling studies have focused on the sub-polar North Atlantic. Results from the mid-nineties showed that transport in this region is dominated by higher order dynamics (Bryan et al., 1995) and that the representation of

topography, especially as it related to the northern overflows, was crucial (Doscher et al., 1994; Boning et al., 1995; Roberts et al., 1996; Roberts and Wood, 1997; Redler and Boning, 1997; Myers, 2002). The sensitivity of model results to mixing and other sub-grid scale processes was also emphasized by a number of authors (e.g. McWilliams, 1996; Large et al., 1997; Willebrand et al., 2001; Deacu and Myers, 2005). For regional process studies, a new trend is towards limited domain models with open boundary conditions permitting exchanges with the surrounding oceans (Redler and Boning, 1997; Myers, 2002). Regional models of the eastern North Atlantic, North Atlantic, as well as the South Atlantic have recently been developed and shown to reproduce the main features of the circulation (Penduff et al., 2000, 2001; Treguier et al., 2001; Willebrand et al., 2001).

Myers (2002) developed a regional eddy-permitting sub-polar ocean model configuration (SPOM) with an open southern boundary and restoring surface boundary conditions. Extensive experiments (Myers and Deacu, 2003; Deacu and Myers, 2005) suggested that with improved representation of topographic and sub-grid scale eddy parameterizations, the model is capable of accurately simulating many aspects of the circulation and hydrography in the sub-polar gyre, although limitations remain (see Myers, 2002; Myers and Deacu, 2003). It is therefore expected that the model will provide a good base for simulations using flux forcing. The focus in this chapter is to show that a regional ocean general circulation model (OGCM) can be stably run under flux forcing for many decades, while highlighting some relevant issues. Following

a brief description of the model in section 2.2, section 2.3 introduces the parameterization of surface fluxes and the associated experiment design. The model behavior is examined in section 2.4. Finally, a summary and discussion are given in section 2.5.

2.2 A brief description of the model

SPOM is a regional configuration of the Modular Ocean Model-Array (MOMA) set up specifically for process and sensitivity studies of ocean variability questions in the sub-polar North Atlantic. The original model formulation is based on a Bryan-Cox-Semtner type ocean general circulation model using the inviscid version of the Killworth et al. (1991) free surface scheme. The biharmonic horizontal viscosity coefficient is $A_h = 7.5 \times 10^{18} \text{ cm}^4 \text{ s}^{-1}$ and the horizontal diffusion coefficient is $K_h = 7.5 \times 10^{18} \text{ cm}^4 \text{ s}^{-1}$. The vertical viscosity is $A_v = 1.5 \text{ cm}^2 \text{ s}^{-1}$ and the vertical diffusion is $K_v = 0.3 \text{ cm}^2 \text{ s}^{-1}$. Convective adjustment is performed using the complete convection scheme of Rahmstorf (1993). The effect of eddies not resolved by the model's $1/3^\circ$ resolution is parameterized by the Gent and McWilliams eddy parameterization scheme (Gent and McWilliams, 1990), using a constant eddy transfer coefficient $2.0 \times 10^5 \text{ cm}^2 \text{ s}^{-1}$.

Zonal boundaries are set at $68^\circ W$ and Greenwich, 0° . The open southern boundary is set at $38^\circ N$, while the closed northern boundary is set at $70^\circ N$ with restoring buffers in Hudson Strait, Baffin Bay and the region to the north of the Iceland. The model z-coordinate has 36 vertical layers, unevenly spaced, with finer resolution in the upper

water column. A partial cell finite-volume technique (Adcroft et al., 1997) is applied to better represent the topography, which is taken from the $1/12^\circ$ ETOPO5 (NOAA, 1988) dataset, linearly interpolated to the model's $1/3^\circ$ resolution. The interpolated depths are used other than ensuring no partially filled level has less than 10 m of water in it. Further details about the model can be found in Myers (2002).

2.3 Surface boundary conditions and experiment design

2.3.1 Restoring control experiment

Our restoring control experiment is taken from Myers (2002). As discussed in that paper, the surface temperature and salinity are relaxed towards the monthly data, taken from the NODC (1994) dataset, with the forcing repeating each year. The relaxation timescale is essentially clamped, with a 2-hour timescale, acting on the top surface layer. The reasoning for such a short restoring timescale is given in Myers (2002).

2.3.2 Forcing Data

The buoyancy (heat and freshwater) forcing is taken from two different monthly climatologies. The first of these originates from ship/buoy measurements of the Southampton Oceanography Center (Josey et al., 1998) - which we refer to as the original SOC climatology. The $1^\circ \times 1^\circ$ climatology has been calculated using ship

meteorological reports contained in the COADS1a dataset (Woodruff et al., 1993), which covers the period 1980 ~ 1993, blended with additional metadata describing observational procedure (height of observing platforms etc.) from the WMO47 list of ships (WMO, 1994), which allows corrections to be made for various observational biases. One deficiency of the original SOC climatology is a global heat flux bias of 30 Wm^{-2} (Josey et al., 1999). To deal with this issue, Grist and Josey (2003) use a linear inverse analysis based upon 10 hydrographic ocean heat transport constraints to reduce the heat flux bias to -2 Wm^{-2} . We will refer to this version as the adjusted SOC climatology. We also use the reanalysis data of the National Centers for Environmental Prediction (NCEP)-National Center for Atmospheric Research (NCAR). This reanalysis data ($2.5^\circ \times 2.5^\circ$), stems from the numerical atmospheric modelling and data assimilation systems (Kalnay et al., 1996), and are based on a long time series (1958 ~ 1998). We will refer to this data as the NCEP climatology.

In both cases, we use the climatological monthly means, repeated as a perpetual year. The net heat flux is a sum of the climatological long wave radiation, net solar radiation, latent and sensible heat fluxes. Precipitation is taken directly from the climatologies while evaporation is calculated by dividing the latent heat flux by the latent heat of vaporization L . To ensure consistency, the SOC formula

$L = 10^6[2.501 - 0.00237(T_s - 273.16)]$ (Josey et al., 1998) is used for the NCEP data as well, where T_s is SST and coefficients 2.501, 0.00237 and 273.16 are obtained from Stull (1988). We also note that we apply the E-P (evaporation E minus precipitation

P) as a virtual salt flux, whereby the amount of salt in the model upper layer is changed rather than actually adding or removing freshwater, i.e. a volume change of the model's free surface.

Two wind stress climatologies are used. One, based on NCEP data, is consistent with the buoyancy fluxes described above. The other is from the European Center for Medium Range Weather Forecast (ECMWF). Assembled by Trenberth et al. (1990) for the period 1980 ~ 1986, it has been shown to give a good representation of LSW formation and dispersal in SPOM (Myers, 2003). Note that we do not use SOC wind stress since there is no data over the area with sea ice cover.

2.3.3 Sub-polar North Atlantic SOC-NCEP flux comparison

The wintertime (DJF) heat fluxes from the two climatologies (original SOC, NCEP) and the differences between them are shown in Figure 2.1. Both show strong wintertime heat loss throughout the sub-polar gyre, with the strongest losses along the pathway of the North Atlantic Current (NAC), in the Labrador Sea and off Iceland. The overall model domain heat loss is larger in NCEP, with the wintertime mean (DJF) being -173 Wm^{-2} and the annual mean -30 Wm^{-2} , as compared to -150 Wm^{-2} and -24 Wm^{-2} in original SOC. The overestimation of heat loss in NCEP data has been documented by a number of studies (Smith et al., 2001; Zeng et al., 1998), focused on the areas with large air-sea temperature difference and high wind speed, such as the Labrador Sea, the Norwegian Sea and the Gulf Stream (Ren-

frew et al., 2002; Moore and Renfrew, 2002). The adjusted SOC climatology provides enhanced heat loss over our domain, -201 Wm^{-2} and -57 Wm^{-2} for wintertime and annual means respectively, even stronger than the NCEP climatology. Differences between this field and the original SOC field can be seen in Figure 3c of Grist and Josey (2003).

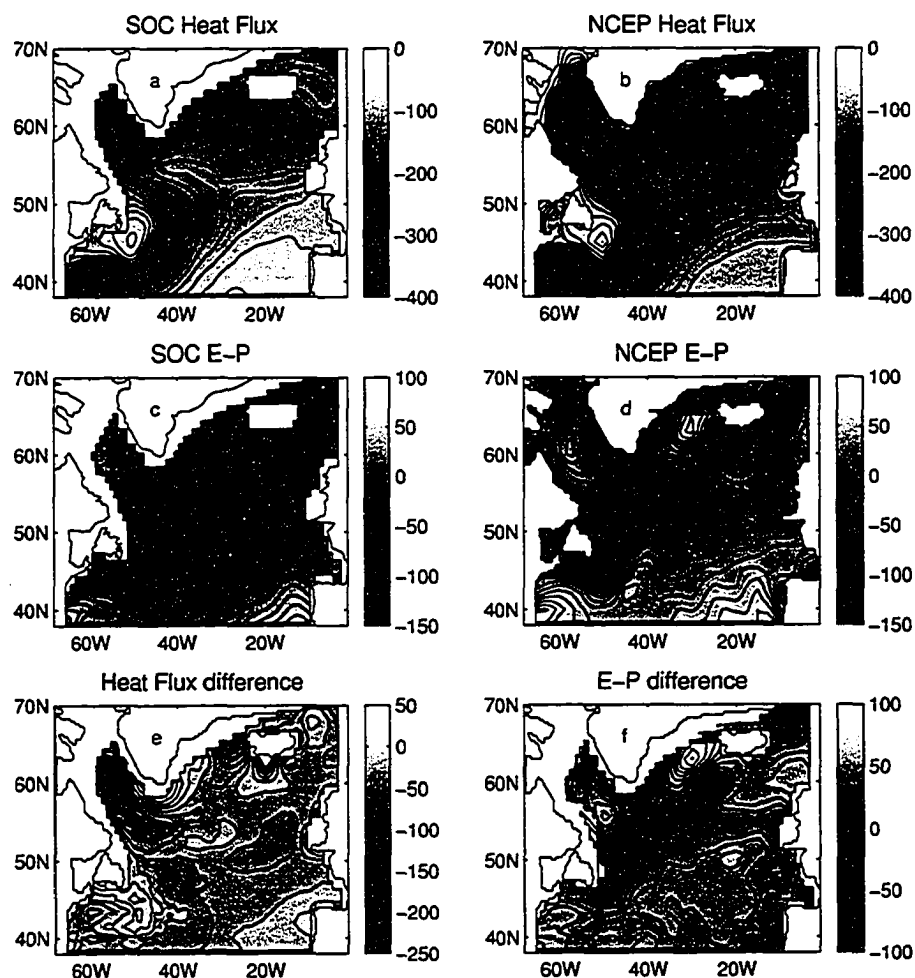


Figure 2.1: Heat fluxes averaged over Dec.-Feb. (unit: Wm^{-2}) for a) original SOC and b) NCEP; annual mean E minus P (unit: cm yr^{-1}) for c) original SOC and d) NCEP and the difference of NCEP minus original SOC for e) heat flux (unit: Wm^{-2}) and f) E minus P (unit: cm yr^{-1}). Some blank regions along Greenland and Labrador coasts indicate missing data in original SOC climatology due to sea ice.

The annual E-P fields from the climatologies and their difference are also given in Figure 2.1. Both give net excess precipitation with annual means of -30.8 cmyr^{-1} for original SOC and -2.7 cmyr^{-1} for NCEP over model domain. Josey and Marsh (2005) noted a large area of net evaporation south of about $45 \sim 50^\circ N$, as well as localized regions of net evaporation north of $50^\circ N$ in NCEP, with the most notable one appearing over the Irminger Sea (similar to Figure 2.1d). In contrast, the border between net precipitation and net evaporation is shifted further south in original SOC, effectively out of our model domain (Figure 2.1c). The discrepancy between NCEP and original SOC likely ascribes to E being much stronger in NCEP than SOC owing to the use of a stronger transfer coefficient for the latent heat. Despite the different time periods the two climatologies are built over, we note the differences are not temporal. If we compute the net excess precipitation over our domain in NCEP based on 1980 \sim 1993, the years considered by the original SOC climatology, we calculate -2.5 cmyr^{-1} .

2.3.4 Modifications

A number of additional modifications were then made so that we could use these climatological fields to successfully force the ocean model. As the use of linearly interpolated monthly means underestimates the actual monthly buoyancy means, we follow Killworth (1996) to remove this bias by multiplying the buoyancy fluxes by 1.4, making them closer to the observations.

Deep convection in the Labrador Sea is a “plumes” scale event (Marshall and Schott, 1999), triggered by intensive heat loss. This strong surface forcing may be caused by the passing of meso- or synoptic scale systems, which contributes significant high-frequency variability in the buoyancy fluxes and is not resolved by monthly means (Moore et al., 1996; Rasmussen et al., 1996; Sathiyamoorthy and Moore, 2002). For example, an instantaneous sensible heat flux of about 750 Wm^{-2} was deduced when a convective event was observed during March 1976. Heat fluxes exceeding 650 Wm^{-2} were reported during the winter of 1997 (Renfrew et al., 2002). Extreme values in the wintertime heat flux, up to 1500 Wm^{-2} , were seen during the 1990s in the Labrador Sea (discussed by Sathiyamoorthy and Moore, 2002). However, the monthly mean sensible heat flux during winter months found by Smith and Dobson (1984) is around 100 Wm^{-2} (discussed by Sathiyamoorthy and Moore, 2002).

We thus crudely parameterize the effect of this unresolved high frequency variability in the heat flux by increasing the heat flux over the potential model convective region ($55 \sim 59^\circ N$ and $51 \sim 56^\circ W$) during winter months (Nov.-Mar.). The heat fluxes are increased 5-fold for the original SOC data and 3-fold for NCEP data. This reflects that the triggering mechanism for oceanic convection is probably related to the high frequency portion of heat loss, rather than the monthly means. Consequently, the maximum monthly heat losses are 1074 Wm^{-2} for the original SOC data and 1170 Wm^{-2} for NCEP data, comparable to an observational maximum of 1500 Wm^{-2} (discussed by Sathiyamoorthy and Moore, 2002). As such, winter (DJF)

averaged heat loss is 968 Wm^{-2} for original SOC and 1099 Wm^{-2} for the NCEP. If this adjustment is not used, the model mixed layer depths are too shallow in the Labrador Sea and LSW formation is severely curtailed.

Formally, the surface freshwater flux term includes a runoff component not directly present in the data we use to force the model. We parameterize this effect as an additional “precipitation” term in the coastal regions of Greenland and Canada based on observational data, modifying the original SOC fluxes. However, since the provision of additional runoff is small, equivalent to 5.7 mSv from the Labrador Coast and 1.4 mSv from the north coast of Newfoundland, which had negligible effect on our results, we did not use this simplified river parameterization in the NCEP experiments.

The model lacks a sea-ice component. Without an explicit representation of the freshwater processes associated with sea-ice drift and melt, it was found that the model salinities drifted unacceptably. Therefore, a 30-day restoring term is added to the surface salinity to reduce this drift.

Finally, both versions of the SOC dataset lack data for areas that are ice-covered in winter due to its origin in ship and buoy based observations. E-P was set to zero in these regions. However, this choice could not be made for the heat fluxes. Sea ice is not a perfect heat insulator and if no heat flux was applied in these regions (which are often not completely ice covered, especially considering the coarse resolution of the atmospheric data), an unacceptable model drift in temperature was observed. Thus,

a flux equals to 0.67 of the domain averaged heat flux (for a given month) was applied in these areas since it produces the best water mass properties from our extensive experiments.

2.3.5 Experiment Design

A number of experiments were performed and those discussed in this chapter are summarized in Table 2.1. Our baseline for comparing the model results will be the experiment of Myers (2002) using restoring boundary conditions (which was run for 40 years), here called RES. We then ran the model for 80 years under each of the two climatologies (original SOC, NCEP), as experiments SOC1 and NCEP1. A third experiment, to attempt to disentangle the relative importance of the buoyancy and momentum forcing was run using NCEP buoyancy forcing and ECMWF momentum forcing. This experiment, NCEP2, was integrated for the base 80 years, and then for an additional 40 years to assist with its understanding. SOC2 is a similar experiment as SOC1 but with the adjusted SOC, integrated for 40 years.

Table 2.1: Summary of experiments reported in this chapter

Names	Buoyancy fluxes	Labrador Sea convection region heat flux increase	Momentum forcing
RES	Relaxation to climatology		ECMWF
SOC1	Original SOC	×5	ECMWF
SOC2	Adjusted SOC	×5	ECMWF
NCEP1	NCEP	×3	NCEP
NCEP2	NCEP	×3	ECMWF

2.4 Model results

2.4.1 Model stability

Basin averaged temperatures and salinities are shown in Figure 2.2 for the first 40 years of integration for several experiments. After an adjustment from the initial conditions, a quasi-equilibrium is approached by year 23. Over the last 10 years of integration (years 71 ~ 80), the basin averaged temperature and salinity only change by $-0.0015\text{ }^{\circ}\text{C}$ and $-0.0004\text{ }psu$ for SOC1, $0.0184\text{ }^{\circ}\text{C}$ and $0.0008\text{ }psu$ for NCEP1. The adjustment to equilibrium is slower under flux forcing. Although the model properties have drifted away from the observationally based initial conditions, they are in line with many other models of the sub-polar gyre. Treguier et al. (2005) reported the LSW with unrealistic high salinity in a series of high resolution ocean models they assessed.

The amplitudes of the annual cycles in basin- and top 200 m- averaged temperatures have increased by 42% and 55% for SOC1, and 62% and 76% for NCEP1 respectively compared to RES. This is produced by the flux surface boundary conditions. The annual salinity amplitudes (top 200 m) in SOC1 ($0.026\text{ }psu$) and NCEP1 ($0.018\text{ }psu$) are only a 1/3 of that from Levitus climatology ($0.068\text{ }psu$) while the annual temperature amplitudes ($2.00\text{ }^{\circ}\text{C}$ in SOC1 and $2.26\text{ }^{\circ}\text{C}$ in NCEP1) are relatively close to the observation ($1.59\text{ }^{\circ}\text{C}$).

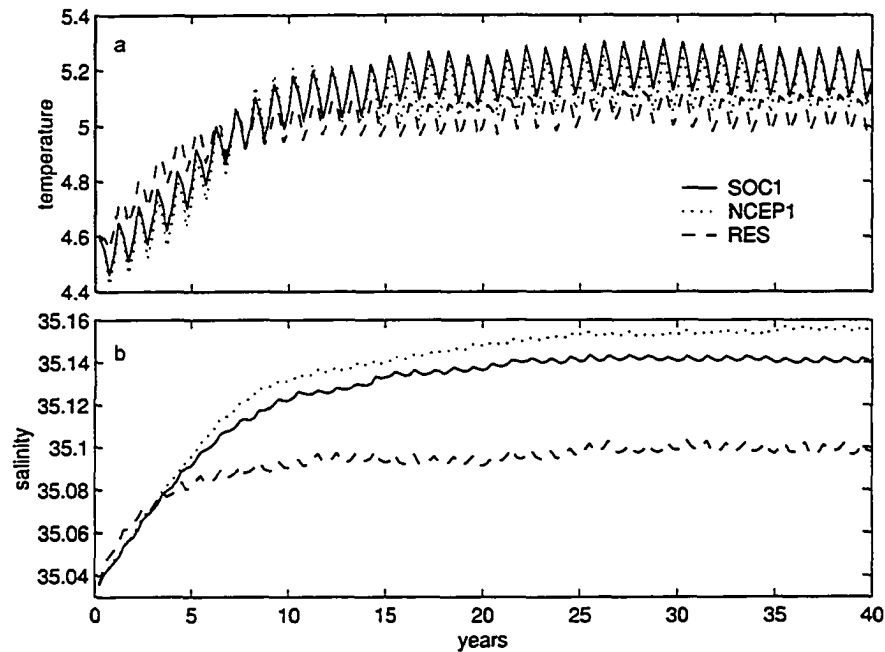


Figure 2.2: Time series of a) temperature ($^{\circ}\text{C}$) and b) salinity (psu) for experiments SOC1, NCEP1 and RES, averaged over the entire model domain

2.4.2 Experiment SOC1

The large-scale structure of the sub-polar gyre in SOC1 is very similar to that in RES, but with a few significant differences (Figure 2.3). The unrealistic anti-cyclonic inflow to the interior of the Labrador Sea found in RES is stronger and more energetic despite the eastward branch of the NAC also being intensified. The Labrador Sea counter-current is intensified, with significant flow into the Irminger Basin, weakening the IC, as well as the flow along the Reykjanes Ridges.

The depth-integrated freshwater content in the central Labrador Sea region (boxed area in Figure 2.4a) averaged over years 37 ~ 40, relative to a salinity of 35.0, is $-2.84 \times 10^{12} \text{ m}^3$, much less than $5.13 \times 10^{12} \text{ m}^3$ in RES averaged over last 4 years

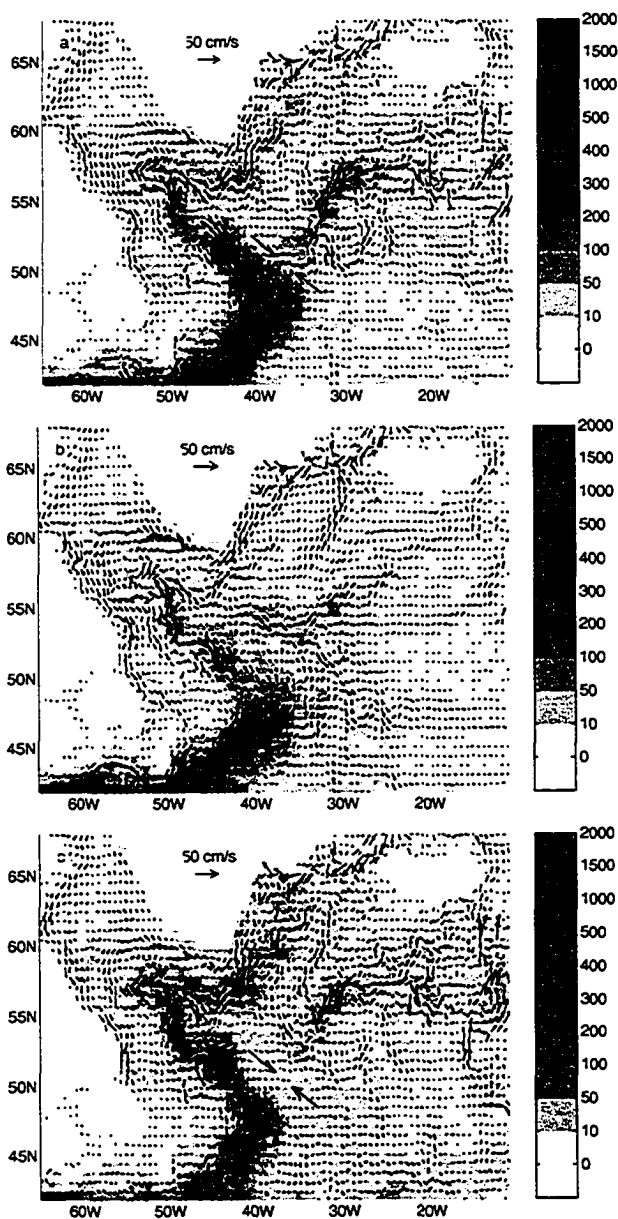


Figure 2.3: Annual current fields (arrows) and EKE fields (cm^2s^{-2}) (gray scale) at 52.5 m (3rd model level) averaged over years 37 ~ 40 for (a) SOC1; (b) RES; (c) NCEP1. Every second vector is plotted.

of integration. Both are a significant drop from an initial value of $1.30 \times 10^{13} \text{ m}^3$ (NODC climatology). Although a reduced freshwater import through a too salty East Greenland Current (EGC) plays a role in the salinification, the main component of the drift is driven by a strong salt import from the south, with the unrealistic NAC inflow to the Labrador Sea. Myers and Deacu (2003) examined the NAC inflow to the Labrador Sea in RES. They suggested that this current was accelerated by a strong rectification process with the conversion of eddy kinetic energy (EKE) to mean kinetic energy (MKE). Our results suggest this process is occurring here, with the enhanced amplitude of the inflow in this experiment related to a significant increase in the conversion of EKE to MKE ($1.6531 \times 10^{-4} \text{ cm}^2\text{s}^{-2}$ in SOC1 versus $5.7688 \times 10^{-5} \text{ cm}^2\text{s}^{-2}$ in RES, averaged over our central Labrador Sea box). Moreover, the higher EKEs around the “Northwest Corner” (near 51°N 43°W where the NAC takes a 90° turn to the right - first defined by Worthington (1976); it scatters a bit far to the east in the model) ($300 \sim 400 \text{ cm}^2\text{s}^{-2}$ in SOC1) are closer to the satellite-tracked surface drifter observations ($500 \sim 1000 \text{ cm}^2\text{s}^{-2}$) (Fratantoni, 2001; Cuny et al., 2002), in comparison with RES ($100 \sim 200 \text{ cm}^2\text{s}^{-2}$).

Another change compared to RES is seen in the sub-polar mode waters (SPMWs), a series of thick layers of low stability waters (McCartney and Talley, 1982) formed locally (associated with topography) by vertically deep mixing due to intensive heat loss to the atmosphere in the sub-polar gyre (Talley, 1999), with a density scope of 26.9 to 27.75 (Hanawa and Talley, 2001). Figure 2.4a illustrates the annual mean

potential vorticity (PV) field, given by $q = \pm \frac{f}{\rho} \frac{\partial \rho}{\partial z}$ (relative vorticity ignored), mapped on $\sigma_0 = 27.6$ averaged over years 37 ~ 40, which effectively signals the formation sites of this density of the SPMW. Comparing with RES (Figure 9 in Myers, 2002), SOC1 gives us a better representation of the water formation on the above isopycnal, with formation along the outcropping edge of the isopycnals (Irminger Basin, the Reykjanes Ridge and Iceland-Scotland Ridge), following the cyclonic circulation around the northern edge of the gyre (Talley, 1999).

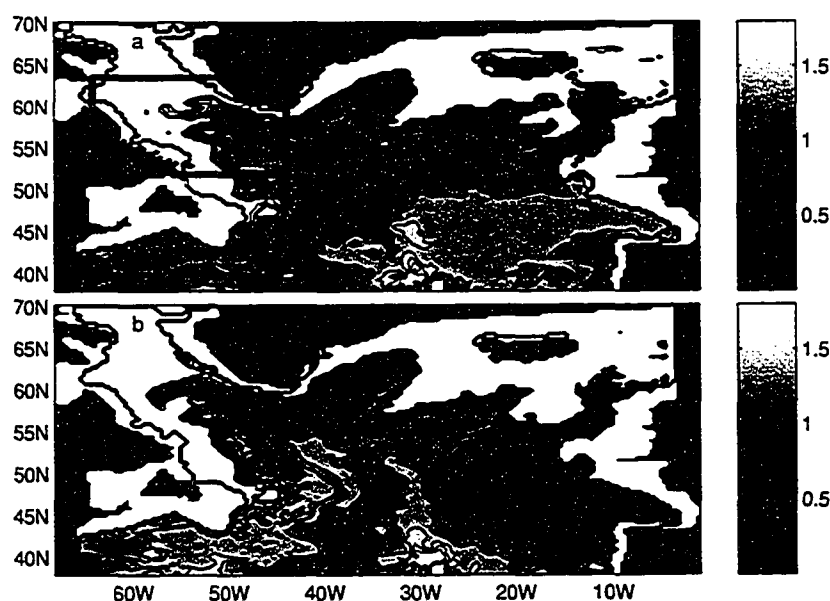


Figure 2.4: Annually-averaged PV over years 37 ~ 40 on $\sigma_0 = 27.6$ for a) SOC1 and b) NCEP1. Contour intervals are in $0.2 \times 10^{-10} m^{-1} s^{-1}$ but no value larger than $2.0 \times 10^{-10} m^{-1} s^{-1}$ is contoured. The small box indicates the central Labrador Sea region discussed in our analysis.

The LSW formed in the Labrador Sea by winter deep convection is characterized by cold, fresh properties (Table 2.2) and a weak vertical density gradient. Deep convection has mainly been observed in the western interior of the basin, with an

average depth of 1500 m (Table 2.2). SOC1 produces the LSW with reasonable density, convective depth and location, but with high temperature and salinity (Table 2.2) due to the entrainment of excess warm and saline water advected into this region through the NAC, as mentioned previously in this section. Potentially unrealistic deep convection nevertheless appeared in the Irminger Sea (not shown) due to a local surface flux maximum. In contrast, RES produces unrealistic deep convection to the southwest of Greenland, attributable to unrealistically warm model EGC water and the subsequent heat loss derived from the restoring boundary conditions, although the properties of the model LSW are otherwise good (Table 2.2, see also Myers (2002)).

Table 2.2: Properties of the LSW in March of 40th year (1: Averaged over years 37 ~ 40; 2: Clarke and Gascard (1983); Wallace and Lazier (1988); Lilly et al. (1999); http://www.mar.dfo-mpo.gc.ca/science/ocean/woce/labsea/labsea_poster.html; 3: Levitus climatology)

	Location of convection	Depth (m)	σ_θ	T(°C)	S(psu)	Annual mean ¹ over central Labrador Sea box	
						T(°C)	S(psu)
SOC1	58.5°N 52 ~ 53°W	1500	27.78	3.8	35.02	4.3	35.03
NCEP1	57.8°N 52 ~ 53°W	1650	27.82	3.9	35.03	4.4	35.06
RES	58.3 ~ 59°N 57°W, 48°W	1500, 1700 ~	27.77	2.8	34.88	3.7	34.93
OBSERVATION (winter) ²	56 ~ 58°N 52 ~ 55°W	1500	27.74	2.75	34.83	3.2 ³	34.86 ³
			~ 27.81	~ 3.65	~ 34.91		

2.4.3 Experiment NCEP1

Several major differences stand out between SOC1 and NCEP1 (Figure 2.3). In NCEP1, the offshore and shelf branches of the Labrador Current do not merge, as in

SOC1 (and in reality), and the shelf branch is purely fed by the Baffin Island Current. This is related to NCEP wind stresses, which are weaker, and more zonal than the ECMWF stresses in winter (Figure 3 in Myers, 2003).

The NAC is generally thought to follow the steep topography of the western boundary in NNE direction from the Southeast Newfoundland Ridge (around $40^{\circ}N$, $45^{\circ}W$) to Flemish Cap ($47^{\circ}N$, $45^{\circ}W$), turn northwest into the “Northwest Corner”, then shift sharply towards the east around $50 \sim 52^{\circ}N$, and finally become a weaker, more diffusive eastward flow (discussed by Luo et al., 2003). In NCEP1, the NAC is more meridional entering the model domain east of $50^{\circ}W$ and then anomalously penetrates northwest into the Labrador Sea, not turning eastward after reaching the “Northwest Corner”. This northward current then winds northeast toward Irminger Sea. The NAC portion east of $36^{\circ}W$ is fed instead by southward flow west of Reykjanes Ridge (Figure 2.3c). The connection between the “Northwest Corner” and the NAC in the eastern basin basically breaks (indicated by a pair of arrows in Figure 2.3c). The response to this anomalous NAC path is a greater inflow of salinity into the Labrador Sea and a further reduction in freshwater content ($-5.36 \times 10^{12} m^3$). The anomalous NAC path is accompanied by enhanced eddy activities (with EKEs of $300 \sim 400 cm^2s^{-2}$ between 52 to $57^{\circ}N$, higher than the $100 \sim 300 cm^2s^{-2}$ from observations - Fratantoni (2001); Cuny et al. (2002)).

Higher surface salinities lead to enhanced deep convection in the Labrador Sea (Table 2.2). We also note deep-reaching, potentially unrealistic vertical mixing (up

to 1300 m) occurring west of the Bay of Biscay and south of Rockall Plateau/Trough (Figure 2.4). The salinity distributions (not shown) on the $\sigma_0 = 27.6$ surface demonstrate that this newly-formed water mass then disperses southeastward. More intensive wintertime heat losses in the NCEP fluxes in this region are responsible. Once initiated, this water mass formation remains a stable feature of the model integration.

Renfrew et al. (2002) suggested that NCEP surface fluxes would be inappropriate in driving ocean models due to an overestimation of the turbulent fluxes in high wind regions, such as the Labrador Sea. Our results seem to show more extensive drawbacks of using the NCEP fluxes to drive an ocean model of the sub-polar gyre.

2.4.4 A diagnosis of two modes of circulation in NCEP2

NCEP2 has same buoyancy forcing as NCEP1 and the same momentum forcing as SOC1. This experiment might be more suitable to be thought as an idealized experiment in a sense that buoyancy and momentum forcings are produced from different time periods and sources with a possibility of being inconsistent with each other. This is however a common option with the availability of the flux data. An analysis of the basin averaged quantities unexpectedly revealed an abrupt increase in both the temperature and salinity around year 34 (following a quasi-equilibrium that developed after the initial spin-up). That the new equilibrium was stable was verified by extending the integration to 120 years (Figure 2.5). These two states correspond to two modes of circulation.

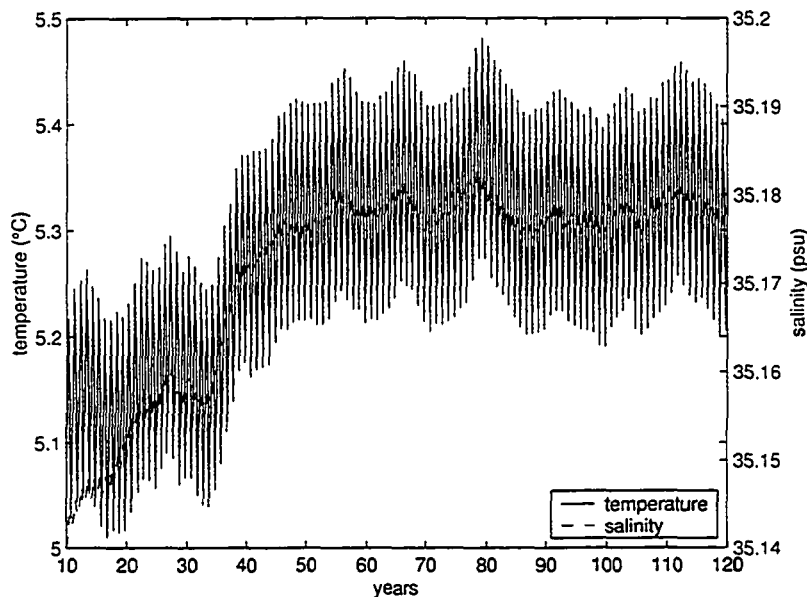


Figure 2.5: Time series of temperature ($^{\circ}C$) and salinity (psu) averaged over the entire model domain in NCEP2

As in NCEP1 (Figure 2.4b), we note deep SPMW formation west of the Bay of Biscay, reaching up to 1350 m by the 34th year (Figure 2.6a), 50 m deeper than in NCEP1 due to probably stronger Ekman pumping from the ECMWF wind stress during winter (see Myers, 2003, Fig3a, b for wind stress comparison). As in NCEP1, the depth of this feature increases through the initial phase of the model integration and is related to the “strong” NCEP heat loss in this region. Following the 34th year of integration, the depth of convection in the eastern region rapidly decreases. By year 80, intermediate depth convection here has completely ceased (Figure 2.6b). Mixed layer depths in this region are now in the 800 ~ 900 m range. This pattern in mixed layer depth is consistent with the changes in heat content over the upper layer (0 ~ 915 m) in this region (Figure 2.7). Heat content is defined as $H = c_p \rho_0 \int_V (T - T_r) dV$,

where c_p is the specific heat capacity of water, ρ_0 the reference density, 1028 kgm^{-3} , T_r a reference temperature (0°C), T the model temperature and V the volume. The initial decrease in heat content implies cumulative surface cooling and hence the deepening of the vertical mixing. The similar evolution pattern as for the time series of domain-averaged temperature after spin-up (Figure 2.5) suggests that the shift in domain-averaged temperature may be caused by the shift in heat content in the eastern basin. A corresponding shift in LSW volume on $\sigma_0 = 27.74 \sim 27.8$ (Figure 2.7) also shows the two circulation modes, with a positive response to the collapse in water mass formation in the eastern basin, with a lag of 2 yrs (albeit with significant interannual variability later in the integration).

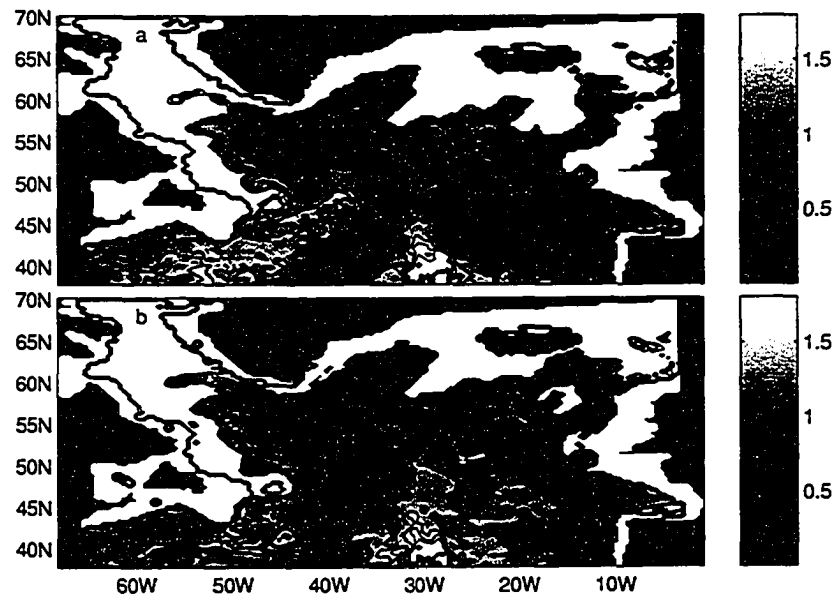


Figure 2.6: Annually-averaged PV on $\sigma_0 = 27.6$ in NCEP2, a) for the 34th year and b) the 80th year. Contour intervals are in $0.2 \times 10^{-10} \text{ m}^{-1} \text{ s}^{-1}$ but no value larger than $2.0 \times 10^{-10} \text{ m}^{-1} \text{ s}^{-1}$ is contoured.

The changes in heat content in this eastern water formation region (Figure 2.7)

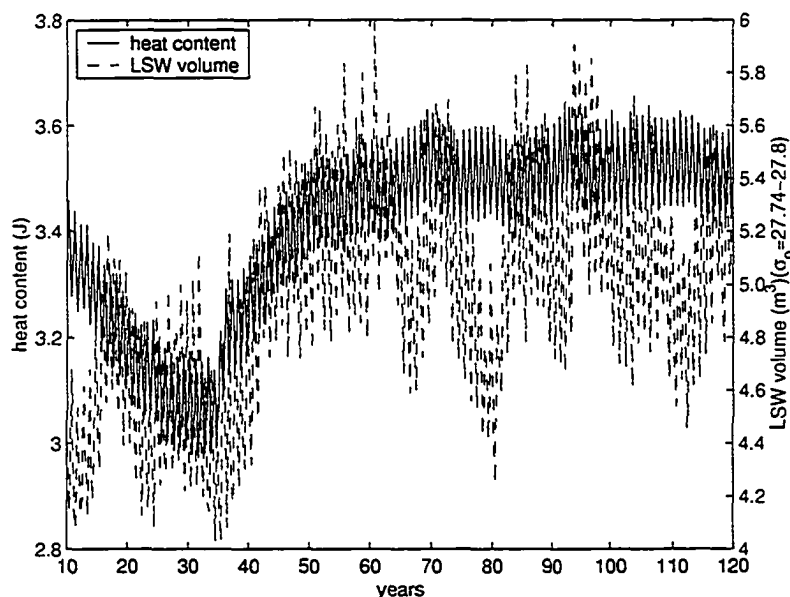


Figure 2.7: A time series of heat content over eastern basin convection region ($43 \sim 52^\circ N$, $12 \sim 24^\circ W$), from the surface to 915 m, and LSW volume ($\sigma_0 = 27.74 \sim 27.8$) over the central Labrador Sea region in NCEP2.

are closely linked to changes in the net inflow of heat to this region through its lateral boundaries. A calculation of total surface heat flux in this region shows an annual mean heat loss of $0.0173 PW$. For an equilibrium to be reached, this must be balanced by the lateral heat fluxes. In NCEP1, a balance in this region is quickly reached (Figure 2.8a), with the main source of heat being a large positive component by the Ekman flux (Figure 2.8b). However in NCEP2, the net lateral heat influx (Figure 2.8a) is not enough to offset the surface heat loss since the different ECMWF wind stress leads to a situation where the net Ekman flux is negligible for this region (heat export almost offsets import) - Figure 2.8b, although non-Ekman component contributes a positive value. Thus, this region rapidly cools, which then drives deep

convection. This situation then excites a spike in positive net non-Ekman heat inflow (Figure 2.8c) around year 35, composed mostly of advective heat flux, leading to a sudden increase in temperature (or heat storage) in this eastern region and a capping of convection. With the cessation of eastern basin convection, the NAC pathway adjusts. No longer is the pathway “broken”, with basically the entire flow into the Labrador Sea, and then Irminger Sea. In year 35 (Figure 2.9a) an eastward branch of the NAC is formed through a bifurcation of the flow as it enters the Irminger Basin, and by year 80 (Figure 2.9b) an eastward branch of the NAC is reestablished in the “Northwest Corner” region (although too much flow is still advected into the Labrador Sea). This transition in NAC pathway is accompanied by temperature changes, with a reduction in the Labrador Sea at 80th year and an increase along the NAC pathway. The excess heat into our domain is provided by an increase in the import of heat through the southern open boundary. As a result, the deep-reaching convection driven by intensive heat loss and high net evaporation (high salinity) west of the Bay of Biscay is eroded by internal advective processes, triggered by the Ekman heat transport.

2.4.5 Adjusted SOC

The model was integrated for 40 years under the adjusted SOC Fluxes which we have further modified as described earlier (Table 2.1). The adjustments, based on the hydrographic constraints to balance the global budget, lead to increased annual

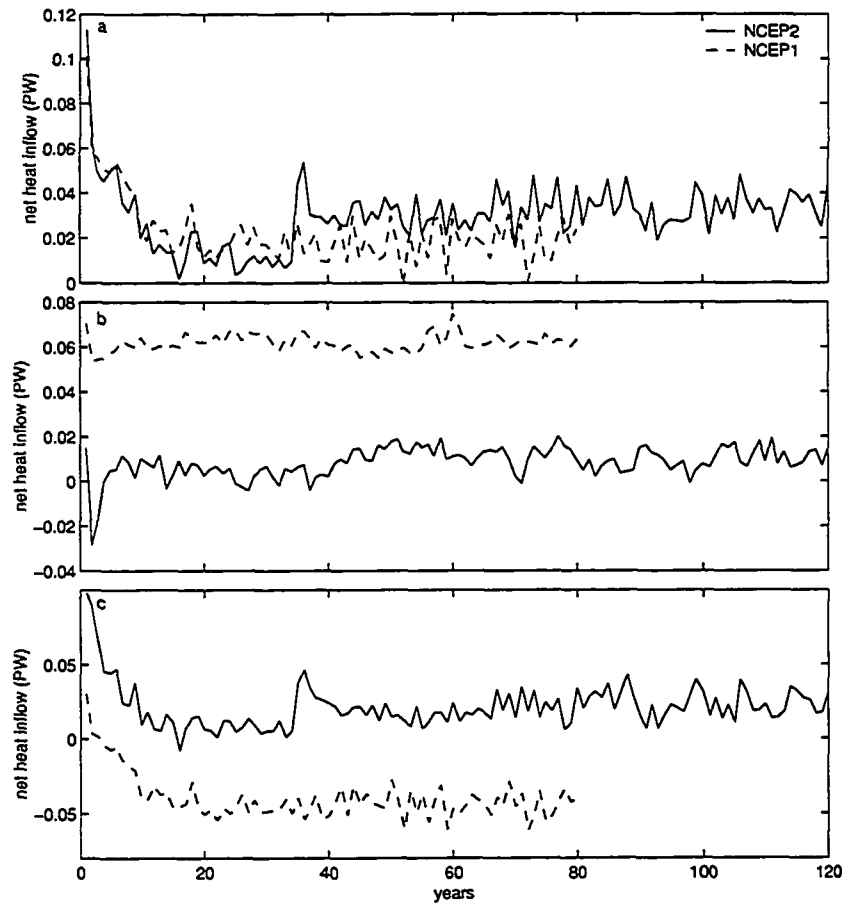


Figure 2.8: Annual a) net heat inflow b) net Ekman heat inflow c) non-Ekman heat inflow (a)-b) through four lateral faces of eastern region ($43 \sim 52^{\circ}N$, $12 \sim 24^{\circ}W$) for whole water column in NCEP1 and NCEP2 (units: PW).

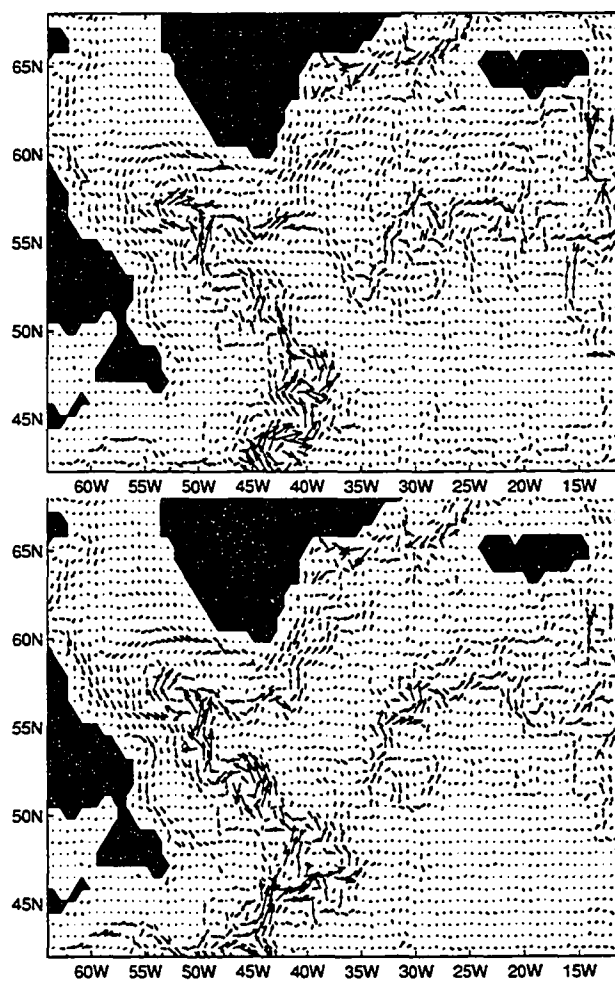


Figure 2.9: Annually-averaged currents at a depth of 52.5 m for NCEP2 in a) the 35th year and b) the 80th year. Every second vector is plotted

mean heat losses everywhere in the model domain in the adjusted climatology. These increases range from 50 Wm^{-2} over the NAC pathway leading into the “Northwest Corner”, to 25 Wm^{-2} over the central Labrador Sea, to $20 \sim 25 \text{ Wm}^{-2}$ over most of the eastern basin.

As might be expected, the enhanced cooling leads to an increase in wintertime mixed layer depths and water formation throughout the model domain. The increased surface heat loss leads to an enhancement of convection in the Labrador Sea, with Labrador Sea water being formed with densities reaching 27.85 (although maximum mixed layer depth over the last 20 years of the simulation is only 1600 m).

The stronger wintertime surface fluxes over the eastern half of the basin lead to an almost complete turn over of the upper 1000 to 1500 m in the eastern part of the Irminger Basin, the Iceland Basin, Rockall Trough and the eastern basin north of 45°N . Densities reach up to 27.78 to the east of Reykjanes Ridge in the western Iceland Basin. These changes are consistent with the analysis of Grist and Josey (2003) who have already noted on the basis of buoy comparisons that the adjusted fluxes are likely to overestimate the heat loss in the eastern basin.

2.5 Summary and discussion

Experiments to examine oceanic variability and climate system change in ocean-only models are often more robust when surface flux forcing is used rather than restoring boundary conditions. We have therefore examined the use of surface flux

forcing in a regional eddy-permitting ocean model of the sub-polar North Atlantic. Our flux forcings originate from original SOC and NCEP monthly climatologies with the addition of crude parameterization of the high frequency portion of heat forcing, so that the model produces sufficient LSW. With the existence of a weak restoring term on salinity, the model remains stable through long decadal integrations although a switch in circulation mode appears in one experiment.

Overall, SOC1 is our most robust experiment with all major features of the sub-polar gyre being represented. Improvements are seen in SPMW formation and dispersal, as well as model eddy kinetic energy fields, with respect to an equivalent run with restoring conditions. The structure of the surface fluxes however leads to potentially unrealistic deep convection in the Irminger Sea, with this situation exacerbated with the hydrographically adjusted SOC fluxes. The drifts in temperature and salinity, seen in most high-resolution models of the sub-polar gyre, appear in all experiments. They seem to be dominated by internal advective processes although surface forcing may indirectly play a role by triggering deep convection and lead to a compensation of surface advection.

Excess heat loss in winter and relative large net evaporation (hence high salinity) in the eastern Atlantic in the NCEP reanalysis lead to potentially unrealistic SPMW formation west of the Bay of Biscay although some mixed layer climatologies (e.g. Kara et al., 2000) suggest mixed layer depths upwards of 600 m in this region. With NCEP wind stress applied (NCEP1), an anomalous NAC penetrates into the

Labrador Sea (does not turn eastward from “Northeast Corner”). This results in deep eastern basin SPMW formation. When replaced by ECMWF wind stress (NCEP2), the eastward NAC path gradually recovers and strengthens, accompanied by more eastward heat transport. As it does so, the deep SPMW formation in the eastern basin fades away, followed by a deepening of the LSW due to a reduction in heat content in the Labrador Sea. Thus a second mode of circulation is achieved in this experiment.

Hansen and Bezdek (1996) depict a preferred propagating pathway of an anomalous warm event in the North Atlantic, developed west of the sub-tropical gyre (Sutton and Allen, 1997). This SST anomaly moved north-westward from south of Newfoundland in 1951 and arrived at the Labrador Sea in 1953 before heading northeast and entering eastern basin (in their Figure 4). This propagation pathway is surprisingly coincident with the transition in our NAC path and heat transport in NCEP2. Bersch (2002) related this event to the shift of NAO phase from positive to negative value. Further work is needed to clarify this point.

Acknowledgements:

This work is part of PhD thesis of Duo Yang and was supported by CFCAS and NSERC grants awarded to Paul Myers. We would like also to acknowledge Daniel Deacu for his generous contribution of a Fortran code.

References

- Adcroft, A., C. Hill, and J. Marshall, 1997: Representation of topography by shaved cell in a height coordinate ocean model. *Mon. Weather Rev.*, **125**, 2293–2315.
- Barnier, B., L. Siefridt, and P. Marchesiello, 1995: Thermal forcing for a global ocean circulation model using a three-year climatology of ECMWF analyses. *J. Mar. Res.*, **6**, 363–380.
- Bersch, M., 2002: North Atlantic Oscillation-induced changes of the upper layer circulation in the North Atlantic Ocean. *J. Geophys. Res.*, **107**, 20–1–20–11.
- Boning, C. W., W. R. Holland, F. O. Bryan, G. Danabasoglu, and J. C. McWilliams, 1995: An overlooked problem in model simulations of the thermohaline circulation and heat transport in the Atlantic Ocean. *J. Climate*, **8**, 515–523.
- Bryan, F., C. W. Boning, and W. R. Holland, 1986: On the midlatitude circulation in a high-resolution model of the North Atlantic. *Nature*, **323**, 301–304.
- 1995: On the midlatitude circulation in a high-resolution model of the North Atlantic. *J. Phys. Oceanogr.*, **25**, 289–305.
- Clarke, R. A. and J.-C. Gascard, 1983: The formation of Labrador Sea Water. Part I: Large-scale processes. *J. Phys. Oceanogr.*, **13**, 1764–1778.
- Cuny, J., P. Rhines, P. P. Niiler, and S. Bacon, 2002: Labrador Sea boundary currents and the fate of the Irminger Sea water. *J. Phys. Oceanogr.*, **32**, 627–647.

- Curry, R. G., M. S. McCartney, and T. M. Joyce, 1998: Oceanic transport of subpolar climate signals to mid-depth subtropical waters. *Nature*, **391**, 575–577.
- Deacu, D. and P. G. Myers, 2005: Effect of a variable eddy transfer coefficient in an eddy-permitting model of the sub-polar North Atlantic. *J. Phys. Oceanogr.*, **35**, 289–307.
- Dickson, R. R., J. R. N. Lazier, J. Meincke, P. Rhines, and J. Swift, 1996: Long-term coordinated changes in the convective activity of the North Atlantic. *Progress in Oceanogr.*, **38**, 241–295.
- Doscher, R., C. W. Boning, and P. Herrmann, 1994: Response of circulation and heat transport in the North Atlantic to changes in thermohaline forcing in north latitudes: A model study. *J. Phys. Oceanogr.*, **24**, 2306–2320.
- Eden, C. and T. Jung, 2001: North Atlantic interdecadal variability: Oceanic response to the North Atlantic Oscillation (1865–1997). *J. Clim.*, **14**, 676–691.
- Eden, C. and J. Willebrand, 2001: Mechanism of interannual to decadal variability of the North Atlantic circulation. *J. Clim.*, **14**, 2266–2280.
- Fratantoni, D. M., 2001: North Atlantic surface circulation during the 1990's observed with satellite-tracked drifters. *J. Geophys. Res.*, **106**, 22067–22093.
- Gent, P. R. and J. C. McWilliams, 1990: Isopycnal mixing in ocean circulation models. *J. Phys. Oceanogr.*, **20**, 150–155.

- Greatbatch, R. J. and S. Zhang, 1995: An interdecadal oscillation in an idealized ocean basin forced by constant heat flux. *J. Clim.*, **8**, 82–91.
- Grist, J. P. and S. A. Josey, 2003: Inverse analysis adjustment of the SOC air-sea flux climatology using ocean heat transport constraints. *J. Climate*, **16**, 3274–3295.
- Han, Y. J., 1984: A numerical world ocean general circulation model. Part 1: A baroclinic experiment. *Dyn. Atmos. Oceans*, **8**, 141–172.
- Hanawa, K. and L. D. Talley, 2001: Mode Waters. *Ocean Circulation and Climate: Observing and Modelling the Global Ocean*, G. Siedler, J. Church, and J. Gould, eds., San Diego: Academic Press, volume 77 of *International Geophysics series*, 373–386.
- Hansen, D. V. and H. F. Bezdek, 1996: On the nature of decadal anomalies in North Atlantic sea surface temperature. *J. Geophys. Res.*, **101**, 8749–8758.
- Huang, R., 1993: Real freshwater flux as a natural boundary condition for the salinity balance and thermohaline circulation forced by evaporation and precipitation. *J. Phys. Oceanogr.*, **23**, 2428–2446.
- Josey, S. A., E. C. Kent, and P. K. Taylor, 1998: The Southampton Oceanography Centre (SOC) Ocean - Atmosphere Heat, Momentum and Freshwater Flux Atlas. report 6, Southampton Oceanography Centre.

- 1999: New insights into the ocean heat budget closure problem from analysis of the SOC air-sea flux climatology. *J. Climate*, **12**, 2856–2880.
- Josey, S. A. and R. Marsh, 2005: Surface freshwater flux variability and recent freshening of the North Atlantic in the eastern subpolar gyre. *J. Geophys. Res.*, **110**, 1–17.
- Kalnay, E., M. Kanamitsu, R. Kistler, W. Collins, D. Deaven, L. Gandin, M. Iredell, S. Saha, G. White, J. Woollen, Y. Zhu, A. Leetmaa, B. R. Chelliah, W. Ebisuzaki, W. Higgins, J. Janowiak, K. C. Mo, C. Ropelewski, J. Wang, R. Jenne, and D. Joseph, 1996: The NCEP/NCAR 40-year reanalysis project. *Bulletin of the American Meteorological Society*, **77**, 437–471.
- Kara, A. B., P. A. Pochford, and H. E. Hurlbert, 2000: An optimal definition for ocean mixed layer depth. *J. Geophys. Res.*, **105**, 16803–16821.
- Killworth, P. D., 1996: Time interpolation of forcing fields in ocean models. *J. Phys. Oceanogr.*, **26**, 136–143.
- Killworth, P. D., D. A. Smeed, and A. J. G. Nurser, 2000: The effects on ocean models of relaxation toward observations at the surface. *J. Phys. Oceanogr.*, **30**, 160–173.
- Large, W. G., G. Danabasoglu, and S. C. Doney, 1997: Sensitivity to surface forcing

- and boundary layer mixing in a global ocean model: annual-mean climatology. *J. Phys. Oceanogr.*, **27**, 2418–2447.
- Lilly, J. M., P. B. Rhines, M. Visbeck, R. Davis, J. R. N. Lazier, F. Schott, and D. Farmer, 1999: Observing deep convection in the Labrador Sea during winter 1994/95. *J. Phys. Oceanogr.*, **29**, 2065–2098.
- Luo, Y., H. Zhang, M. D. Prater, and L. M. Rothstein, 2003: Warm water pathways, transports and transformations in the northwestern North Atlantic and their modification by cold air outbreaks. *J. Geophys. Res.*, **108**, 26–1–26–16.
- Marshall, J. and F. Schott, 1999: Open-ocean convection: observation, theory, and model. *Review of Geophysics*, **37**, 1–64.
- McCartney, M. S. and L. D. Talley, 1982: The subpolar mode water of the North Atlantic Ocean. *J. Phys. Oceanogr.*, **12**, 1169–1188.
- McWilliams, J. C., 1996: Modeling the oceanic general circulation. *Annu. Rev. Fluid Mech.*, **28**, 215–248.
- Moore, G. W. K., M. C. Reader, J. York, and S. Sathiyamoorthy, 1996: Polar lows in the Labrador Sea. A case study. *Tellus*, **48A**, 17–40.
- Moore, G. W. K. and I. A. Renfrew, 2002: An assessment of the surface turbulent heat fluxes from the NCEP-NCAR reanalysis over the western boundary currents. *J. Climate*, **15**, 2020–2037.

- Myers, P. G., 2002: SPOM: A regional model of the sub-polar North Atlantic. *Atmosphere-Ocean*, **40**, 445–463.
- 2003: An examination of wind-stress forcing and circulation in the sub-polar North Atlantic. *Quaternary International*, **99-100**, 89–98.
- Myers, P. G. and D. Deacu, 2003: Labrador Sea freshwater content in a model with a partial cell topographic representation. *Ocean Modelling*, **6**, 359–377.
- NOAA, 1988: Digital relief of the surface of the earth, tech. rep. data announcement 88-mgg-02. National Geophysical Data Center, Boulder, Colorado.
- NODC, 1994: World ocean atlas 1994 cd-rom data set documentation, tech. rep. noaa. US Department of Commerce.
- Penduff, T., B. Barnier, and A. C. D. Verdiere, 2000: Self-adapting open boundaries for a sigma coordinate model of the eastern North Atlantic. *J. Geophys. Res.*, **105**, 11279–11297.
- Penduff, T., A. C. D. Verdiere, and B. Barnier, 2001: General circulation and intergyre dynamics in the eastern North Atlantic from a regional primitive equation model. *J. Geophys. Res.*, **106**, 22313–22329.
- Philander, S. G. H. and A. D. Seigel, 1985: Simulation of El Nino of 1982-1983. *Coupled Ocean-Atmosphere Models*, Elsevier Oceanography Series, volume 40, 517–541.

Rassmussen, E. A., C. Claud, and J. F. Purdom, 1996: Labrador Sea polar lows. *Global Atmos. Ocean Syst.*, **4**, 275–334.

Redler, R. and C. W. Boning, 1997: Effect of the overflows on the circulation in the subpolar North Atlantic: A regional model study. *J. Geophys. Res.*, **102**, 18529–18553.

Renfrew, I. A., G. W. K. Moore, P. S. Guest, and K. Bumke, 2002: A comparison of surface layer and surface turbulent flux observations over the Labrador Sea with ECMWF analyses and NCEP reanalyses. *J. Phys. Oceanogr.*, **32**, 383–400.

Roberts, M. J., R. Marsh, A. L. New, and R. A. Wood, 1996: An intercomparison of Bryan-Cox-type ocean model and an isopycnal ocean model. Part I: The subpolar gyre and high-latitude processes. *J. Phys. Oceanogr.*, **26**, 1495–1527.

Roberts, M. J. and R. A. Wood, 1997: Topographic sensitivity studies with a Bryan-Cox-type ocean model. *J. Phys. Oceanogr.*, **27**, 823–836.

Rosati, A. and K. Miyakoda, 1988: A general circulation model for upper ocean simulation. *J. Phys. Oceanogr.*, **18**, 1601–1626.

Sathiyamoorthy, S. and G. W. K. Moore, 2002: Buoyancy flux at ocean weather station Bravo. *J. Phys. Oceanogr.*, **26**, 458–474.

Smith, R. D., M. E. Maltrud, F. O. Bryan, and M. W. Hecht, 2000: Numerical

- simulation of the North Atlantic Ocean at $1/10^\circ$. *J. Phys. Oceanogr.*, **30**, 1532–1561.
- Smith, S. D. and F. W. Dobson, 1984: The heat budget at ocean weather station Bravo. *Atmos.- Ocean*, **22**, 1–22.
- Smith, S. R., D. M. Legler, and K. V. Verzone, 2001: Quantifying uncertainties in NCEP reanalyses using high-quality research vessel observations. *J. Climate*, **14**, 4062–4072.
- Stull, R. B., ed., 1988: *An introduction to boundary layer meteorology*. Kluwer Academic Publishers, 666pp.
- Sutton, R. T. and M. R. Allen, 1997: Decadal predictability of North Atlantic sea surface temperature and climate. *Nature*, **388**, 563–567.
- Talley, L. D., 1999: Mode waters in the subpolar North Atlantic in historical data and during the WOCE period. *Int. WOCE Newsletter*, **37**, 3–6.
- Treguier, A. M., B. Barnier, A. P. D. Miranda, J. M. Molines, N. Grima, M. Imbard, G. Madec, C. Messenger, T. Reynaud, and S. Michel, 2001: An eddy-permitting model of the Atlantic circulation: evaluating open boundary conditions. *J. Geophys. Res.*, **106**, 22115–22129.
- Treguier, A. M., S. Theetten, E. P. Chassignet, T. Penduff, R. Smith, L. Talley,

- J. Q. Beismann, and C. Boning, 2005: The North Atlantic subpolar gyre in four high-resolution models. *J. Phys. Oceanogr.*, **35**, 757–774.
- Trenberth, K. E., W. G. Large, and J. G. Olson, 1990: The mean annual cycle in global ocean wind stress. *J. Phys. Oceanogr.*, **20**, 1742–1760.
- Tziperman, E., J. R. Toggweiler, Y. Feliks, and K. Bryan, 1994: Instability of the thermohaline circulation with respect to mix boundary conditions: Is it really a problem for realistic models? *J. Phys. Oceanogr.*, **24**, 217–232.
- Wallace, D. W. R. and J. R. N. Lazier, 1988: Anthropogenic chlorofluoromethanes in newly formed Labrador Sea Water. *Nature*, **332**, 61–63.
- Weaver, A. J. and T. M. C. Hughes, 1992: Stability and variability of the thermohaline circulation and its link to climate. *Trends in Physical Oceanography, Research Trends Series, Council of Scientific Research Integration, Trivandrum, India*, **1**, 15–70.
- Weaver, A. J. and E. S. Sarachik, 1991: The role of mixed boundary conditions in numerical models of the ocean's climate. *J. Phys. Oceanogr.*, **21**, 1470–1493.
- Willebrand, J., B. Barnier, C. Boning, C. Dieterich, P. D. Killworth, C. L. Provost, Y. Jia, J. M. Molines, and A. L. New, 2001: Circulation characteristics in three eddy-permitting models of the North Atlantic. *Progress in Oceanography*, **48**, 123–161.

- WMO, 1994: International list of selected, supplementary and auxiliary ships. 1, WMO Geneva.
- Woodruff, S. D., S. J. Lubker, K. Wolter, S. J. Worley, and J. D. Elms, 1993: Comprehensive Ocean-Atmosphere Data Set (COADS) release 1a: 1980-92. *Earth System Monitor*, 4, 4-8.
- Worthington, L. V., 1976: *On the North Atlantic circulation*. The Johns Hopkins University Press, Baltimore and London.
- Zeng, X., M. Zhao, and R. E. Dickinson, 1998: Intercomparison of bulk aerodynamic algorithms for the computation of sea surface fluxes using TOGA COARE and TAO data. *J. Climate*, 11, 2628-2644.

Chapter 3

Role of the high frequency portion of heat flux in Labrador Sea Water formation in an eddy-permitting ocean model

3.1 Introduction

Deep convection in the Labrador Sea region is a “plume” scale event, triggered by intensive heat loss to the atmosphere, under the preconditioning of cyclonic circulation and neutral stratification (Clarke and Gascard, 1983; Marshall and Schott, 1999). This strong surface forcing might be brought about by the passing of mesoscale or synoptic scale cyclones, which contribute significant high-frequency variability to the surface heat flux. In ocean modelling, however, the surface flux forcing, either based on observation or atmospheric general circulation model output, is frequently averaged over some period ranging from annual to monthly, as well as spatially, such

that the extreme surface cooling associated with the synoptic scale events is removed (Killworth, 1996). This can lead to significant drifts in temperature and salinity (e.g. Rosati and Miyakoda, 1988). Rosati and Miyakoda (1988) depicted the role of high frequency variability, unrepresented in monthly means, in producing more realistic mixing-layer structure by a comparison of the model results forced with monthly mean versus 12-hourly averaged surface fluxes. Philander and Seigel (1985) parameterized the high-frequency wind fluctuations in monthly mean winds by stipulating wind speeds to be not less than 4.8 ms^{-1} and thus avoided the overly high surface temperature (discussed by Rosati and Miyakoda, 1988).

The role of the high frequency portion of heat loss in Labrador Sea Water (LSW) formation has been supported by a number of observations. For example, an instantaneous sensible heat flux of about 750 Wm^{-2} was deduced when a convective event was observed during March 1976. However, the monthly mean sensible heat flux during winter months found by Smith and Dobson (1984) are around 100 Wm^{-2} (discussed by Sathiyamoorthy and Moore, 2002). Heat fluxes sometimes exceeding 650 Wm^{-2} were reported during the winter of 1997 (Renfrew et al., 2002). The wintertime heat flux reached extremely high values of up to 1500 Wm^{-2} , during the 1990s (discussed by Sathiyamoorthy and Moore, 2002).

A flux-forced version of an eddy-permitting regional ocean model of the sub-polar North Atlantic is developed in Chapter 2. Initially, the model was forced by monthly averaged fluxes provided either by Southampton Oceanography Center (SOC) or by

the National Centers for Environmental Prediction - National Center for Atmospheric Research (NCEP-NCAR). Neither of them however could produce deep convection and the Labrador Sea Water (LSW). Moreover, model tracer fields drifted away from the initial conditions. To improve water mass formation and model hydrography, they roughly parameterized the effect of synoptic scale events in the model by simply enhancing heat fluxes (five-fold in SOC and three-fold in NCEP-NCAR) during the winter (Nov.- Mar.) over a limited region within the Labrador Sea ($55 \sim 59^{\circ}N$ and $51 \sim 56^{\circ}W$). The focus on this region is that the deep convection in the Labrador Sea is very localized and has mainly been observed in the western interior of the basin, around $56 \sim 58^{\circ}N$ and $52 \sim 55^{\circ}W$ (Clarke and Gascard, 1983; Wallace and Lazier, 1988; Lilly et al., 1999).

Are the results biased by increasing the heat fluxes over the entire winter in contrast to just during high frequency synoptic events? This chapter examines this issue with a series of experiments designed to represent different scenarios for synoptic events. The model is described briefly in section 3.2, followed by the configuration of surface forcing in section 3.3. The model results are analyzed in section 3.4, with a summary and discussion in section 3.5.

3.2 Model description

The Sub-Polar Ocean Model (SPOM) is a regional configuration of the Modular Ocean Model-Array (MOMA) set up specifically for process and sensitivity studies of

ocean variability questions in the sub-polar North Atlantic. The original model formulation is based on a Bryan-Cox-Semtner type ocean general circulation model using the inviscid version of the Killworth et al. (1991) free surface scheme. The biharmonic horizontal viscosity coefficient is $A_h = 7.5 \times 10^{18} \text{ cm}^4 \text{ s}^{-1}$ and the horizontal diffusion coefficient is $K_h = 7.5 \times 10^{18} \text{ cm}^4 \text{ s}^{-1}$. The vertical viscosity is $A_v = 1.5 \text{ cm}^2 \text{ s}^{-1}$ and the vertical diffusion is $K_v = 0.3 \text{ cm}^2 \text{ s}^{-1}$. Convective adjustment is performed using the complete convection scheme of Rahmstorf (1993). The effect of eddies not resolved by the model's $1/3^\circ$ resolution is mainly parameterized by the Gent and McWilliams eddy parameterization scheme (Gent and McWilliams, 1990), using a constant eddy transfer coefficient $2.0 \times 10^5 \text{ cm}^2 \text{ s}^{-1}$.

The zonal boundaries are set at $68^\circ W$ and Greenwich, 0° . The open southern boundary is set at $38^\circ N$, while the closed northern boundary is set at $70^\circ N$ with restoring buffers in Hudson Strait, Baffin Bay and the region to the north of the Iceland. The model z -coordinates have 36 vertical layers, unevenly spaced, with finer resolution in the upper water column. A partial cell finite-volume technique (Adcroft et al., 1997) is applied to better represent the topography, which is taken from the $1/12^\circ$ ETOPO5 NOAA (1988) dataset, linearly interpolated to the model's $1/3^\circ$ resolution. The interpolated depths are used other than ensuring no partially filled level has less than 10 m of water in it. Further details about the model can be found in Myers (2002).

3.3 Surface forcing algorithms

The model formulation used is based upon the flux-forced configuration of the SPOM developed in Chapter 2. The surface momentum forcing is taken from the European Center for Medium Range Weather Forecast (ECMWF), assembled by Trenberth et al. (1990) for the period 1980 ~ 1986. The base buoyancy fluxes are taken from monthly climatology, originating from the comprehensive set of ship/buoy measurements of SOC, with a resolution of $1^\circ \times 1^\circ$ (Josey et al., 1998). This dataset provides heat fluxes and E-P (evaporation E minus precipitation P), the latter of which is used as a virtual salt flux. Some modifications are made over ice-covered areas where there is a lack of data. A 30-day weak restoring is added on salinity in order to account for lack of a sea-ice process in the SPOM (see Chapter 2 for details). We define the resulting monthly heat flux field with monthly bias removed as our base heat flux (BHF).

The intensive heat loss caused by the effect of synoptic-scale systems is then parameterized by increasing the BHF over the Labrador Sea convection region ($55 \sim 59^\circ N$ and $51 \sim 56^\circ W$) during winter (Nov.-Mar.). We design three experiments HEAT1-HEAT3, based on different patterns for the high frequency heat loss associated with the synoptic-scale events. HEAT1 is the same experiment as SOC1 in Chapter 2, with BHF multiplied by five ($5 * BHF$), i.e. a general enhancement of the heat flux during the winter months. To avoid a sudden transition in heat fluxes, the multiplier for the modified fluxes is smoothly ramped down at the boundary of

the enhanced region. However, meso- or synoptic events are intermittent. In general their occurrences have a quasi-period of a week. For simplicity, we employ a period of ten days in two other experiments since there are 30 model days in each month. HEAT2 takes a form of $6 * BHF * HFHF$, employed repeatedly in November through March. $HFHF$ denotes the high frequency heat flux formulated as an absolute value of sinusoid, $|\sin 3\pi x|$, where x is a time variable (varying from 0 to 1 within one month). This pattern implies that intense synoptic processes occur 3 times each month (30 model days). The heat flux variability here is smooth and gradual. However, weather systems often rapidly spin-up or decay. They also may stall, implying significant durations. Experiment HEAT3 therefore utilizes a similar heat flux pattern $6 * BHF * HFHF$ but with $HFHF$ being expressed as a square wave, i.e. a piecewise function $HFHF = 1$ when $x = 0 \sim 0.2, 0.4 \sim 0.6$ and $0.8 \sim 1.0$ and $HFHF = 0$ otherwise. This function is also applied repeatedly over five winter months (November through March). This pattern similarly has a period of 10 days, but with the first event starting at the beginning and the third event lasting until the end of each month. This experiment undergoes longer periods of intense heat loss at the border of each month. Note that when the addition of the high frequency component calculates a heat flux less than BHF , BHF is applied. The resulting idealized high frequency variability of heat fluxes at $57^{\circ}N, 54^{\circ}W$ is shown in Figure 3.1. Other locations have similar patterns although different amplitudes.

Table 3.1 lists the monthly heat flux means and the maxima of instantaneous

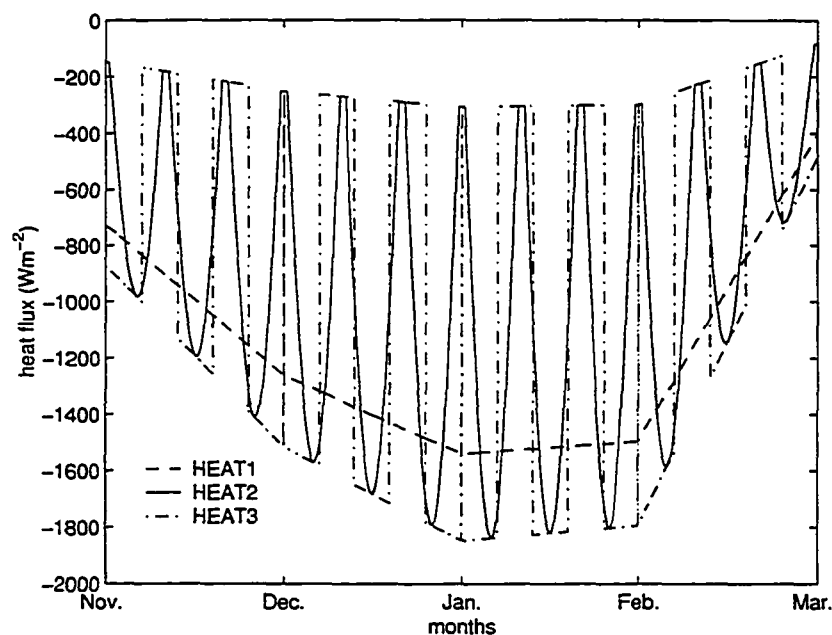


Figure 3.1: Time series of wintertime heat fluxes at $57^{\circ}N$, $54^{\circ}W$ in the Labrador Sea heat fluxes over the Labrador Sea convection region ($55 \sim 59^{\circ}N$ and $51 \sim 56^{\circ}W$) for all three experiments. The winter mean heat loss in HEAT1 differs by only 2.8% and 5.5% from those in HEAT2 and HEAT3 respectively. The maximum heat loss occurs in January. January mean/instantaneous maximum heat fluxes in HEAT1 are 7.2%/22.7% and 10.3%/25.1% smaller than in HEAT2 and HEAT3, respectively. HEAT3 displays the largest amplitude between monthly minimum and maximum.

Table 3.1: Monthly heat flux means and maxima of instantaneous heat fluxes over the Labrador Sea convection region ($55 \sim 59^{\circ}N$ and $51 \sim 56^{\circ}W$) (unit: Wm^{-2})

Exp.	Types	Nov.	Dec.	Jan.	Feb.	Mar.	Winter Mean
HEAT1	Mean	-520.51	-875.93	-1074.60	-954.84	-302.31	-745.64
	Max	-1312	-1645	-1657	-1657		
HEAT2	Mean	-403.15	-942.71	-1158.20	-1034.72	-296.97	-767.15
	Max	-1535	-1983	-2144	-1971		
HEAT3	Mean	-406.27	-971.90	-1198.07	-1076.27	-291.31	-788.76
	Max	-1648	-2096	-2211	-1971		

3.4 Model results

The model was initially spun up for 40 years under HEAT1. This forcing gives a reasonable climatology for the Labrador Sea region, with the LSW being produced to a depth of ~ 1500 m in the western interior of Labrador Sea, albeit with both temperature and salinity higher than observations (Chapter 2). Then the model is run for a further 35 years using the forcing from each HEAT pattern.

As it takes time for the model to adjust after the switch in surface forcing at year 40, we focus on the last 15 years of integration (model years 61 \sim 75). Deep convection is observed to occur during winter months in the Labrador Sea, around $58 \sim 59^\circ N$, $52 \sim 54^\circ W$, in all experiments. There is significant interannual variability in convective depth, ranging from 1000 to 1500 m in HEAT1 and HEAT2. HEAT3 shows similar interannual variability but greater extremes (one year with basically no deep convection and one year reaching 1600 m in depth). A convective depth of 1500 m has been documented by a number of observations (Clarke and Gascard, 1983; Clarke and Coote, 1988; Lilly et al., 1999). Observations also show significant interannual/interdecadal variability (Dickson et al., 1996; The Lab Sea Group, 1998; Lazier et al., 2001), from a potential switching off of convection during the late 1960s/early 1970s (Dickson et al., 1996), to less than 1000 m in the winter of 1995 \sim 1996, to 2300 m in the winter of 1992 \sim 1993 (The Lab Sea Group, 1998; Lazier et al., 2001). Although this variability is most likely thought to be associated with variability in an atmospheric mode (e.g. the North Atlantic Oscillation) and hence surface flux forc-

ing, stratification and stagnation of the previous year's LSW may also play important roles (Clarke and Gascard, 1983; Dickson et al., 1996). At least in our experiments, the variability arises from internal processes, since our forcing is perpetual.

Although our three experiments give rise to somewhat different convection patterns, the LSW properties are very similar in all experiments. Wintertime convection is associated with temperatures of $\sim 4\text{ }^{\circ}\text{C}$ and salinities of $35.1\text{ }psu$. These values are warmer and saltier than observed (Clarke and Gascard, 1983; Wallace and Lazier, 1988; Lilly et al., 1999) but consistent with the drift in properties (especially salinity) seen in most eddy-permitting models of the sub-polar gyre (Treguier et al., 2005; Myers and Deacu, 2004). This leads to formation of the LSW with densities ranging from 27.75 to 27.80 in most years in all experiments. If we integrate the volume of the LSW (in the above density range of 27.75 to 27.80) in the central Labrador Sea in each experiment, we also find few differences between experiments (Figure 3.2), albeit with significant interannual variability. Averaging over the last 15 years of each experiment, we determine the volume of the LSW to be $4.28 \times 10^{14}\text{ }m^3$ in HEAT1, $4.27 \times 10^{14}\text{ }m^3$ in HEAT2 and $4.23 \times 10^{14}\text{ }m^3$ in HEAT3. Thus, despite the net heat fluxes varying by up to 5.5% between experiments (and the maximum instantaneous heat loss varying by up to 25%), the changes in time integrated LSW volume over this 15 year period is only 1%. Although an examination of volumes means that we are considering storage as well as water mass formation, the small discrepancies between experiments suggest that a balance has been reached.

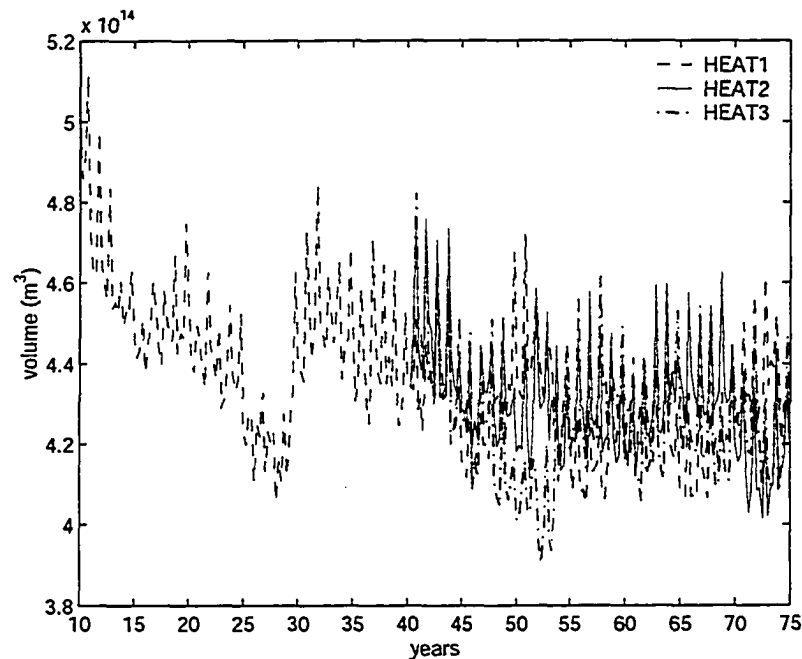


Figure 3.2: Time series of LSW volume on $\sigma_0 = 27.75 \sim 27.8$ over the central Labrador Sea Region

3.5 Summary and discussion

In a previous work (Chapter 2), a flux forced version of an eddy-permitting ocean model of the sub-polar North Atlantic has been developed. In order to obtain “right” LSW climatological properties and prevent the tracer fields from drifting from the observations, the effect of high frequency variability in heat flux is parameterized by simply increasing the heat loss over the Labrador Sea convection region for the entire winter (Nov.-Mar.). In this chapter we design two other parameterization schemes with more realistic time-evolving patterns represented by idealized functions. Despite significant differences in mean and instantaneous heat fluxes among the three experiments, all show very similar LSW properties and an improvement of LSW formation

in comparison with using simple monthly mean. We conclude that this type of idealization of synoptic events is hence appropriate to be used in an ocean model in terms of LSW formation (giving “right” LSW properties in comparison with monthly mean forcing). Advantages of such an approach include a way that permits the continued use of readily available monthly heat flux fields as well as a reduction in computation cost (1% of CPU).

Additionally, two other interesting results are highlighted in this chapter. First, there is the issue of internally driven convective variability. Although in no way disagreeing with the widely observed link between changes in atmospheric modes (such as the NAO) and LSW formation (Curry et al., 1998; Dickson et al., 1996), we show that variability in LSW volume can also be driven by internal oceanic processes. As the surface forcing does not include any interannual (or lower frequency) variability, volume changes must be driven by internal processes (such as changes to stratification or surface properties) that lead to differing amounts of convective water formation each year. Although LSW volumes will also be affected by changes in export, the variable increases seen in each winter do suggest that the volume changes are driven by variability in water mass formation.

A number of climate modelling studies using idealized models or configurations have suggested a link between the Meridional Overturning Circulation (MOC) and changes in the location, intensity and variability of convection (Delworth et al., 1993; Rahmstorf, 1995a,b; Delworth and Greatbatch, 2000). Yet as discussed by Rhein

et al. (2002), there is as of yet no definite knowledge if convective variability can then be linked to variability in aspects of the MOC, such as meridional heat transport or the export of LSW from the subpolar gyre. Albeit very limited in extent, our results argue against such a link. We find significant interannual variability in convection and convective depth in all experiments. Yet, once integrated, we do not find any significant differences in LSW volume or export in these experiments. We would suggest that variability in LSW volumes, or potentially LSW export, may more likely be a relevant proxy to the MOC.

Acknowledgements:

This work is part of the PhD thesis of Duo Yang and was supported by CFCAS (GR-019) and NSERC grants awarded to Paul G. Myers.

References

- Adcroft, A., C. Hill, and J. Marshall, 1997: Representation of topography by shaved cell in a height coordinate ocean model. *Mon. Weather Rev.*, **125**, 2293–2315.
- Clarke, R. A. and A. R. Coote, 1988: The formation of Labrador Sea Water. Part III: The evolution of oxygen and nutrient concentration. *J. Phys. Oceanogr.*, **18**, 469–480.

- Clarke, R. A. and J.-C. Gascard, 1983: The formation of Labrador Sea Water. Part I: Large-scale processes. *J. Phys. Oceanogr.*, **13**, 1764–1778.
- Curry, R. G., M. S. McCartney, and T. M. Joyce, 1998: Oceanic transport of subpolar climate signals to mid-depth subtropical waters. *Nature*, **391**, 575–577.
- Delworth, T. L. and R. J. Greatbatch, 2000: Multidecadal Thermohaline Circulation variability driven by atmospheric surface flux forcing. *J. Clim.*, **13**, 1481–1495.
- Delworth, T. L., S. Manabe, and R. J. Stouffer, 1993: Interdecadal variations of the Thermohaline Circulation in a coupled ocean-atmosphere model. *J. Clim.*, **6**, 1993–2011.
- Dickson, R. R., J. R. N. Lazier, J. Meincke, P. Rhines, and J. Swift, 1996: Long-term coordinated changes in the convective activity of the North Atlantic. *Progress in Oceanogr.*, **38**, 241–295.
- Gent, P. R. and J. C. McWilliams, 1990: Isopycnal mixing in ocean circulation models. *J. Phys. Oceanogr.*, **20**, 150–155.
- Josey, S. A., E. C. Kent, and P. K. Taylor, 1998: The Southampton Oceanography Centre (SOC) Ocean - Atmosphere Heat, Momentum and Freshwater Flux Atlas. report 6, Southampton Oceanography Centre.
- Killworth, P. D., 1996: Time interpolation of forcing fields in ocean models. *J. Phys. Oceanogr.*, **26**, 136–143.

- Killworth, P. D., D. Stainforth, D. J. Webb, and S. M. Peterson, 1991: The development of a free-surface Bryan-Cox-Semtner ocean model. *J. Phys. Oceanogr.*, **21**, 1333–1348.
- Lazier, J., R. Pickart, and P. Rhines, 2001: Deep convection. *Ocean Circulation and Climate: Observing and Modelling the Global Ocean*, G. Siedler, J. Church, and J. Gould, eds., San Diego: Academic Press, volume 77 of *International Geophysics series*, 387–400.
- Lilly, J. M., P. B. Rhines, M. Visbeck, R. Davis, J. R. N. Lazier, F. Schott, and D. Farmer, 1999: Observing deep convection in the Labrador Sea during winter 1994/95. *J. Phys. Oceanogr.*, **29**, 2065–2098.
- Marshall, J. and F. Schott, 1999: Open-ocean convection: observation, theory, and model. *Review of Geophysics*, **37**, 1–64.
- Myers, P. G., 2002: SPOM: A regional model of the sub-polar North Atlantic. *Atmosphere-Ocean*, **40**, 445–463.
- Myers, P. G. and D. Deacu, 2004: Labrador Sea freshwater content in a model with a partial cell topographic representation. *Ocean Modelling*, **6**, 359–377.
- NOAA, 1988: Digital relief of the surface of the earth, tech. rep. data announcement 88-mgg-02. National Geophysical Data Center, Boulder, Colorado.
- Philander, S. G. H. and A. D. Seigel, 1985: Simulation of El Nino of 1982-1983.

- Coupled Ocean-Atmosphere Models*, Elsevier Oceanography Series, volume 40, 517–541.
- Rahmstorf, S., 1993: A fast and complete convection scheme for ocean models. *Ocean Modelling*, **101**, 9–11.
- 1995a: Bifurcations of the Atlantic Thermohaline Circulation in response to changes in the hydrological cycle. *Nature*, **378**, 145–149.
- 1995b: Multiple convection patterns and thermohaline flow in an idealized OGCM. *J. Clim.*, **8**, 3028–3039.
- Renfrew, I. A., G. W. K. Moore, P. S. Guest, and K. Bumke, 2002: A comparison of surface layer and surface turbulent flux observations over the Labrador Sea with ECMWF analyses and NCEP reanalyses. *J. Phys. Oceanogr.*, **32**, 383–400.
- Rhein, M., J. Fischer, W. M. Smethie, D. Smythe-Wright, R. F. Weiss, C. Mertens, D.-H. Min, U. Fleischmann, and A. Putzka, 2002: Labrador Sea Water: Pathways, CFC inventory, and formation rates. *J. Phys. Oceanogr.*, **32**, 648–665.
- Rosati, A. and K. Miyakoda, 1988: A general circulation model for upper ocean simulation. *J. Phys. Oceanogr.*, **18**, 1601–1626.
- Sathiyamoorthy, S. and G. W. K. Moore, 2002: Buoyancy flux at ocean weather station Bravo. *J. Phys. Oceanogr.*, **26**, 458–474.

- Smith, S. D. and F. W. Dobson, 1984: The heat budget at ocean weather station Bravo. *Atmos.- Ocean*, **22**, 1–22.
- The Lab Sea Group, 1998: The Labrador Sea deep convection experiment. *Bull. Amer. Meteo. Soc.*, **79**, 2033–2058.
- Treguier, A. M., S. Theetten, E. P. Chassignet, T. Penduff, R. Smith, L. Talley, J. Q. Beismann, and C. Boning, 2005: The North Atlantic subpolar gyre in four high-resolution models. *J. Phys. Oceanogr.*, **35**, 757–774.
- Trenberth, K. E., W. G. Large, and J. G. Olson, 1990: The mean annual cycle in global ocean wind stress. *J. Phys. Oceanogr.*, **20**, 1742–1760.
- Wallace, D. W. R. and J. R. N. Lazier, 1988: Anthropogenic chlorofluoromethanes in newly formed Labrador Sea Water. *Nature*, **332**, 61–63.

Chapter 4

Response of the sub-polar North Atlantic to extreme NAO phase-related flux forcing in a regional eddy-permitting ocean model

4.1 Introduction

Since Bjerknes (1964) and others since (e.g. Deser and Blackman, 1993; Kushnir, 1994) introduced the notion of the timescale dependent nature of the North Atlantic air-sea interaction, there has been intensive interest toward understanding variability in ocean circulation and heat transport in the North Atlantic, concentrating on the North Atlantic Oscillation (NAO) - related atmospheric forcing. The NAO is a dominant mode of the atmospheric variability over the North Atlantic, expressed as the

⁰A version of this chapter has been submitted for publication. Duo Yang and Paul G. Myers 2005. *Geophysical Research Letters*.

surface pressure difference between subpolar and subtropical action centers and hence representing the strength of the westerly winds blowing over the North Atlantic Ocean between $40 \sim 60^\circ N$ (Rogers, 1984; Hurrell, 1995). The rationale for the interest in the NAO is its intimate relationship with latent and sensible heat (Cayan, 1992), freshwater (Hurrell, 1996) and momentum fluxes (Visbeck et al., 1998) provided to high latitude North Atlantic on inter-annual and inter-decadal scales, which thus puts its signature on water mass formation, circulation and oceanic heat and freshwater transport (e.g. Dickson et al., 1996; Curry et al., 1998; Curry and McCartney, 2001).

The subpolar North Atlantic is our focus, where the formation of the Labrador Sea Water (LSW) is associated with the sinking branch of the meridional overturning circulation (MOC), while the North Atlantic Current (NAC), an extension of the Gulf Stream (Clarke et al., 1980), is unique in transporting warm waters to much higher latitudes than currents in any other ocean (Rossby, 1996), and acts as part of the upper layer branch of the MOC. The NAC is associated with strong temperature and salinity gradients, separating the warm, saline waters of tropical-subtropical origin from the cold, fresh waters of the Labrador Sea (Rossby, 1996). Observations show that LSW formation and the NAC have displayed significant interannual and interdecadal variability. Weak convection, thinning and warming LSW can be related to a low NAO index (weaker westerlies) and vice versa (Curry et al., 1998). The remote impact of the LSW on subtropical deep water also appears to be regulated by NAO variability (Curry et al., 1998). Curry and McCartney (2001) reveal the

response of the Gulf Stream - NAC system intensity to the NAO forcing by constructing an oceanic analogue of the NAO index. Bersch (2002) suggested a subpolar gyre contraction, as the NAO changed from its positive phase to the negative phase.

Studies from Ocean General Circulation Models (OGCMs) have linked NAO-related interannual or interdecadal atmospheric forcing to low-frequency variations in the horizontal and meridional circulation and heat transport (Hakkinen, 1999; Delworth and Greatbatch, 2000; Eden and Jung, 2001; Eden and Willebrand, 2001; Gulev et al., 2003). However, a series of idealized models forced by idealized, stable flux forcing did exhibit internal oceanic oscillation, independent of varying surface forcing (e.g. Weaver and Sarachik, 1991; Weaver et al., 1993; Greatbatch and Zhang, 1995; te Raa et al., 2004). We hence inspect this issue in a more realistic (geometry, topography and stable, extreme NAO related surface forcing) and eddy-permitting regional ocean model configuration. With better resolved LSW formation and NAC pathway, we reveal interactions of water mass formation and boundary currents, as well as their role in the initiation and maintenance of an internal oceanic mode.

4.2 Model configuration and experiment design

The model is a flux-forced version (Chapter 2) of a regional eddy-permitting ($1/3^\circ$) ocean model of the sub-polar North Atlantic ($68^\circ W \sim 0^\circ$ and $38 \sim 70^\circ N$) (Myers, 2002) having 36 unevenly spaced vertical z-levels. The climatological surface buoyancy (heat and freshwater) forcing originates from ship/buoy measure-

ments of the Southampton Oceanography Center (SOC) (Josey et al., 1998) (mean of 1980 ~ 1993), with the addition of a crude parameterization of the effect of high-frequency variability resulting from the passages of synoptic scale events on the heat flux over the convective region of Labrador Sea during winter months. Wind stress is from an European Center for Medium Range Weather Forecast (ECMWF) climatology, assembled by Trenberth et al. (1990) for the period 1980 ~ 1986. The model also features a finite volume partial cell (Adcroft et al., 1997) topography, taken from ETOPO5 (NOAA, 1988) dataset, as well as open boundary conditions dealing with connections with the rest of the Atlantic Ocean at $38^{\circ}N$ and buffer zones used in the northern boundary regions. The model is described in more detail in Myers (2002) and in Chapter 2.

Using the above configuration, the model is spun up for 40 years from rest (and climatological temperature and salinity). Then we conduct three experiments, starting from the end of the spin-up. Our control experiment (hereafter CTL) is a further integration of 40 years under climatological forcing and is the same experiment as SOC1 in Chapter 2. The major features of the large-scale circulation of the sub-polar North Atlantic are well represented except our “Northwest Corner” is too far to the east, as shown in Chapter 2. Two other experiments, named HNAO and LNAO, are forced by anomalous monthly heat and freshwater fluxes corresponding to extreme high and low NAO phases superposed upon the climatological forcing (wind stress unchanged), and integrated over years 41 ~ 150 and 41 ~ 100 respectively. The

extreme NAO phase related anomalous heat and freshwater fluxes are synthesized from three extreme high NAO index years (1989, 1990 and 1995) in HNAO and from three extreme low NAO index years (1969, 1996 and 1963) in LNAO, taken from the NCEP-NCAR reanalysis (Kalnay et al., 1996). The December-February (DJF) heat flux anomalies show an obvious seesaw pattern with heat loss being most intense over the Labrador Sea and decreasing towards the southeast during the extreme high NAO phase and strongest in southeast corner of our domain, around the Bay of Biscay, and reducing towards the Labrador Sea in the extreme low NAO phase (Figure 4.1). Our anomalous pattern is similar to the sum distribution of anomalous latent and sensible heat fluxes over the sub-polar North Atlantic in Marshall et al. (2001) (their Figure 3a) during the high NAO phase although our heat flux includes long wave and net solar radiations. The DJF averaged heat flux difference between two extreme NAO phases over Labrador Sea reaches up to 200 Wm^{-2} .

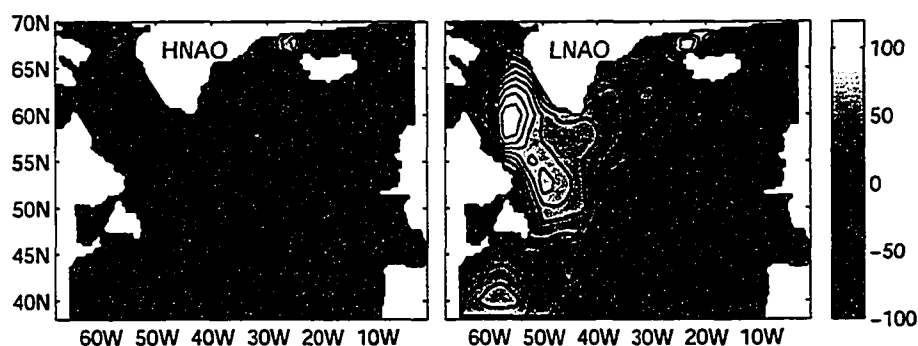


Figure 4.1: Heat flux anomalies averaged over Dec.-Feb. (NCEP-NCAR). HNAO anomalies are synthesized from three extreme high NAO years (1989, 1990 and 1995) and LNAO anomalies from three extreme low NAO years (1969, 1996 and 1963)

4.3 Model response of the sub-polar North Atlantic

4.3.1 Less “stable” oceanic response in HNAO vs. LNAO

An examination of the meridional stream function (MSF) at $55^{\circ}N$, the model domain averaged heat content and the eastern basin ($43 \sim 52^{\circ}N$ $12 \sim 24^{\circ}W$) averaged heat content (Figure 4.2) reveals a potential multi-decadal oscillation in HNAO while a quasi-equilibrium is established in LNAO following an initial adjustment. Interannual variability is ubiquitous in both experiments. This variability in HNAO has an irregular period that changes over time. *de Raai et al. (2004)* suggest from an idealized model study that changing the model complexity can result in interdecadal variability comprising more than one period. Our irregular period might hence be attributed to the complexity of our model and could thus reflect the superposition of different periods resulting from the persistent surface forcing signal in HNAO. Note, however, that an additional experiment with a more “realistic” persistence for high NAO forcing (lasting for ten years before a return to climatological forcing, a situation not unusual - e.g. during late 1980 ~early 1990s) displays the same feature of multi-decadal variability and period superposition, albeit with slightly different details.

The MSF at $55^{\circ}N$ mirrors to a great extent the strength and timing of Labrador Sea convection. Figure 4.2 shows that the changes in the MSF lead variations in domain (and eastern basin) heat content by 4 (6) years, with maximum correlation

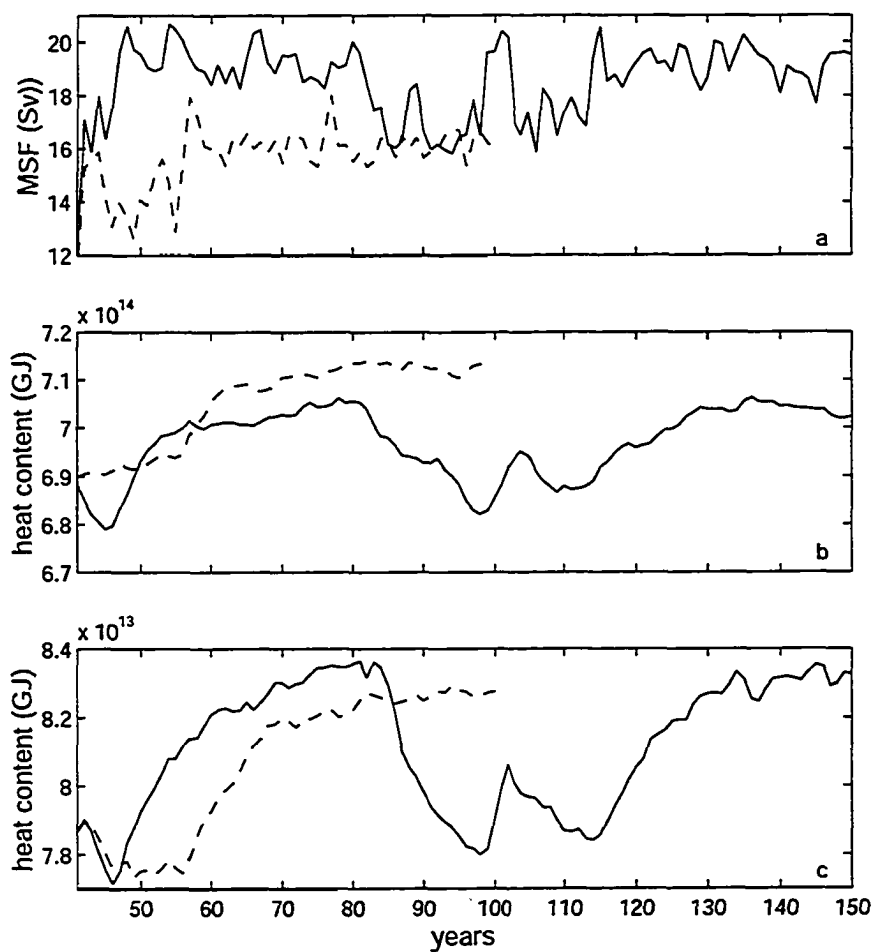


Figure 4.2: Time series of a) meridional stream function at $55^{\circ}N$; b) domain-averaged heat content; c) heat content in eastern basin ($43 \sim 52^{\circ}N$ $12 \sim 24^{\circ}W$) for HNAO (solid line) and LNAO (dashed line).

coefficients between the timeseries of 0.73 (0.66), significant at the 99% level, and therefore suggest a driving role of Labrador Sea convection, triggered by atmospheric forcing. However, since there is no variability other than the seasonal cycle in our surface forcing, the different evolving patterns, especially the multi-decadal variability appearing in HNAO, must be brought about by internal oceanic processes. Figure 4.3 gives snapshots of annual temperature anomalies in HNAO over a full oscillation (years 46 ~ 94) and depicts such an internal mode - anomalous heat transport evolution. After switching to anomalously high NAO forcing in year 41, the increased heat loss over the Labrador Sea produces colder and hence denser surface water, enhancing deep vertical convection. Subsequently, the NAC transports more heat to the Labrador Sea, warming it and leading to less heat influx to the eastern basin, and a drop in heat content (Figure 4.2c). We see more heat concentrates around Labrador Sea basin at year 46 (Figure 4.3), accompanied by reduced convection and low LSW volume in Labrador Sea (not shown). After that, more northeastward heat transport causes increased temperature in eastern basin during years 52 ~ 80 and decreased temperature in Labrador Sea, accompanied by the deep convection up to 1700 m and high LSW volume. Then, this deep convection provokes a gradual heat transport toward Labrador Sea again such that the eastern basin cools and the Labrador Sea warms up with weakened vertical convection (1100 m) and diminished LSW volume. This process then repeats in the remaining years, accompanied by the subsequent oscillations. The low-frequency variability in HNAO is therefore closely

associated with anomalous heat transport in the upper layers, leading to temperature anomalies. In LNAO, heat transports are consistently directed northeastward after the spin-up, giving rise to a stable equilibrium situation.

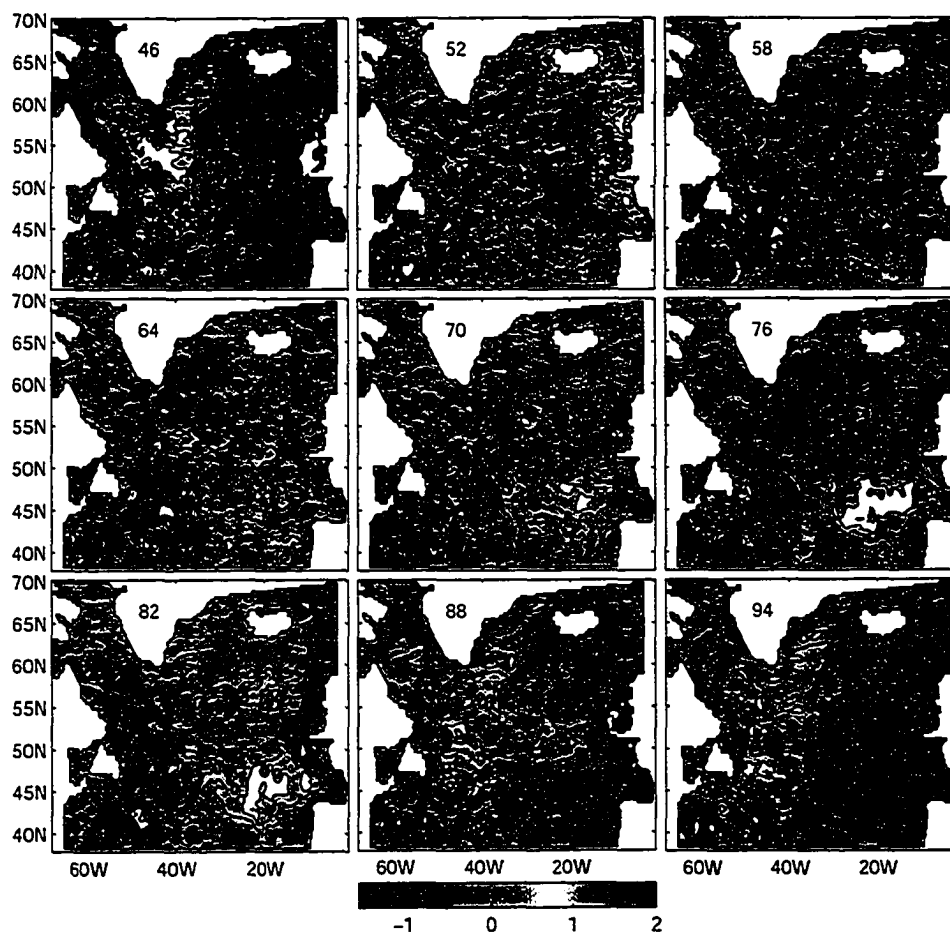


Figure 4.3: Snapshots of annual temperature anomalies in HNAO (with respect to annual temperature mean over the entire integration period - years 40 ~ 150) averaged over the upper 658 m (model levels 1 ~ 14) during a full oscillation (years 46 ~ 94), plotted every six model years.

Our results therefore suggest that surface forcing in response to the high NAO phase is more likely to induce internal oceanic heat transport variability than the low

NAO case.

4.3.2 Anomalous NAC pathway

Now let us investigate the NAC and link it to the variability in anomalous heat transport discussed above. Classically, the NAC is thought to flow to the northwest into the “Northwest Corner” from around the Flemish Cap, then shift sharply towards the east around $52^{\circ}N$ (Krauss et al., 1987). However, the complexity and variability of the flow around “Northwest Corner”, associated with significant meanders and eddies, has been documented by a number of authors (e.g. Mann, 1967; Krauss et al., 1987; Clarke et al., 1980; Rossby, 1996). We focus on the NAC’s evolving patterns in the region $46 \sim 52^{\circ}N$ $33 \sim 44^{\circ}W$ by examining the model sea surface height (SSH) field. These variations are nicely demonstrated using the SSH isolines of 0 and -5 cm. We plot the isolines for years 46, 76 and 94 for HNAO (covering the oscillation previously discussed) and a representative year (80) for LNAO (Figure 4.4). In HNAO, a more westward NAC axis is evident, accompanied by low-frequency shifts in orientation of the pathway: northwest (years 46 and 94) - northeast (year 76). These changes are consistent with the anomalous heat transport and low-frequency variability in heat content discussed previously. Similar switches also appear in the subsequent oscillation. We do not observe a north-south NAC shift (Bersch, 2002), possibly due to the longitude of the model northwest corner and the proximity of this region to the model southern boundary. In LNAO, the NAC manifests a stable, more eastward

(in contrast to HNAO) and then northeast oriented pathway, without interdecadal changes.

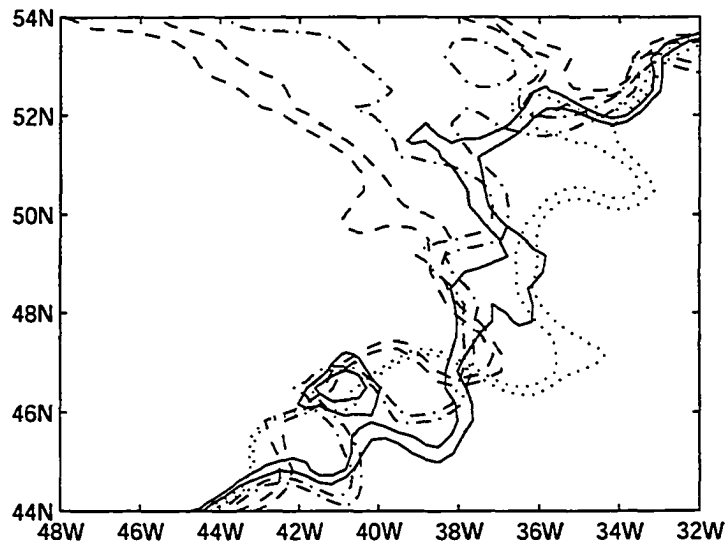


Figure 4.4: 0 and -5 cm sea surface height contours for years 46 (dashed line), 76 (solid line) and 94 (dash-dot line) in HNAO and in year 80 (dotted line) in LNAO, output from our model.

Bersch (2002) documented changes in the upper layer circulation along Greenland-Ireland and Newfoundland-France sections when the NAO index dropped significantly in 1996 and 1997. He suggested a contraction of the subpolar gyre with a westward shift accompanied by an eastward shift of the Subarctic Front (SAF) was observed in the Iceland and the Newfoundland Basins. This feature seems consistent with our LNAO experiment. A comparison of salinity in the upper 1000 m vs. longitude in LNAO against our CTL (not shown) shows the occurrence of higher salinity water in the Iceland Basin, Rockall Trough and western European Basin, as well as lower salinity water in the Irminger Basin during extreme low NAO years. A further comparison

of salinity on $\sigma_0 = 27.2$ and $\sigma_0 = 27.5$ in LNAO indicates an increased northward spreading of warm, saline, and less dense Subpolar Mode Water and Mediterranean Water, as suggested by Bersch (2002) (his Figure 3 and 5). The modeled NAC axis shown in Figure 4.4 is further east in LNAO.

4.4 Discussion

Using a hierarchy of increasingly complex model configurations under prescribed, idealized heat flux forcing, te Raa et al. (2004) proposed that interdecadal variability in the North Atlantic was caused by an internal oceanic mode: northwestward propagation of large-scale temperature anomalies gives rise to a phase difference between meridional and zonal temperature gradient anomalies; anomalous east-west temperature difference leads anomalous north-south temperature difference; and anomalous east-west/north-south temperature difference further leads to anomalous meridional/zonal overturning. We feel that such a mechanism can be seen in our more “realistic” situations. If we reexamine our temperature anomalies by only looking at Figure 4.3 without considering the potentially realistic heat transport directions via the NAC, our temperature anomalies also propagate northwestward, in a form of negative, positive, . . . , phases, similar to their Figure 1. Then, by a decomposition of these temperature anomalies into anomalous east-west and north-south temperature differences, we would expect a similar internal oceanic mode, driving the low-frequency variability in our MSF and then basin-averaged heat content. However,

such a process involves an interaction between LSW formation and the NAC path in our case. Therefore we delineate this process in such a way: the intensive heat loss over Labrador Sea and subsequent vertical convection during the high NAO phase (initiation of anomalous east-west temperature difference) increases the meridional heat flux via an anomalous NAC north-south transport, leading to anomalous north-south temperature difference; which then produces anomalous zonal heat flux via an anomalous NAC east-west transport; thus the internal low-frequency mode.

Curry and McCartney (2001) plot the potential energy anomaly (PEA) distributions for years 1990 ~ 97 (high NAO phase) and 1965 ~ 74 (low NAO phase), as well as the difference between these two periods (their Figure 4 and Figure 8). A north-south dipole with increased (uplifted) subtropical PEA and decreased (deepened) subpolar PEA appears around Mann Eddy-Grand Banks and an east-west dipole with decrease to the west and increase to the east, north of Mann Eddy. These dipoles would seem to suggest strength variations of the NAC, and possibly also reflect an axis shift (Curry and McCartney, 2001), after a transit of the NAO index from low to high phase although the authors could not further verify it due to a lack of data. Our results appear to be a verification of such a situation.

4.5 Summary

Using a regional eddy-permitting ocean model of the sub-polar North Atlantic forced with anomalous buoyancy fluxes corresponding to extreme high and low NAO

phases, we reexamine the issue of internal oceanic variability suggested by a series of “idealized” studies. Our results show potentially multi-decadal variability in LSW formation and heat transport under anomalous high NAO related forcing, in comparison to an equilibrium like circulation under anomalous low NAO related forcing. A less stable state is therefore suggested to occur under the high NAO phase and it appears to be brought about by oceanic internal process, i.e., changes in the NAC strength and pathway but excited by Labrador Sea deep convection, triggered by intensive heat loss during winter. The oscillation in both Labrador Sea convection and the NAC path then self-maintains without a change in surface forcing (such as a switch to low NAO-related forcing).

Model simulations (Shindell et al., 1999; Fyfe et al., 1999) suggest that observed NAO/Arctic Oscillation (AO) positive phase since 1980s appears more likely under greenhouse induced climate warming scenario although stratospheric dynamics may need to be involved (Paeth et al., 1999). Delworth and Dixon (2000) pointed out that the thermohaline circulation response to the intensifying NAO/AO can delay the weakening of the former due to increase of greenhouse gases concentrations. Our results implicate the possibility for enhanced variability of the climate system under the high NAO phase and thus in a warmer world. Hence this study emphasizes the importance of understanding how the ocean circulation will evolve in such a situation.

Acknowledgements:

This work is part of PhD thesis of Duo Yang and was funded by CFCAS (GR-019) and NSERC grants awarded to Paul G. Myers.

References

- Adcroft, A., C. Hill, and J. Marshall, 1997: Representation of topography by shaved cell in a height coordinate ocean model. *Mon. Weather Rev.*, **125**, 2293–2315.
- Bersch, M., 2002: North Atlantic Oscillation-induced changes of the upper layer circulation in the North Atlantic Ocean. *J. Geophys. Res.*, **107**, 20–1–20–11.
- Bjerknes, J., 1964: Atlantic air-sea interaction. *Adv. Geophys.*, **10**, 1–82.
- Cayan, D., 1992: Latent and sensible heat flux anomalies over the northern oceans: The connection to monthly atmospheric circulation. *J. Clim.*, **5**, 354–369.
- Clarke, R. A., H. W. Hills, R. F. Reiniger, and B. A. Warren, 1980: Current system south and east of the Grand Banks of Newfoundland. *J. Phys. Oceanogr.*, **10**, 25–65.
- Curry, R. G. and M. S. McCartney, 2001: Ocean gyre circulation changes associated with the North Atlantic Oscillation. *J. Phys. Oceanogr.*, **31**, 3374–3400.
- Curry, R. G., M. S. McCartney, and T. M. Joyce, 1998: Oceanic transport of subpolar climate signals to mid-depth subtropical waters. *Nature*, **391**, 575–577.

- Delworth, T. L. and K. W. Dixon, 2000: Implications of the recent trend in the Arctic/North Atlantic Oscillation for the North Atlantic thermohaline circulation. *J. Clim.*, **13**, 3721–3727.
- Delworth, T. L. and R. J. Greatbatch, 2000: Multidecadal Thermohaline Circulation variability driven by atmospheric surface flux forcing. *J. Clim.*, **13**, 1481–1495.
- Deser, C. and M. L. Blackman, 1993: Surface climate variations over the North Atlantic Ocean during winter: 1900–1989. *J. Clim.*, **6**, 1743–1753.
- Dickson, R. R., J. R. N. Lazier, J. Meincke, P. Rhines, and J. Swift, 1996: Long-term coordinated changes in the convective activity of the North Atlantic. *Progress in Oceanogr.*, **38**, 241–295.
- Eden, C. and T. Jung, 2001: North Atlantic interdecadal variability: Oceanic response to the North Atlantic Oscillation (1865–1997). *J. Clim.*, **14**, 676–691.
- Eden, C. and J. Willebrand, 2001: Mechanism of interannual to decadal variability of the North Atlantic circulation. *J. Clim.*, **14**, 2266–2280.
- Fyfe, J. C., G. J. Boer, and G. M. Flato, 1999: The Arctic and Antarctic Oscillation and their projected changes under global warming. *Geophys. Res. Lett.*, **26**, 1601–1604.
- Greatbatch, R. J. and S. Zhang, 1995: An interdecadal oscillation in an idealized ocean basin forced by constant heat flux. *J. Clim.*, **8**, 82–91.

- Gulev, S. K., B. Barnier, H. Knochel, J. Molines, and M. Cottet, 2003: Water mass transformation in the North Atlantic and its impact on the meridional circulation: insights from an ocean model forced by NCEP-NCAR reanalysis surface fluxes. *J. Clim.*, **16**, 3085–3110.
- Hakkinen, S., 1999: Variability of the simulated meridional heat transport in the North Atlantic for the period 1951-1993. *J. Geophys. Res.*, **104**, 10991–11007.
- Hurrell, J. W., 1995: Decadal trends in the North Atlantic Oscillation: Regional temperatures and precipitation. *Science*, **269**, 676–679.
- 1996: Influence of variations in extratropical wintertime teleconnections on Northern Hemisphere temperature. *Geophys. Res. Lett.*, **23**, 665–668.
- Josey, S. A., E. C. Kent, and P. K. Taylor, 1998: The Southampton Oceanography Centre (SOC) Ocean - Atmosphere Heat, Momentum and Freshwater Flux Atlas. report 6, Southampton Oceanography Centre.
- Kalnay, E., M. Kanamitsu, R. Kistler, W. Collins, D. Deaven, L. Gandin, M. Iredell, S. Saha, G. White, J. Woollen, Y. Zhu, A. Leetmaa, B. R. Chelliah, W. Ebisuzaki, W. Higgins, J. Janowiak, K. C. Mo, C. Ropelewski, J. Wang, R. Jenne, and D. Joseph, 1996: The NCEP/NCAR 40-year reanalysis project. *Bulletin of the American Meteorological Society*, **77**, 437–471.
- Krauss, W., E. Fahrbach, A. Aitsam, J. Elken, and P. Koske, 1987: The North

- Atlantic Current and its associated eddy field southeast of Flemish Cap. *Deep-Sea Research*, **34**, 1163–1185.
- Kushnir, Y., 1994: Interdecadal variations in North Atlantic sea surface temperature and associated atmospheric conditions. *J. Clim.*, **7**, 141–157.
- Mann, C. R., 1967: The termination of the Gulf Stream and the beginning of the North Atlantic Current. *Deep-Sea Research*, **14**, 337–359.
- Marshall, J., H. Johnson, and J. Goodman, 2001: A study on the interaction of the North Atlantic Oscillation with ocean circulation. *J. Clim.*, **14**, 1399–1421.
- Myers, P. G., 2002: SPOM: A regional model of the sub-polar North Atlantic. *Atmosphere-Ocean*, **40**, 445–463.
- NOAA, 1988: Digital relief of the surface of the earth, tech. rep. data announcement 88-mgg-02. National Geophysical Data Center, Boulder, Colorado.
- Paeth, H., A. Hense, R. Glowienka-Hense, R. Voss, and U. Cubasch, 1999: The North Atlantic Oscillation as an indicator for greenhouse-gas induced regional climate change. *Clim. Dyn.*, **15**, 953–960.
- Rogers, J. C., 1984: The association between the North Atlantic Oscillation and the Southern Oscillation in the Northern Hemisphere. *Mon. Wea. Rev.*, **112**, 1999–2015.
- Rosby, T., 1996: The North Atlantic Current and surrounding waters: at the crossroads. *Rev. Geophys.*, **34**, 463–481.

- Shindell, D. T., R. L. Miller, G. A. Schmidt, and L. Pandolfo, 1999: Simulation of recent northern winter climate trends by greenhouse-gas forcing. *Nature*, **399**, 452–455.
- de Raaf, L. A., J. Gerrits, and H. A. Dijkstra, 2004: Identification of the mechanism of interdecadal variability in the North Atlantic ocean. *J. Phys. Oceanogr.*, **34**, 2792–2807.
- Trenberth, K. E., W. G. Large, and J. G. Olson, 1990: The mean annual cycle in global ocean wind stress. *J. Phys. Oceanogr.*, **20**, 1742–1760.
- Visbeck, M., H. Cullen, G. Krahnemann, and N. Naik, 1998: An ocean model's response to North Atlantic Oscillation-like wind forcing. *Geophys. Res. Lett.*, **25**, 4521–4524.
- Weaver, A. J., J. Marotzke, P. F. Cummings, and E. S. Sarachik, 1993: Stability and variability of the thermohaline circulation. *J. Phys. Oceanogr.*, **23**, 39–60.
- Weaver, A. J. and E. S. Sarachik, 1991: Evidence for decadal variability in an ocean general circulation model: An advective mechanism. *Atmos.-Ocean*, **29**, 197–231.

Chapter 5

Sensitivity of the sub-polar North Atlantic to LGM surface forcing and sea-ice distribution in an eddy-permitting regional ocean model

5.1 Introduction

The importance of the sub-polar North Atlantic in climate change is connected to its role in poleward heat transport. This is linked to Labrador Sea deep convection and hence the formation of Labrador Sea Water (LSW), as well as the North Atlantic Current (NAC), an extension of the Gulf Stream (Clarke et al., 1980). Currently, the former, one component of the North Atlantic Deep Water (NADW), helps to drive the sinking branch of the meridional overturning circulation (MOC), a global

^oA version of this chapter has been submitted for publication. Duo Yang and Paul G. Myers and Andrew B. G. Bush 2005. *Paleoceanography*.

system of surface and subsurface ocean currents, while the latter is unique as an upper layer branch in transporting warm waters to much higher latitudes than in any other ocean (Rossby, 1996). Both of them have displayed interannual and interdecadal variability over the last five decades (Dickson et al., 1996; Curry et al., 1998; Curry and McCartney, 2001). LSW formation and the NAC experienced major fluctuations between today and the last glacial period. The Last Glacial Maximum (LGM - about 22 to 14 kyr BP), was characterized by significantly lower temperature than today with large continental areas covered by great ice sheets and a consequent sea level drop of 121 m (Fairbanks, 1989) with extensive sea ice in the northern latitudes (Crowley and North, 1991).

Paleo proxy data have provided us with some evidence in terms of the discrepancy in water mass formation and heat transport during the LGM, in comparison with modern values. Weakening and shallowing of NADW (e.g. Curry and Lohmann, 1983; Oppo and Fairbanks, 1987; Boyle and Keigwin, 1987; Veum et al., 1992), with a shift in its formation to relatively southern latitudes (Alley and Clark, 1999), were deduced from the decreased flux of NADW into the Southern Ocean (Oppo and Fairbanks, 1987; Rutberg et al., 2000) and consequently a further northward penetration of South Ocean Water (SOW) into the benthic Atlantic Ocean (Thomas et al., 2002). With the southward shift of NADW formation came a similar shift in the Gulf Stream/NAC system which became more zonally-orientated (Ruddiman and McIntyre, 1977, 1984; CLIMAP, 1981). Consequently, poleward ocean heat transport in the North Atlantic

was reduced (Miller and Russell, 1989). Weakening and shallowing of the NADW (e.g. Weaver et al., 1998, 2001; Seidov et al., 1996) with southward shift (e.g. Seidov and Haupt, 1997), as well as reduced poleward heat transport (e.g. Seidov and Maslin, 1996) have been reproduced in coupled and ocean-only models configured for the LGM. Cottet-Puinel et al. (2004) note from their simulations of the last glacial cycle that the MOC systematically weakens when LSW formation ceases and strengthens when it resumes. The authors further point out the dependence of the intensity of the MOC on LSW formation and properties as convection on the east side of the Atlantic shows relative stability.

The sensitivity of water mass formation and the ocean circulation to changes in North Atlantic surface fluxes has become a major factor in explaining climate variability. From reconstructions, de Vernal and Hillaire-Marcel (2000, 2002) infer a strong stratification between a low salinity surface layer (due to seasonal sea ice spreading) and the underlying waters, implying diminished LSW formation. Keffer et al. (1988) and Bush and Philander (1999) attribute the southward migration in the Gulf/NAC system to the prevailing wind field modified by the great ice sheets (Manabe and Broccoli, 1985) 3500 ~ 4000 m thick (e.g. the Laurentide in eastern North America) (e.g. CLIMAP, 1981).

Sea ice can alter sea-surface salinity and hence the density and stratification of the water column. Vertical convection is therefore affected, as suggested by de Vernal and Hillaire-Marcel (2000, 2002), as well as the energy and mass exchanges at the ocean-

atmosphere interface. Our focus here is to investigate the impact of atmospheric and sea ice forcing on the circulation of the sub-polar North Atlantic during the LGM. We carry this out by focusing on LSW formation (and thus variations in strength for the Atlantic MOC - AMOC) as well as the pathway of the NAC. The tool we use is a high resolution eddy-permitting ocean model of the sub-polar North Atlantic. We feel this tool is consistent with our focus, since coarser resolution (and consequently poorer representation of eddy and frontal processes) can lead to a weakening and broadening of frontal features and currents (including the NAC). Section 5.2 describes briefly the model configuration and experiment design, as well as the ocean-atmosphere general circulation model (CGCM) output (similar to Bush and Philander, 1999) and sea-ice reconstructions (Crowley and North, 1991; de Vernal and Hillaire-Marcel, 2000) we use. The model results are analyzed in section 5.3, followed by a discussion and summary in section 5.4.

5.2 A brief description of the model and experiment design

The model is a flux-forced version (Chapter 2) of a regional eddy-permitting ($1/3^\circ$) ocean model of the sub-polar North Atlantic ($68^\circ W \sim 0^\circ$ and $38 \sim 70^\circ N$) (Myers, 2002) having 36 unevenly spaced vertical z-levels. The model also features a finite volume partial cell (Adcroft et al., 1997) topography, taken from ETOPO5 (NOAA, 1988) dataset, as well as open boundary conditions dealing with connections with the

rest of the Atlantic Ocean at $38^{\circ}N$ and buffer zones used in the northern boundary regions. The model is described in more detail in Myers (2002).

For our present day control run, the climatological surface buoyancy (heat and freshwater) forcing originates from ship/buoy measurements of the Southampton Oceanography Center (SOC) (Josey et al., 1998) (mean of 1980 ~ 1993), with the addition of a crude parameterization of the effect of high-frequency variability resulting from the passages of synoptic scale events on the heat flux over the convective region of Labrador Sea during winter months. Wind stress is from an European Center for Medium Range Weather Forecast (ECMWF) climatology, assembled by Trenberth et al. (1990) for the period 1980 ~ 1986. The model thus manifests the important processes associated with water mass formation and dispersal, as well as circulation in this region at the present day (see Chapter 2).

Paleo fluxes (both buoyancy fluxes and wind stress) are taken from a 70-yr CGCM simulation configured for the LGM (21 kyr BP), as described in Bush and Philander (1999). Since the direct application of CGCM surface fluxes to force an OGCM can lead to model instability and drift (Rosati and Miyakoda, 1988), the paleo heat and freshwater flux forcing used is obtained by adding anomalies derived from two CGCM simulations (LGM minus control) (Figure 5.1) to the present day flux fields used in the control experiment. The major features are much stronger heat losses over the Labrador Sea at the LGM, associated with strong northwest prevailing winds off the ice cap (Manabe and Broccoli, 1985; Bush and Philander, 1999). These winds also

lead to strong evaporation and low precipitation and thus freshwater losses over the Labrador Sea. Together, this forcing implies significantly greater buoyancy loss over the Labrador Sea and hence denser surface waters. In contrast, increased precipitation under the stronger Atlantic stormtrack decreases surface salinity in low latitudes.

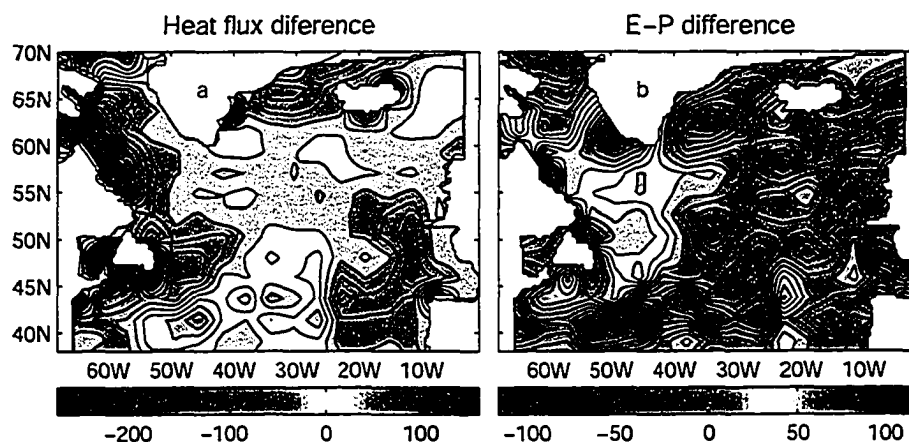


Figure 5.1: Differences in a) winter (DJF) heat flux (Wm^{-2}); b) annual E-P ($cm yr^{-1}$) between the LGM and present, based on CGCM output

The CGCM has a limited (thermodynamic) representation of sea ice. In the LGM simulation, sea ice location is confined to a region north of $61^{\circ}N$ to the west of Greenland and north of $66^{\circ}N$ to the east of Greenland (Figure 5.2). A comparison with two different reconstructions of sea ice (Crowley and North, 1991; de Vernal and Hillaire-Marcel, 2000) implies an underestimation of sea ice in the CGCM output. We therefore parameterize sea-ice by using distributions consistent with the two above listed reconstructions and modify the flux fields accordingly. Based on the pattern shown by Crowley and North (1991, p49, Figure 3.2) for the northern hemisphere for January 18 kyr BP (when Labrador Sea was surrounded by the Laurentide, Inuitian

and Greenland ice sheets), we assume sea-ice extends southward to $48^{\circ}N$ across the entire sub-polar region (Figure 5.2). Here, we assume this “extra” ice is present through the entire winter (December to May) while using the CGCM representation for the rest of the year. A more recent and detailed seasonal reconstruction is the one of de Vernal and Hillaire-Marcel (2000), based upon sea-ice cover during the period from 20 to 16 kyr BP. We hence assume different seasonality as one moves away from the margins (Figure 5.2). Perennial sea-ice is set for Baffin Bay and along the Labrador shelf. Offshore along the Labrador slope, as well the Greenland slope, and in Davis Strait, complete ice cover is assumed in winter. For the rest of the Labrador and Irminger Seas, including all areas north of $55^{\circ}N$ and west of $30^{\circ}W$, a shorter winter ice season (February through to April) is assumed. Again, except as specified above, the CGCM ice field is then used in all other months. Since the presence of sea-ice modifies air-sea fluxes (Parkinson et al., 1987), the paleo-fluxes are then modified in months when ice cover is present in a given grid cell. Our simple parameterization assumes no freshwater exchange and only limited heat flux exchange (10% of that given by the CGCM - Parkinson et al. (1987)) through the ice, as sea ice is a good insulator. This is just the first order picture which this chapter focuses on. By doing do, we don't question the roles of freshening due to sea-ice melt and brine rejection (salinity increase) because of sea-ice formation. Parkinson et al. (1987) suggest two orders of magnitude difference between heat released by an sea-ice covered ocean and heat released from the open ocean. Sea-ice with a thickness larger than 1 meter can

block more than 95% of the heat exchange. In terms of the thickness difference of sea ice, the percentile of 10% is determined.

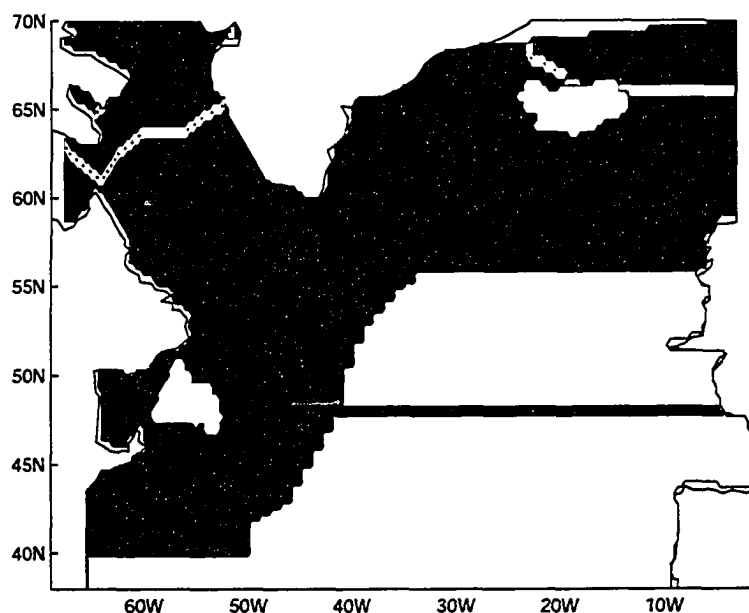


Figure 5.2: LGM sea ice distributions. CGCM output in Feb. (maximum sea ice coverage) is indicated by the thick white line, north of which is covered by sea ice. Sea ice cover north of thick black line ($48^{\circ}N$) is based upon Crowley and North (1991). Shaded sea ice areas are consistent with de Vernal and Hillaire-Marcel (2000), with black color representing perennial sea ice, dark gray color winter (Dec.- May) sea ice cover, light gray color a shorter (Feb.- Apr.) sea ice season and the white area ice-free.

We performed four experiments that depend on the surface forcing and sea-ice conditions. SOCE is our control experiment with the present day surface forcing configuration discussed above, and is the same experiment as SOC1 in Chapter 2. This experiment does a good job of reproducing the large-scale circulation of the sub-polar North Atlantic, other than the model “Northwest Corner” being too far to the east, as shown in Chapter 2. LGME1 is an experiment for the LGM, forced by the CGCM surface forcing. LGME2 and LGME3 are experiments for the LGM

with modified buoyancy fluxes based upon two sea ice reconstructions. Details on the experiments, including integration lengths, are given in Table 5.1. The extension of some experiments by 10 years was to confirm that the given simulations were approaching some form of quasi-equilibrium. An extended integration of 80 years for SOCE (discussed in Chapter 2) further verifies an achievement of the model stability and hence the results obtained by integrations of these lengths (20 or 30 years) are robust.

Table 5.1: Summary of experiments performed in this chapter

Names	length of integration (years)	Heat Flux	E-P	Wind Stress	Sea-ice
SOCE	30~80	SOC	SOC	ECMWF	no
LGME1	20	CGCM	CGCM	CGCM	white line in Fig.5.2
LGME2	20	modified CGCM	modified CGCM	CGCM	black line in Fig.5.2
LGME3	30	modified CGCM	modified CGCM	CGCM	shaded in Fig.5.2

5.3 Model results

Wintertime deep convection and LSW formation are observed around $58.5^{\circ}N$, $52 \sim 53^{\circ}W$ in both SOCE and LGME1. The depth of convection reaches 1500 m and 1700 m, respectively. This location, as well as depths ranging from 1500 to 1700 m have been noted in a number of modern observational studies (e.g. Clarke and Gascard, 1983; Clarke and Coote, 1988; Lilly et al., 1999). The similarity of LGME1 to SOCE can be attributed to the under-representation of sea-ice in the Labrador

Sea by the CGCM. Without sea-ice, strong atmospheric fluxes lead to decrease in buoyancy of the upper waters and enhanced convective overturning. In contrast, there is no LSW formation in either LGME2 and LGME3. Using proxy data to reconstruct sea surface temperature (SST), sea surface salinity (SSS), surface density, as well as vertical density gradients, de Vernal and Hillaire-Marcel (2000, 2002) suggest that a strong stratification developed between a shallow, low salinity surface water layer and the underlying intermediate waters, that was unfavorable for the LSW formation. Although the melt process must be important in terms of providing freshwater to a surface cap, our results support the idea, first suggested by Weaver et al. (2001), that the insulation effect is sufficient on its own to shutdown LSW formation. As the LSW makes up the upper component of NADW, these results support the sensitivity of this water mass (and thus the AMOC) to the sea-ice reconstruction and to model flux field. This can be seen by comparing the maximum meridional overturning streamfunction from each experiment (Table 5.2).

Table 5.2: Maximum meridional stream function (Sv) for all experiments

SOCE	LGME1	LGME2	LGME3
16	20	6	12

At present, the NAC is thought to follow the steep topography of the western boundary in a NNE direction from the Southeast Newfoundland Ridge (around $40^{\circ}N$, $45^{\circ}W$) to Flemish Cap ($47^{\circ}N$, $45^{\circ}W$), turn northwest into the “Northwest Corner”, then shift sharply towards the northeast around $50 \sim 52^{\circ}N$ (discussed by Luo et al.,

2003). The NAC is characterized by strong temperature, salinity and hence density gradients as it currently separates warm, saline waters of tropical-subtropical origin and the cold, fresh waters from the Labrador Sea (Rossby, 1996). It thus represents the position of the sub-polar front. Figure 5.3 gives annual temperature fields from last year of integration on the third model level (52 m) for all four experiments. The strong temperature and thus density gradients along the NAC path can be clearly seen in all cases. The NACs in SOCE and LGME1 have quite similar flow patterns, flowing northwest into “Northwest Corner” west of $42^{\circ}W$ and then turning northeast. The gradients (and thus the flow) are stronger in LGME1 owing to stronger heat loss over the Labrador Sea. An extremely zonal NAC appears several degrees to the south of the ice edge in LGME2. As the mid-Atlantic ridge is approached, the flow weakens, leading to only broad and diffuse transport into the eastern basin. The situation in LGME3 is intermediate to LGME1 and LGME2. Initially, the flow is more zonal, similar to LGME2 (albeit with some northward component). However, east of $38^{\circ}W$, the flow begins to resemble LGME1, with a significant meridional component, allowing significant penetration into the Labrador Sea as well as the Iceland Basin. Unlike in LGME1, where the NAC (and thus the (sub)-Arctic Front) is not constrained, in LGME2 and LGME3 the more southerly paths are constrained by the imposed southern limit of sea-ice cover.

Atmospheric general circulation model (AGCM) and CGCM experiments indicate a split of the atmospheric wind field into northern and southern branches around the

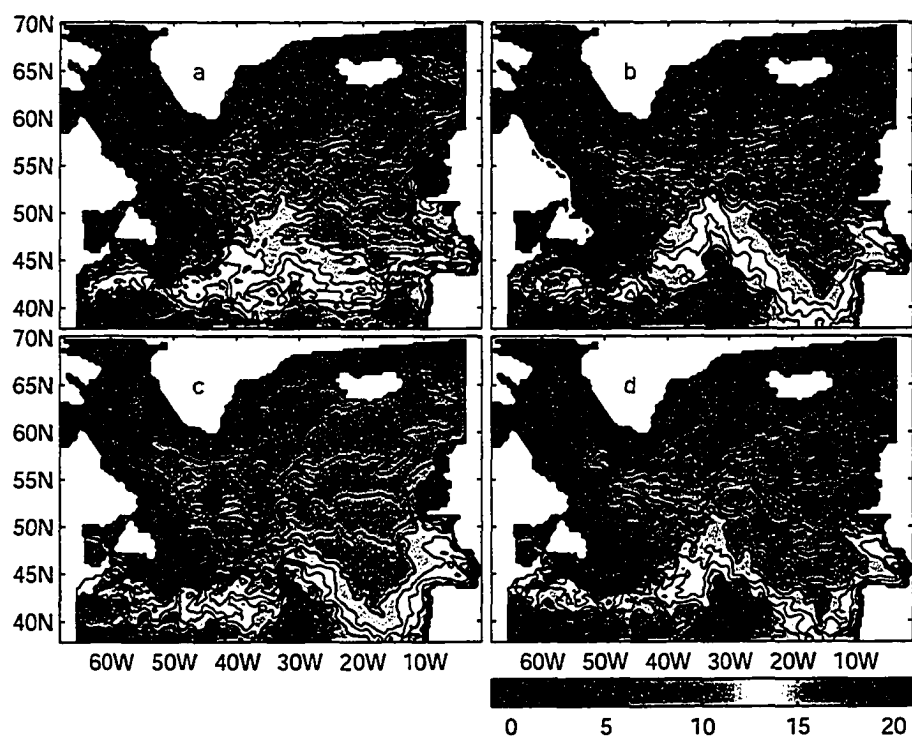


Figure 5.3: Annual temperature at 3rd model level (52 m) for a) SOCE b) LGME1 c) LGME2 d) LGME3

Laurentide Ice Sheet, with the northern branch passing through the Laurentide and Greenland ice sheets and then over the Labrador Sea (Manabe and Broccoli, 1985; Hall et al., 1996; Bush and Philander, 1999). It has been suggested that this modified atmospheric circulation leads to more zonal orientation and a southward shift of the zero line of wind stress curl. This zero line then represents the boundary between the subtropical and subpolar gyres and hence the NAC (Keffer et al., 1988). Our results would tend to contradict this hypothesis. In the three LGM experiments, the same paleo-wind stress pattern is used yet each has a different NAC orientation. Here the NAC path is controlled primarily by the shape and location of the sea-ice edge based on the different reconstructions. This result implies that interactions between ocean circulation and sea ice are likely to have some measure of control on oceanic meridional heat transport in this region.

5.4 Discussion and Summary

We examine the impact of atmospheric forcing and its modulation by sea ice in a regional eddy-permitting ocean model of the sub-polar North Atlantic. We focus on water mass formation (LSW) and the pathway of the NAC. When using the LGM fluxes from a paleo-CGCM (Bush and Philander, 1999), we find a strengthening of LSW formation and the NAC, consistent with the stronger air-sea fluxes believed to have been present during this time. The difference between this result and observations of weakened or curtailed LSW during this time are related to an

under-estimation of sea-ice in the CGCM. When we include extended sea-ice, based upon a pair of reconstructions, our results come more into line with that based on the paleo reconstructions. LSW formation is curtailed, leading to a weaker AMOC. The NAC also weakens, and shifts to a more zonal pathway south of the ice edge.

Our results also support the notion of a positive feedback between ice growth and climate cooling, as suggested by de Vernal and Hillaire-Marcel (2000). In our case, the key aspect of the link is the role of isolating the underlying ocean from the strong atmospheric fluxes and thus shutting down intermediate and deep water formation. These results also present a cautionary tale for the analysis of paleo-general circulation model results. Significantly different circulations, including a wide range of values for the commonly examined AMOC, are found in our simulations with different sea-ice reconstructions, one of the less well known paleo-fields. This suggests the need for further work to attempt to accurately refine the LGM sea-ice extent, including its seasonal variations (e.g. monthly).

Acknowledgements:

This work is part of PhD thesis of Duo Yang and was funded by CFCAS (GR-019) and NSERC grants awarded to Paul G. Myers.

References

- Adcroft, A., C. Hill, and J. Marshall, 1997: Representation of topography by shaved cell in a height coordinate ocean model. *Mon. Weather Rev.*, **125**, 2293–2315.
- Alley, R. B. and P. U. Clark, 1999: The deglaciation of the Northern Hemisphere: A global perspective. *Annu. Rev. Earth Planet. Sci.*, **27**, 149–182.
- Boyle, E. A. and L. Keigwin, 1987: North Atlantic Thermohaline Circulation during the past 20,000 years linked to high-latitude surface temperature. *Nature*, **330**, 35–40.
- Bush, A. B. G. and S. G. H. Philander, 1999: The climate of the Last Glacial Maximum: Results from a coupled atmosphere-ocean general circulation model. *J. Geophys. Res.*, **104**, 24509–24525.
- Clarke, R. A. and A. R. Coote, 1988: The formation of Labrador Sea Water. Part III: The evolution of oxygen and nutrient concentration. *J. Phys. Oceanogr.*, **18**, 469–480.
- Clarke, R. A. and J.-C. Gascard, 1983: The formation of Labrador Sea Water. Part I: Large-scale processes. *J. Phys. Oceanogr.*, **13**, 1764–1778.
- Clarke, R. A., H. W. Hills, R. F. Reiniger, and B. A. Warren, 1980: Current system south and east of the Grand Banks of Newfoundland. *J. Phys. Oceanogr.*, **10**, 25–65.

- CLIMAP, 1981: Seasonal reconstruction of the earth's surface at the last glacial maximum. *Geol. Soc. Am. Map Chart Ser. MC-36*.
- Cottet-Puinel, M., A. J. Weaver, C. Hillaire-Marcel, A. de Vernal, P. U. Clark, and M. Eby, 2004: Variation of Labrador Sea Water formation over the Last Glacial cycle in a climate model of intermediate complexity. *Quaternary Sciences Reviews*, **23**, 449–465.
- Crowley, T. J. and G. R. North, eds., 1991: *Paleoclimatology*. New York: Oxford University Press; Oxford: Clarendon Press.
- Curry, R. G. and M. S. McCartney, 2001: Ocean gyre circulation changes associated with the North Atlantic Oscillation. *J. Phys. Oceanogr*, **31**, 3374–3400.
- Curry, R. G., M. S. McCartney, and T. M. Joyce, 1998: Oceanic transport of subpolar climate signals to mid-depth subtropical waters. *Nature*, **391**, 575–577.
- Curry, W. B. and G. P. Lohmann, 1983: Reduced advection into Atlantic Ocean deep eastern basins during last glaciation maximum. *Nature*, **306**, 577–580.
- de Vernal, A. and C. Hillaire-Marcel, 2000: Sea-ice cover, sea-surface salinity and halo-/thermocline structure of the northwest North Atlantic: modern versus full glacial conditions. *Quaternary Sciences Reviews*, **19**, 65–85.
- 2002: Structure of the upper water column in the northwest North Atlantic: Modern versus Last Glacial Maximum conditions. *Paleoceanography*, **17**, 2–1–2–15.

- Dickson, R. R., J. R. N. Lazier, J. Meincke, P. Rhines, and J. Swift, 1996: Long-term coordinated changes in the convective activity of the North Atlantic. *Progress in Oceanogr.*, **38**, 241–295.
- Fairbanks, R. G., 1989: A 17,000-year glacio-eustatic sea level record: Influence of glacial melting rates on Younger Dryas event and deep-ocean circulation. *Nature*, **342**, 637–642.
- Hall, N. M. J., P. J. Valdes, and B. Dong, 1996: The maintenance of the last great ice sheets: A UGAMP GCM study. *J. Clim.*, **9**, 1004–1019.
- Josey, S. A., E. C. Kent, and P. K. Taylor, 1998: The Southampton Oceanography Centre (SOC) Ocean - Atmosphere Heat, Momentum and Freshwater Flux Atlas. report 6, Southampton Oceanography Centre.
- Keffer, T., D. G. Martinson, and B. H. Corliss, 1988: The position of the Gulf Stream during quaternary glaciations. *Science*, **241**, 440–442.
- Lilly, J. M., P. B. Rhines, M. Visbeck, R. Davis, J. R. N. Lazier, F. Schott, and D. Farmer, 1999: Observing deep convection in the Labrador Sea during winter 1994/95. *J. Phys. Oceanogr.*, **29**, 2065–2098.
- Luo, Y., H. Zhang, M. D. Prater, and L. M. Rothstein, 2003: Warm water pathways, transports and transformations in the northwestern North Atlantic and their modification by cold air outbreaks. *J. Geophys. Res.*, **108**, 26–1–26–16.

- Manabe, S. and A. J. Broccoli, 1985: The influence of continental ice sheets on the climate of an ice-age. *J. Geophys. Res.*, **90**, 2167–2190.
- Miller, J. R. and G. L. Russell, 1989: Ocean heat transport during the Last Glacial Maximum. *Paleoceanog.*, **4**, 141–155.
- Myers, P. G., 2002: SPOM: A regional model of the sub-polar North Atlantic. *Atmosphere-Ocean*, **40**, 445–463.
- NOAA, 1988: Digital relief of the surface of the earth, tech. rep. data announcement 88-mgg-02. National Geophysical Data Center, Boulder, Colorado.
- Oppo, D. W. and R. G. Fairbanks, 1987: Variability in the deep and intermediate water circulation of the Atlantic Ocean during the past 25,000 years: North Hemisphere modulation of the Southern Ocean. *Earth and Planetary Science Letters*, **86**, 1–15.
- Parkinson, C. L., J. C. Comiso, H. J. Zwally, D. J. Cavalieri, P. Gloersen, and W. J. Campbell, 1987: Arctic Sea Ice, 1973-1976: Satellite Passive-Microwave Observations. NASA Pub. SP-489, NASA Scientific and Technical Information Program, Washington DC.
- Rosati, A. and K. Miyakoda, 1988: A general circulation model for upper ocean simulation. *J. Phys. Oceanogr.*, **18**, 1601–1626.

- Rossby, T., 1996: The North Atlantic Current and surrounding waters: at the crossroads. *Rev. Geophys.*, **34**, 463–481.
- Ruddiman, W. F. and A. McIntyre, 1977: Late quaternary surface ocean kinematics and climate change in the high-latitude North Atlantic. *J. Geophys. Res.*, **82**, 3877–3887.
- 1984: Ice-age thermal response and climatic role of the surface North Atlantic Ocean, 43°–63°. *Geological Society of America Bulletin*, **95**, 381–396.
- Rutberg, R. L., S. R. Hemming, and S. L. Goldstein, 2000: Reduced North Atlantic Deep Water flux to the glacial Southern Ocean inferred from neodymium isotope ratios. *Nature*, **405**, 935–938.
- Seidov, D. and B. J. Haupt, 1997: Simulated ocean circulation and sediment transport in the North Atlantic during the last glacial maximum and today. *Paleoceanography*, **12**, 281–305.
- Seidov, D. and M. Maslin, 1996: Seasonally ice free glacial Nordic Seas without deep water ventilation. *TERRA NOVA*, **8**, 245–254.
- Seidov, D., M. Sarnthein, K. Statterger, R. Prien, and M. Weinelt, 1996: North Atlantic ocean circulation during the last glacial maximum and subsequent meltwater event: A numerical model. *J. Geophys. Res.*, **101**, 16305–16332.
- Thomas, M., J. Marchitto, D. W. Oppo, and W. B. Curry, 2002: Paired benthic

- foraminiferal cd/ca and zn/ca evidence for a greatly increased presence of Southern Ocean Water in the glacial North Atlantic. *Paleoceanography*, **17**, 10-1-10-16.
- Trenberth, K. E., W. G. Large, and J. G. Olson, 1990: The mean annual cycle in global ocean wind stress. *J. Phys. Oceanogr.*, **20**, 1742-1760.
- Veum, T., E. Jansen, M. Arnold, I. Beyer, and J. Duplessy, 1992: Water mass exchange between the North Atlantic and the Norwegian Sea during the past 28,000 years. *Nature*, **356**, 783-785.
- Weaver, A. J., M. Eby, A. F. Fanning, and E. C. Wiebe, 1998: Simulated influence of carbon dioxide, orbital forcing and ice sheets on the climate of the Last Glacial Maximum. *Nature*, **394**, 847-853.
- Weaver, A. J., M. Eby, E. C. Wiebe, C. M. Bitz, P. B. Duffy, T. L. Ewen, A. F. Fanning, M. M. Holland, A. MacFadyen, H. D. Matthews, K. J. Meissner, O. Saenko, A. Schmittner, H. Wang, and M. Yoshimori, 2001: The UVic earth system climate model: Model description, climatology, and applications to past, present and future climates. *Atmosphere-Ocean*, **39**, 361-428.

Chapter 6

Summary and Future Work

6.1 Summary and Conclusions

This study examines the impact of anomalous surface forcing associated with extreme NAO phases and the LGM on water mass formation and circulation over the sub-polar North Atlantic, in order to further clarify the mechanisms of variability and changes in oceanic circulation and heat transport so as to contribute to an understanding of variations and stability in future climate system. It involves four themes.

1) A version of a regional eddy-permitting ocean general circulation model of the sub-polar North Atlantic driven by flux forcing was developed for specific application to recent outstanding questions of ocean and climate variability and change. It is based upon a previous version using restoring boundary conditions (Myers, 2002). The buoyancy fluxes originate from SOC and NCAR-NCEP monthly climatologies, with the addition of a crude parameterization of the high frequency portion of heat fluxes that provides sufficient LSW in the model. Although a weak restoring term on

salinity is needed to parameterize non-included sea-ice effects and thus control salinity drift, the model remains stable, albeit with a shift between two modes of circulation in one experiment. All major features of the sub-polar gyre are well represented in the experiment with SOC buoyancy forcing. Sub-polar mode water formation and dispersal, as well as the model eddy kinetic energy fields are improved with respect to an equivalent run with restoring boundary conditions. A drift in temperature and salinity exists, a common feature in high resolution ocean model of this region, which is brought about by an internal advection process. Nevertheless, the variability and change in oceanic circulation can be easily identified against such a control run.

2) The sensitivity of water mass formation to high frequency variability is explored with a series of experiments designed to represent different scenarios of synoptic events (time evolving patterns) to justify the crude parameterization of high frequency events in the model development mentioned above. The results show that while variations in convective activity do occur, LSW formation (volume) is basically consistent in all experiments, suggesting that the exact form of the high frequency heat flux representation may not be key if one is looking at end results of the water formation process in an integrated sense. This type of idealization of synoptic events is therefore appropriate for use in an ocean model in terms of LSW formation.

3) The response of LSW formation and the NAC to extreme high and low NAO phase-related surface forcing is inspected with above flux forced model. A potentially multi-decadal variability in LSW formation and heat transport occurs under

anomalous high NAO related forcing, in contrast to a stable state under anomalous low NAO related forcing. This variability appears to be brought about by an oceanic internal process, which is similar to the results from a series of “idealized” studies (e.g. Weaver and Sarachik, 1991; te Raa et al., 2004). However, the result from this study is that this internal mode exists only during high NAO phase, and is produced by the changes in the NAC strength and pathway.

4) The potential impact of paleo-atmospheric forcing and its modulation by sea ice is also explored with the model. The focus is on water mass formation and the pathway of the NAC. Paleo fluxes are obtained from a CGCM while the seasonal sea ice cover is based on a pair of LGM sea ice reconstructions (Crowley and North, 1991; de Vernal and Hillaire-Marcel, 2000). LSW formation, the NAC pathway and the AMOC strength are found to be dependent on the structure of the sea-ice representation. The key role played by the sea-ice is its isolation of the underlying ocean from the wintertime atmospheric fluxes.

A few salient conclusions are achieved in this thesis. First, extensive experiments suggest that use of flux forcing is important for an eddy-permitting ocean model to properly represent the important processes associated with water mass formation and dispersal in the sub-polar North Atlantic and to better resolve the NAC pathway. The results also show that SOC buoyancy fluxes are more robust to force regional ocean model. Second, the results implicate a less stable oceanic state and hence the possibility for enhanced variability of climate system to occur under the high phase

of the NAO. Since the high phase of the NAO becomes more likely under climate warming scenarios (Shindell et al., 1999; Fyfe et al., 1999), this result emphasizes the importance of understanding how the ocean circulation will evolve in such a situation. Finally, this study stresses the significance of the isolation of the ocean from atmospheric forcing by sea-ice, and hence highlights the need for accurate seasonal sea ice fields for paleo modelling simulations.

6.2 Future Work

By imposing diverse anomalous surface forcings in response to extreme high and low NAO phases, as well as the extreme climate interval - LGM, this study reveals variant oceanic responses. It is of great interest to further investigate the feedback of these responses on the atmosphere and a subsequent atmosphere-ocean interaction, hence variations and stability of climate system, especially for the less stable high NAO state. This could be done by coupling an atmospheric model to SPOM in the future.

This thesis suggests a considerable discrepancy in oceanic circulations in response to different sea-ice distributions in the model simulations during the LGM. A limitation in the process of its parameterization of sea-ice effect is that it does not consider complete sea-ice impact, such as an inclusion of the effects of freeze and thaw processes and hence resulted freshening and brine rejection, although it compromised my focus. This could be a future work based on modern sea-ice information or further

availability of refined paleo-reconstruction of sea-ice or a coupling of sea-ice model. It is also expected that an examination of oceanic behavior during other intervals of the last glacial cycle in response to the atmospheric forcing and sea-ice distributions could be done when additional sea ice reconstructions are generated.

Model hydrography drift has become a major issue in developing a regional high resolution ocean model in the North Atlantic, as discussed in this thesis. The SPOM uses constant vertical diffusion coefficients, as discussed in Section 1.2. It is noted that ocean model solutions are sensitive to their subgrid-scale vertical tracer diffusivity (McWilliams, 1996). The incorporation of vertical mixing schemes could be tested in order to solve this problem in the future. Moreover, coupling of a sea ice model to the flux version of the SPOM again would be expected to add more freshwater into the sub-polar North Atlantic domain. This work could reduce the model drift, as suggested by the results from a coupled sea-ice sigma-coordinate ocean model (Hakkinen, 1999), where the model SST and SSS have very little drift in areas with deep mixed layer.

References

- Crowley, T. J. and G. R. North, eds., 1991: *Paleoclimatology*. New York: Oxford University Press; Oxford: Clarendon Press.
- de Vernal, A. and C. Hillaire-Marcel, 2000: Sea-ice cover, sea-surface salinity and

- halo-/thermocline structure of the northwest North Atlantic: modern versus full glacial conditions. *Quaternary Sciences Reviews*, **19**, 65–85.
- Fyfe, J. C., G. J. Boer, and G. M. Flato, 1999: The Arctic and Antarctic Oscillation and their projected changes under global warming. *Geophys. Res. Lett.*, **26**, 1601–1604.
- Hakkinen, S., 1999: Variability of the simulated meridional heat transport in the North Atlantic for the period 1951–1993. *J. Geophys. Res.*, **104**, 10991–11007.
- McWilliams, J. C., 1996: Modeling the oceanic general circulation. *Annu. Rev. Fluid. Mech.*, **28**, 215–248.
- Myers, P. G., 2002: SPOM: A regional model of the sub-polar North Atlantic. *Atmosphere-Ocean*, **40**, 445–463.
- Shindell, D. T., R. L. Miller, G. A. Schmidt, and L. Pandolfo, 1999: Simulation of recent northern winter climate trends by greenhouse-gas forcing. *Nature*, **399**, 452–455.
- te Raa, L. A., J. Gerrits, and H. A. Dijkstra, 2004: Identification of the mechanism of interdecadal variability in the North Atlantic ocean. *J. Phys. Oceanogr.*, **34**, 2792–2807.
- Weaver, A. J. and E. S. Sarachik, 1991: Evidence for decadal variability in an ocean general circulation model: An advective mechanism. *Atmos.-Ocean*, **29**, 197–231.